

**UNIVERSITY OF OSLO**  
**Department of Physics**

**Attitude Control  
of a Nano Satellite**

Master thesis

Fredrik Stray

October 1, 2010





---

# Preface

---

This master thesis is part of the fulfillment of the Master of Science in engineering cybernetics at the Department of Physics, Faculty of Mathematics and Natural Science, University of Oslo. The work has primarily been done at UNIK, University Graduate Center at Kjeller.

I would like to thank my supervisor Professor Oddvar Hallingstad and my advisor Associate Professor Torfinn Lindem for their support during this work.

Last, but not least, I would like to thank my wife Sissel, and our three beautiful girls, Alva Fredrikke, Veslemøy Marie and Astrid Louise. I'm very thankful for the love you have given me, and for the patience you have shown during the work on my master thesis.

Kjeller, October 2010

---

Fredrik G. Stray



---

# Summary

---

The CubeSTAR satellite is a student satellite project at the University of Oslo. The main mission is to measure the turbulence in the electron plasma using a novel Multi Needle Langmuir Probe system developed at the University of Oslo. In order to get correct measurements, it's important that the probes are located in the front of the satellite in the orbit velocity direction.

In this thesis, the attitude control problem of the CubeSTAR nano-satellite is the main topic. The satellite will use three electromagnetic coils as actuators, mounted on each axis. These coils can generate a magnetic moment, and together with the Earth's geomagnetic field, create a torque able to change the attitude of the spacecraft. The problem with using magnetic coils is that the magnetorquers only work in the direction perpendicular to the geomagnetic field, and there will always exist one axis that is not controllable. However, because the geomagnetic field is approximately periodic, the spacecraft becomes controllable over one orbit.

The spacecraft dynamics and the environmental models are derived and analyzed, and the design of the magnetic coils are presented. An adaptive PD-like controller and the LQR optimal control problem are presented and investigated for magnetic stabilization of the spacecraft, in addition to the B-dot detumbling control law. Simulations of the different controllers shows the performance when realistic disturbances are added to the system, and a recommendation based on these results are presented.

The attitude determination and control system will be implemented on a FPGA on-board the satellite. Implementation of the attitude control is achieved by using the DSP-builder software by Altera. The source code is compiled to HDL, and downloaded onto the FPGA. The performance of the FPGA is shown through hardware in-the-loop simulations.



---

# Contents

---

<b>Preface</b>	<b>iii</b>
<b>Summary</b>	<b>v</b>
<b>1 Introduction</b>	<b>1</b>
1.1 The CubeSat Standard . . . . .	1
1.2 The CubeSTAR student satellite project . . . . .	2
1.2.1 Scientific mission . . . . .	3
1.3 Attitude Control and Determination System . . . . .	3
1.3.1 Control actuators . . . . .	3
1.3.2 Attitude determination . . . . .	5
1.4 CubeSTAR attitude control actuators . . . . .	5
1.5 Previous work . . . . .	6
1.5.1 Similar Missions . . . . .	7
1.6 Outline of the thesis . . . . .	8
<b>2 Attitude Parametrization</b>	<b>11</b>
2.1 Direction cosine matrix . . . . .	11
2.1.1 Kinematic differential equation . . . . .	12
2.1.2 Skew-symmetric form . . . . .	12
2.2 Euler angles . . . . .	12
2.3 Euler parameters . . . . .	14
2.4 Discussion . . . . .	15
<b>3 Spacecraft Dynamics</b>	<b>17</b>
3.1 Coordinate Reference frames . . . . .	18
3.2 Equations of Motion . . . . .	19
3.2.1 Angular momentum . . . . .	19
3.2.2 Dynamics . . . . .	20
3.2.3 Kinematics . . . . .	20

3.3	Magnetic torquers . . . . .	21
3.4	Environmental Models . . . . .	22
3.4.1	Earth's Geomagnetic Field . . . . .	22
3.4.2	Gravity Gradient torque . . . . .	25
3.4.3	Aerodynamic Torque . . . . .	26
3.4.4	Solar Radiation Torque . . . . .	28
3.4.5	Residual Dipole Torques . . . . .	29
3.5	Linearized model . . . . .	29
3.5.1	Linearized equations of motion . . . . .	32
3.6	Controllability . . . . .	33
3.7	Stabilizability . . . . .	33
3.8	Summary . . . . .	34
<b>4</b>	<b>Magnetorquer Design</b>	<b>35</b>
4.1	Design specification . . . . .	35
4.2	Magnetic coil design . . . . .	35
4.3	Design results . . . . .	38
4.4	Summary . . . . .	38
<b>5</b>	<b>Attitude Control</b>	<b>41</b>
5.1	Detumbling . . . . .	41
5.2	Magnetic Stabilization . . . . .	42
5.2.1	Proportional-Derivative Control . . . . .	43
5.2.2	Linear-Quadratic Regulator . . . . .	44
5.3	Summary . . . . .	49
<b>6</b>	<b>Simulations</b>	<b>51</b>
6.1	The Uncontrolled Satellite . . . . .	52
6.2	Detumbling simulation . . . . .	55
6.3	PD-Control simulation . . . . .	58
6.4	LQR Control . . . . .	62
6.4.1	Constant Gain . . . . .	62
6.5	Discussion . . . . .	66
<b>7</b>	<b>Implementation</b>	<b>69</b>
7.1	HIL Simulation . . . . .	70
<b>8</b>	<b>Conclusions</b>	<b>75</b>
8.1	Discussion of Results . . . . .	75
8.2	Recommendation for Future Work . . . . .	76



---

<b>Bibliography</b>	<b>82</b>
<b>A Abstract submitted to the 61st International Astronautical Congress (IAC)</b>	<b>83</b>
<b>B MATLAB source code</b>	<b>85</b>
<b>C SIMULINK source code</b>	<b>97</b>
<b>D DSP builder source code</b>	<b>105</b>



---

# List of Figures

---

1.1	Sketch of the CubeSTAR satellite. . . . .	2
3.1	The geomagnetic field seen from the orbit frame at 300 km altitude. The circular orbit has an inclination of $90^\circ$ . . . . .	23
3.2	The geomagnetic field seen from the orbit frame at 500 km altitude. The circular orbit has an inclination of $90^\circ$ . . . . .	24
3.3	The geomagnetic field seen from the orbit frame at 800 km altitude. The circular orbit has an inclination of $90^\circ$ . . . . .	25
3.4	The geomagnetic field seen from the orbit frame at 500 km altitude using the dipole approximation. The circular orbit has an inclination of $90^\circ$ . . . . .	26
6.1	Euler angles from the uncontrolled satellite . . . . .	53
6.2	Quaternions from the uncontrolled satellite . . . . .	54
6.3	Angular velocity from the uncontrolled satellite . . . . .	54
6.4	Disturbance torques acting on the uncontrolled satellite . . . . .	55
6.5	Euler angles from the B-dot control simulation . . . . .	56
6.6	Quaternions from the B-dot control simulation . . . . .	56
6.7	Angular velocity from the B-dot control simulation . . . . .	57
6.8	Magnetic moments from the B-dot control simulation . . . . .	57
6.9	Magnetic torques from the B-dot control simulation . . . . .	58
6.10	Euler angles from the PD control simulation . . . . .	59
6.11	Quaternions from the PD control simulation . . . . .	60
6.12	Angular velocity from the PD control simulation . . . . .	60
6.13	Magnetic moments from the PD control simulation . . . . .	61
6.14	Magnetic torques from the PD control simulation . . . . .	61
6.15	Disturbance torques from the PD control simulation . . . . .	62
6.16	Euler angles from the constant gain LQR control simulation . . . . .	63
6.17	Quaternions from the constant gain LQR control simulation . . . . .	64
6.18	Angular velocity from the constant gain LQR control simulation . . . . .	64
6.19	Magnetic moments from the constant gain LQR control simulation . . . . .	65

6.20	Magnetic torques from the constant gain LQR control simulation . . . . .	65
6.21	Disturbance torques from the constant gain LQR control simulation . . . . .	66
7.1	Euler angles from the FPGA HIL simulation . . . . .	71
7.2	Quaternions from the FPGA HIL simulation . . . . .	71
7.3	Angular velocity from the FPGA HIL simulation . . . . .	72
7.4	Magnetic moments from the FPGA HIL simulation . . . . .	72
7.5	Magnetic torques from the FPGA HIL simulation . . . . .	73
C.1	Top-Level Block Diagram . . . . .	97
C.2	Non-Linear System . . . . .	98
C.3	Spacecraft Dynamics . . . . .	98
C.4	Spacecraft Kinetics . . . . .	98
C.5	orbit to body . . . . .	99
C.6	Magnetic Coils model . . . . .	99
C.7	Environmental Model . . . . .	100
C.8	Gravity Gradient Block . . . . .	101
C.9	Magnetic Field Block . . . . .	101
C.10	Magnetic Dipole Disturbance Block . . . . .	102
C.11	Sun Preassure Block . . . . .	102
C.12	Aerodynamic Preassure Block . . . . .	103
C.13	Adaptive PD . . . . .	103
C.14	Adaptive PD gamma . . . . .	104
C.15	Adaptive PD gamma average . . . . .	104
D.1	Top-Level Block Diagram of the FPGA attitude control. . . . .	105
D.2	Block Diagram of the FPGA gain . . . . .	106
D.3	Block Diagram of the FPGA matrix calculation . . . . .	107
D.4	Block Diagram of the FPGA matrix calculation . . . . .	107

---

# List of Tables

---

3.1	Air density in the atmosphere for specific altitudes. . . . .	27
4.1	Magnetorquer design constraints . . . . .	36
4.2	Copper properties . . . . .	38
4.3	Magnetorquer design results for the short side coil . . . . .	39
4.4	Magnetorquer design results for the long sides . . . . .	39
6.1	Simulation Model Parameters . . . . .	51
6.2	Initial conditions for the uncontrolled satellite simulation . . . . .	53
6.3	Initial conditions and gain value for the B-dot detumbling simulation . . .	55
6.4	Initial conditions and gain value for the adaptive PD-control simulation .	58
6.5	Initial conditions and gain value for the constant gain LQR control simulation . . . . .	63



## Chapter 1

---

# Introduction

---

Since the beginning of the space age, a lot of work has been done regarding the Attitude Determination and Control System (ADCS) on satellites. The ADCS is of great importance because satellites, also called spacecrafts, usually needs to point in specific directions in order to perform its assigned tasks. This tends to be towards the Earth, sun or stars, while other parts such as antennas may need to point towards the Earth, while solar panels needs to be directed towards the sun.

The purpose of this thesis is to examine the problem of using magnetic control to stabilize a 2 kg nano satellite, i.e. satellite with mass less then 10 kg. The mass is assumed evenly distributed over the volume. First, a reasonable model of the satellite must be established and investigated. Then the magnetic coils, also called magnetorquers, must be designed in such a way that they are able to control the spacecraft and meets the design specifications. Control strategies are proposed and simulated with the spacecraft and environmental models. A constant gain Linear Quadratic Regulation (LQR) control law will be implemented on a Altera Cyclone III FPGA using the DSP-builder software by Altera, and tested using Hardware In the Loop (HIL) simulations.

## 1.1 The CubeSat Standard

The CubeSat concept, developed at the Stanford University, was designed in order to make it easier to launch student satellite projects at a lower cost comparing to commercial satellites. The original CubeSat was a cube of size 10cm  $\times$  10cm  $\times$  10cm, named 1-U and weighing at most 1 kg. A deployer was also developed, namely P-POD (Poly Pico-satellite Orbital Deployer). This deployer could stack three CubeSats on top of each other, and launch them into space. Later, 2-U and 3-U CubeSats where developed. They consist of the original area, but is 20cm and 30cm high, respectively. The satellites is usually launched as secondary payloads in order to lower the costs, resulting in a large amount of student satellite projects. In recent revisions, the weight specifications has been changed, allowing heavier satellites [40]. However, in this thesis

the original weight specifications are assumed.

## 1.2 The CubeSTAR student satellite project

The Space Technology And Research development center (STAR) project is a collaboration between UiO (University of Oslo) and UNIS (University Center in Svalbard) amongst others. It's main focus is to study the Sun-Earth relationship including turbulence in ionospheric plasma. The CubeSTAR project was initiated as a spin-off from this project with support from the Norwegian Space Center, NAROM (Norwegian Center for Space-related Education) and ANSAT Student Satellite Program. The idea behind the project is to build a satellite from scratch using the CubeSat framework. This results in a project which involves several disciplines, and gives students an opportunity to examine the field of space technology.

The CubeSTAR student satellite project has decided to use a 2-U CubeSat, as this size gives the necessary space and weight required. The subsystems consist of Power Supply, Communication, Ground Control, Attitude Control and Determination System and the payload (scientific mission). The satellite will operate at an altitude between 300 and 800 km height. A sketch of the CubeSTAR satellite borrowed from the Instrument Workshop at the Department of Physics, UiO is shown in figure 1.1. On the left side of the satellite, the communication antennas are mounted. The multi-Needle Langmuir Probe (m-NLP) system, consisting of four probes, is to the right.

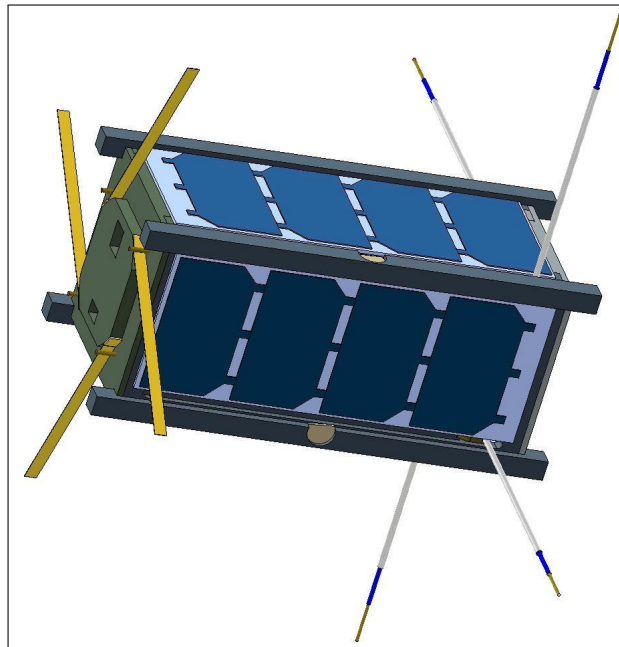


**Figure 1.1:** Sketch of the CubeSTAR satellite.



### 1.2.1 Scientific mission

As mentioned, the STAR-project is working with measurements of the electron density in ionospheric plasma. The scientific mission of CubeSTAR is to use a novel Langmuir probe system for determination of absolute electron density in ionospheric plasma, called m-NLP. This system is developed at the University of Oslo (UiO), and has been successfully demonstrated on the ICI-2 (Investigation of Cusp Irregularities) sounding rocket in 2008[4]. The m-NLP system has a spatial resolution down to the sub-meter scale, while common systems usually has a spatial resolution of kilometers. For the CubeSTAR system, a low-power version of the system used on ICI-2 will be developed. The system consist of compromising four cylindrical probes with a diameter of 0.5 mm and a length of about 25 mm. Each of these probes are operated at different fixed bias voltages in the electron saturation region. On-board, a Altera Cyclone IV FPGA will do the calculations of the electron density. In order to get correct measurements, it's important that the m-NLP system is placed in the front of the velocity direction with an accuracy of about  $10^\circ$ . For more information about the scientific experiment, see Bekkeng [4].

## 1.3 Attitude Control and Determination System

The following gives a short introduction to the most used control and determination concepts. For simplicity, only Earth orbital spacecraft missions are considered.

### 1.3.1 Control actuators

There exists several ways to control a spacecraft. Stabilization of satellites can be divided into two categories, passive stabilization and active stabilization.

#### Passive stabilization methods

Passive stabilization methods usually stabilizes in two axes only. These methods are often easy to apply, inexpensive, and tends to be very robust. However, the passive stabilization methods usually doesn't give good accuracy, and it's therefore necessary to implement active stabilization methods as well.

Gravity gradient stabilization, usually realized with a boom, uses the gravitational force to stabilize the spacecraft. Gravity gradient stabilization stabilizes in two axes only, and excludes stabilization in the direction of the gravity gradient. The property of this kind of stabilization lies in the position of the center of gravity of the satellite. With a gravity gradient boom, the center of gravity is moved towards the boom, causing the effect that the boom will be aligned in the direction of the Earth.

Spin stabilization is caused by spinning the satellite about a stable axis. This creates a gyroscopic effect, making it hard to change the attitude in the spin stabilized axes. This two-axes stabilization is however not suitable for a large amount of spacecrafts. A large amount of satellites are not symmetric, and it is therefore often hard to spin stabilize the satellite. In order to get spin stabilization, an active control actuator must be applied.

Passive magnets will force the spacecraft to follow the Earth's magnetic field. The orientation will only point with limited accuracy, and in most cases not with the desired attitude. When using magnetometers, the passive magnets will also disturb the measurements because the passive magnets are much stronger than the Earth's magnetic field. In most missions, the orientation of the satellite must be known, and can therefore be hard to achieve with the use of passive magnets. However, this type of stabilization is very easy to implement and very robust in terms of failure.

### **Active stabilization methods**

In order to get high accuracy on the attitude control, active stabilization methods are often required. They are more expensive and harder to implement than passive methods, but is in most cases necessary to be able to carry out the satellite's main mission.

Magnetic coils, or magnetorquers, are winded electromagnetic coils with or without metallic cores. The magnetic coils creates a magnetic field when electrical current is applied. This field then acts on the Earth's geomagnetic field, creating a torque acting on the satellite. The magnetic coils are cheap and light. The problem with magnetic coils however is the dependency of the Earth's magnetic field. It's only possible to apply a control torque in the direction perpendicular to the geomagnetic field vector. This means that there will always be an axis not controllable. However, the geomagnetic field is not homogeneous, and can be considered periodic. Because of this it's possible to have a 3-axes stabilization using magnetic coils solely. In addition, the geomagnetic field is very weak, and attitude control based on magnetorquers will therefore tend to be slow.

Momentum wheels and reaction wheels is well used methods to get very high accuracy. They consist of mechanical moving wheels creating gyroscopic effects. Momentum wheels are usually used for gyroscopic stabilization as these operate at high rotation speeds. Reaction wheels can change the spacecrafts angular momentum, and operates at zero nominal rotation speed. This gives a very fast response, and is able to act independent on the three axes. The disadvantages with these types of wheels are high power consumption, moving parts that can easily fail, large mass, expensive and large volume. In addition, because momentum wheels operates at high rotation speeds, they need support for momentum dumping. This is usually realized with magnetorquers. The placement of the wheels is also of high importance as a small misplacement will severely change the spacecrafts properties.

Thrusters are propulsive devices. They shoot out mass in one direction, and thus creating a force in the opposite direction. Thrusters can be realized with liquid fuel, plasma and ions to name a few. The most common way to use thrusters for attitude control of satellites are with liquid fuel. This bang-bang solution creates a very fast response, with great accuracy. However, liquid fuel have a limited life time, is very heavy and can be hard to implement. In addition, liquids are hard to model because they can not be modeled as rigid bodies, and creates more complex models of the spacecraft.

### 1.3.2 Attitude determination

Although not treated in this thesis, the attitude determination system is a very important system. Without it, it's not possible to estimate the attitude of the spacecraft, and hence the active attitude control mat be useless. In the following, a short introduction to selected attitude sensors will be presented.

The magnetometer is an absolute attitude sensor that measures the Earth's geomagnetic field. With a 3-axis magnetometer, it's possible to estimate the attitude by comparing the measurements with a model of the Earth's geomagnetic field. It's therefore vital that the geomagnetic model is good, and that the position of the satellite in the orbit is known. Because the magnetometer measures magnetic fields, there may occur difficulties regarding use of magnetic coils and internal magnetic dipole disturbances.

A sun sensor is a absolute attitude sensor that senses the direction of the sun, and can also be implemented with solar cells. When the satellite is in eclipse, that is in the shadow of the Earth, the sun sensors are not usable.

Star trackers can identify thousands of different stars, and can hence be used as an absolute attitude sensor. These sensors can give very high accuracy, but requires low angular velocities, in addition to being very expensive.

The gyroscope is a relative attitude sensor that senses rotation. It can not be used alone for attitude determination, but can severely improve the attitude estimation together with absolute attitude sensors.

## 1.4 CubeSTAR attitude control actuators

Up to now, there exists very little data on the results on the use of active attitude control, including magnetorquers, on nano-satellites. This is due to the fact that developers other than student projects tends to rely on passive attitude control on nano satellites. In addition, the failure of the ADCS has been a huge problem on CubeSat projects. Different types of actuators has above been presented. CubeSTAR is a small satellite, without much space and a strict weight restriction. A gravity boom could be of interest,

but can be difficult to realize as a boom deployment must be designed. Momentum wheels and reaction wheels gives great pointing accuracy, but is big and expensive. It's possible to buy commercial, "off the shelf" ADCS with magnetorquers and momentum wheels, but these are of the size of 1-U, and therefore use half of the available space in a 2-U CubeSat.

As of this stage, it's desirable to use three perpendicular magnetic coils solely for attitude control on the CubeSTAR satellite. This because of its light weight, it's easy to implement and design, have a low power consumption and is inexpensive. Because of the shape of the satellite, two different types of coils must be designed. These coils will have the dimensions dimensions  $190 \times 75\text{mm}$  and  $75 \times 75\text{mm}$ , and a max cross section of  $2 \times 5\text{mm}$  ( $10\text{mm}^2$ ). The satellite has limited supply of electrical energy, and has a limit of 100 mA current in the coils and the voltage set to 3V.

## 1.5 Previous work

At this stage of the project, there exists no previous work on the ADCS for the CubeSTAR project. Some of the work in this thesis has been to explore the literature on the magnetic attitude control problem. As already mentioned, there exists a large amount of literature on attitude control of spacecrafts. In this section, some of the mentionable work on attitude control using magnetic coils as actuator are presented, followed by some projects similar to CubeSTAR.

In 1961 White et al. [44] was the first to mention that the Earth's magnetic field could be used for attitude control by installing magnets on a spacecraft. Later, in 1988 Martel et al. [28] examined using magnetic control for gravity-gradient stabilized spacecrafts. In 1989 Musser and Ward [29] attempted to use a fully magnetic attitude three-axis stability. The general attitude was formulated in Wen and Kreutz-Delgado [41] and Fjellstad and Fossen [12]. However, this work does not directly relate to the problem of using magnetorquers solely because of the problems regarding uncontrollability in the geomagnetic field. The work of Wisniewski [47] in 1996 has become a reference literature, investigating different controllers. This includes Lyapunov stability theory, and linear theory was used to obtain both time-variant and time-invariant constant gain controllers. In addition, non-linear control theory based on sliding mode control where developed.

In recent years, Bolandi and Vaghei [7] designed an adaptive controller for spinning satellites was designed with high attitude accuracy. The design included a supervisory-adaptive controller with sliding control. Proportional-Derivate (PD)-control has been investigated by for example Lovera and Astolfi [23], Makovec et al. [26]. The LQR optimal control approach has been investigated by Lovera et al. [24], Psiaki [32], Pulecchi et al. [33], Wisniewski [47] to name a few. Here, the general LQR

problem is investigated, in addition to periodic and constant gain LQR solutions. Hegrenæs et al. [17], Krogstad et al. [20], Silani and Lovera [37], Wood et al. [48] has examined the Model Predictive Control (MPC) approach to the attitude control. The designs demonstrates improvement in the performance compared with PD control problem. The MPC problem is very similar to the LQR control problem. Even though the two problems finds the optimal control input, the main difference between the two is that MPC also predicts the optimal control input and the state space model for the future in a given horizon. In this way, the present computed control input is adjusted according to the information about the future. Although the improved results, the MPC approach is more difficult to implement and is more computational demanding compared to the more classical approaches such as PD control. MPC solutions with look-up tables, such as the explicit MPC method used in Hegrenæs [16], requires large amounts of memory, but give good results.

### 1.5.1 Similar Missions

The following will present some of the previous satellite missions similar to the CubeSTAR project. The satellites mission objectives and ADCS are of special interest, and the focus will be on these parts.

#### Ørsted

Ørsted is a 60kg Danish satellite from the University of Aalborg launched in 1999, and is still operative. The satellite is considered as the first satellite using three magnetic coils for attitude control solely together with a gravity gradient boom, and the work of Wisniewski [47] has become a classic reference on attitude control of satellites using magnetorquers. Several controllers where derived and tested. The main scientific objective of the spacecraft was to map the Earth's magnetic field and to determine the changes in the field. More theory on the Ørsted satellite can be found in Bøgh and Blanke [5], Bøgh et al. [6], Wisniewski and Blanke [46] and some lessons learned from the project in Bak et al. [3].

#### nCube

The nCube student satellite project consisted of two satellites, named nCube-1 and nCube-2, developed mainly at NTNU (Norwegian University of Science and Technology)[8, 30, 31, 39]. The two satellites shared the same main mission, namely to demonstrate and test ship traffic surveillance and reindeer tracking using a space-born AIS(Automatic Identification System). The satellites used active magnetic coils together with a deployable gravity boom. The attitude determination system consisted of 3-axis magnetometers and sun sensors. However, one satellite was lost in a failed launch attempt, and there where never communication with the second one.

### Compass-1

Compass-1 is a pico-satellite developed at University of Applied Sciences Aachen, Germany [14]. It's a 1-U CubeSat, and uses magnetic coils only. The satellite was launched in 2008 in a Low Earth Orbit (LEO), with a camera as it's main payload. Pointing error was detected in simulation to be approximately  $10^\circ$ . A constant gain full-state feedback LQR controller where implemented, and the attitude determination consisted of a 3-axis magnetometer and five sun sensors.

### AAU CubeSat

The AAU CubeSat was a 1-U CubeSat developed at Aalborg University, Denmark [15, 19]. The main mission consisted of taking photographs of the Earth from a LEO at approximately 700km. Three perpendicular magnetorquers was used as actuators, with a total magnetic coil mass budget of 150g, and a power budget with maximum 450 mW. For detumbling, the B-dot algorithm was used. The constant gain LQR was investigated for attitude stabilization. This controller requires very little on-line computation. A LMI(Linear matrix inequality) controller based on  $H_2$  optimal control was also investigated, but not found suitable. However, both controllers gave usable results. The satellite used a three-axis magnetometer and six sun sensors as attitude determination sensors. The satellite experienced severely limited operations in the first few months after the launch. This was due to problems concerning communications and power supply.

## 1.6 Outline of the thesis

The thesis is organized as follows:

- **Chapter 2:** Different attitude parametrizations including their properties are presented.
- **Chapter 3:** The spacecraft dynamics are presented along with the environmental models and the magnetic coils.
- **Chapter 4:** The design of the magnetorquers are investigated.
- **Chapter 5:** An adaptive PD-controller and the LQR optimal control problem are given, in addition to a detumbling control law.
- **Chapter 6:** The performance of the different controllers investigated by simulations.
- **Chapter 7:** In this chapter, a constant gain attitude controller is implemented on a FPGA and the performance is shown through HIL simulations.

- **Chapter 8:** In this chapter, the conclusions and recommendations for further work are given.
- **Appendix A:** An abstract based on the work done in this thesis was submitted to the 61st International Astronautical Congress (IAC) 2010, Prague, Czech Republic.
- **Appendix B:** The Matlab source code is included
- **Appendix C:** Printouts of the Simulink block diagrams.
- **Appendix D:** Printout of the DSP builder block diagrams.





## Chapter 2

---

# Attitude Parametrization

---

When working with dynamic models, for example spacecraft attitude dynamics, several Cartesian frames are often used. These frames can be used to evaluate how different objects are oriented according to each other. Before describing the spacecraft dynamics, it's necessary to look at how orientation can be described. In this chapter, the most used attitude parametrizations are presented. The different methods are evaluated and compared, and based on this, the attitude parameterization used for this work is chosen. For simplicity, orthonormal basis vectors is assumed throughout. A geometric vector,  $\vec{v}$ , can be described in the coordinate frame  $\mathcal{F}_a$  as an algebraic vector  $v^a$ . For simplicity, algebraic vector notation is used. For more information on the subject, see for example Egeland and Gravdahl [11].

## 2.1 Direction cosine matrix

The direction cosine matrix, or simply the rotation matrix, is a way to coordinate transform a vector from one frame to another. The rotation matrix has three interpretations. It can be used to rotate a vector within a reference frame, represent a vector from one reference frame to another or to represent the orientation between two different reference frames.

A rotation matrix,  $\mathbf{R}$ , is a rotation matrix if and only if [11]

$$\mathbf{R} \in \text{SO}(3) \tag{2.1}$$

where  $\text{SO}(3)$  is defined as

$$\text{SO}(3) = \{ \mathbf{R} | \mathbf{R} \in \mathbb{R}^{3 \times 3}, \mathbf{R}^T \mathbf{R} = \mathbf{I}, \det \mathbf{R} = 1 \} \tag{2.2}$$

where  $\mathbf{I}$  is the  $3 \times 3$  identity matrix.

The coordinate transformation of a vector,  $\vec{v}$ , from frame  $\mathcal{F}_a$  to the  $\mathcal{F}_b$  frame can be expressed as

$$v^b = \mathbf{R}_a^b v^a \tag{2.3}$$

The rotation matrix,  $\mathbf{R}_a^b$ , in equation 2.3 represents the orientation between the two

frames. Because the rotation matrix is in  $SO(3)$ , transposing the rotation matrix yields

$$\mathbf{R}_b^a = \mathbf{R}_a^{bT} = \mathbf{R}_a^{b^{-1}} \quad (2.4)$$

The reverse transformation of the vector  $\mathbf{v}$ , that is from frame  $\mathcal{F}_b$  to  $\mathcal{F}_a$ , can then be expressed as

$$\mathbf{v}^a = \mathbf{R}_a^{bT} \mathbf{v}^b = \mathbf{R}_b^a \mathbf{v}^b \quad (2.5)$$

### 2.1.1 Kinematic differential equation

From the properties of 2.2, the kinematic differential equation of the rotation matrix can be expressed as two alternative equations.

$$\dot{\mathbf{R}}_a^b = \boldsymbol{\omega}_a^{ab} \times \mathbf{R}_a^b \quad (2.6)$$

or

$$\dot{\mathbf{R}}_a^b = \mathbf{R}_a^b \boldsymbol{\omega}_b^{ab} \times \quad (2.7)$$

where  $\boldsymbol{\omega}_a^{ab}$  is the angular velocity of  $\mathcal{F}_b$  relative to  $\mathcal{F}_a$  represented in  $\mathcal{F}_a$ , and similar for  $\boldsymbol{\omega}_b^{ab}$ .

### 2.1.2 Skew-symmetric form

The vector cross product found in equation 2.6 and 2.7 can be shown to be skew symmetric. The skew symmetric form of a vector cross product of the vector  $\boldsymbol{\omega} = [\omega_x \ \omega_y \ \omega_z]^T$  can be expressed as

$$\mathbf{S}(\boldsymbol{\omega}) = \boldsymbol{\omega} \times = \begin{bmatrix} 0 & -\omega_z & \omega_y \\ \omega_z & 0 & -\omega_x \\ -\omega_y & \omega_x & 0 \end{bmatrix} \quad (2.8)$$

Equation 2.6 and 2.7 can then, with the skew-symmetric form, be expressed as

$$\dot{\mathbf{R}}_a^b = \mathbf{S}(\boldsymbol{\omega}_a^{ab}) \mathbf{R}_a^b = \mathbf{R}_a^b \mathbf{S}(\boldsymbol{\omega}_b^{ab}) \quad (2.9)$$

## 2.2 Euler angles

The Euler angle parametrization is an intuitive way of describing one coordinate frame to another using three successive rotations. It's physical interpretation consist of using the direction matrix to post multiply three rotation matrices, which are obtained from rotations about three fixed axes in the system. It's common to define the rotations as roll, pitch and yaw, where the Euler roll angle  $\phi$  is a rotation about the  $x$ -axis, the pitch angle  $\theta$  about the  $y$ -axis and the yaw angle  $\psi$  about the  $z$ -axis. These axes are orthonormal to

each other, following the right hand rule. From this, three principal rotation matrices about the three axes can be described as

$$\mathbf{R}_x(\phi) = \begin{bmatrix} 1 & 0 & 0 \\ 0 & c(\phi) & -s(\phi) \\ 0 & s(\phi) & c(\phi) \end{bmatrix} \quad (2.10a)$$

$$\mathbf{R}_y(\theta) = \begin{bmatrix} c(\theta) & 0 & s(\theta) \\ 0 & 1 & 0 \\ -s(\theta) & 0 & c(\theta) \end{bmatrix} \quad (2.10b)$$

$$\mathbf{R}_z(\psi) = \begin{bmatrix} c(\psi) & -s(\psi) & 0 \\ s(\psi) & c(\psi) & 0 \\ 0 & 0 & 1 \end{bmatrix} \quad (2.10c)$$

where  $s(\cdot)$  and  $c(\cdot)$  represents  $\sin(\cdot)$  and  $\cos(\cdot)$ , respectively.

It can be shown that there exists 12 possible rotation sequences. To calculate the rotation sequence, evaluation of 6 trigonometric functions, 4 additions and 16 multiplications are needed. In addition to being computational demanding, singularities occurs for certain angles.

The usual way when dealing with rigid bodies with six degrees of freedom is the yaw-pitch-roll (3-2-1 or z-y-x) rotation. This rotation matrix can then be written as

$$\mathbf{R}_b^a = \mathbf{R}_z(\psi)\mathbf{R}_y(\theta)\mathbf{R}_x(\phi) \quad (2.11)$$

By inserting 2.10 into 2.11 we get the rotation matrix expressed in the terms of the Euler angles

$$\mathbf{R}_a^b = \begin{bmatrix} c(\psi)c(\theta) & c(\psi)s(\theta)s(\phi) - s(\psi)c(\phi) & c(\psi)c(\phi)s(\theta) + s(\psi)s(\phi) \\ s(\psi)c(\theta) & s(\psi)s(\theta)s(\phi) + c(\psi)c(\phi) & s(\psi)s(\theta)c(\phi) - c(\psi)s(\phi) \\ -s(\theta) & c(\theta)s(\phi) & c(\theta)c(\phi) \end{bmatrix} \quad (2.12)$$

It must be noted however, that  $\mathbf{R}_a^b$  is singular for  $\theta = \pm\frac{\pi}{2}$ . This means that the representation will introduce singularities when rotating the *pitch* axis  $\pm\frac{\pi}{2}$ . In many cases, for example ship navigation, it's possible to place the reference frame in such a way that singularities does not occur. However, satellites can have all possible orientations, and singularities may occur. When dealing with euler angles in these types of systems, extra precaution is necessary to avoid numerical errors.

## 2.3 Euler parameters

The Euler parameters, or unit quaternions, was discovered by Leonhard Euler. These are essentially the same as quaternions formulated by Sir William Hamilton. Due to the small difference, mainly in notation, unit quaternions will therefore be called quaternions and Euler parameters interchangeably. The Euler parameters are attractive due to non-singularities unlike the Euler angles, and require less computation than Euler angles. However, there is no physical interpretation, and it's therefore hard to understand the orientation. It's therefore often necessary to transform the quaternions to Euler angles in order to evaluate the orientation. In this work, the Euler parameters is defined as [11]

$$\mathbf{q} = \begin{bmatrix} \boldsymbol{\epsilon} \\ \eta \end{bmatrix} \quad (2.13)$$

$$\boldsymbol{\epsilon} = \begin{bmatrix} q_1 \\ q_2 \\ q_3 \end{bmatrix} = \mathbf{k} \sin\left(\frac{\theta}{2}\right) \quad (2.14)$$

$$\eta = q_4 = \cos\left(\frac{\theta}{2}\right) \quad (2.15)$$

The quaternions must be normalized in order to be unit quaternions, that is

$$\mathbf{q}^T \cdot \mathbf{q} = 1 \quad (2.16)$$

It's interesting to note that

$$\mathbf{q} = -\mathbf{q} \quad (2.17)$$

as this may cause trouble when using quaternions as equilibrium in attitude control. In many cases, only using the positive or negative quaternion equilibrium doesn't imply the shortest way of rotation, and unnecessary rotations may occur.

The Euler parameters can also be expressed on the alternative form

$$q_1 = e_1 \cdot \sin\left(\frac{\phi}{2}\right) \quad (2.18a)$$

$$q_2 = e_2 \cdot \sin\left(\frac{\phi}{2}\right) \quad (2.18b)$$

$$q_3 = e_3 \cdot \sin\left(\frac{\phi}{2}\right) \quad (2.18c)$$

$$q_4 = \cos\left(\frac{\phi}{2}\right) \quad (2.18d)$$

The rotation matrix for quaternions can be described as

$$\mathbf{R}(\boldsymbol{\epsilon}, \eta) = \mathbf{I} + 2\eta\mathbf{S}(\boldsymbol{\epsilon}) + 2\mathbf{S}^2(\boldsymbol{\epsilon}) \quad (2.19)$$

The kinematic differential equations can be expressed as [11]

$$\dot{\boldsymbol{\epsilon}} = \frac{1}{2}[\eta\mathbf{I} + \mathbf{S}(\boldsymbol{\epsilon})]\boldsymbol{\omega}_a^{ab} \quad (2.20)$$

$$\dot{\eta} = -\frac{1}{2}\boldsymbol{\epsilon}^T\boldsymbol{\omega}_b^{ab} \quad (2.21)$$

## 2.4 Discussion

In the previous sections Euler angles and Euler parameters has been introduced. The Euler angles are intuitive and easy to use do to the fact that they has a physical interpretation. However, Euler angles include singularities which may cause numerical problems. A spacecraft is able to orientate in all directions, and singularities can therefore become a reality. Euler parameters are four dimensional, and does not suffer from singularities. This makes Euler parameters a popular choice in the literature and in many applications. Other parametrizations such as the modified Rodrigues parameters and the  $(w, z)$  parameterization has not been treated due their little use in the literature. Because of the avoidance of singularities and the massive usage in the literature makes the Euler parameters a suitable choice for attitude parametrization for the CubeSTAR attitude control system.



## Chapter 3

---

# Spacecraft Dynamics

---

Spacecraft dynamics is the science in understanding and predicting a spacecraft's orientation and rotational motion. The field can roughly be divided into two parts. The attitude dynamics, or rotational dynamics, describes the attitude and rotational motion of the spacecraft about its own axes. The other part is the orbital dynamics, or translation dynamics, which describe the orientation and rotational motion seen from another reference, e.g. the earth. When a spacecraft is orbiting a planet or another object, the attitude dynamics and orbital dynamics are mutually coupled [18]. If we remove all the forces working on the spacecraft and the planet, except, off course, the gravitation field keeping the spacecraft orbiting, the orbital dynamics will affect the attitude dynamics and vice versa because the gravitation field is a conservative field. In conservative fields, the system-energy, momentum and spin is extant, and this includes the translation and rotation dynamics to both the spacecraft and the orbited object, and hence the mutually coupling.

In this chapter, the spacecraft dynamics is presented. The reference frames used in this work is defined before the equations of motion is derived. From here the dynamic and kinematic equations are found, and these equations are essential to describe how the satellite acts in space. Before the dynamic equations are completed, the magnetorquers and environmental models must be investigated. In order to use linear system theory a linearized model is derived, and controllability and stabilizability are analyzed.

For the orbit propagation, Kepler's laws are usually used to describe the orbit motion around the Earth. However, because this thesis is assuming a circular orbit, a more simpler orbit propagation is used. This model assumes that the Earth is spherical, and the orbit has a constant altitude in addition to a constant angular velocity. By knowing the orbit's radius, the orbit's angular rate, the orbit inclination on the Earth, and the Earth's angular velocity about its own axis, it's possible to calculate the position of the spacecraft over time. ECSS [10] includes standard parameters of the Earth, and is used as reference. The interested reader should refer to Hughes [18], Sidi [36], Wertz [42], Wertz and Larson [43].

## 3.1 Coordinate Reference frames

In order to analyze and describe the dynamics of the spacecraft, it's necessary to define coordinate reference frames that the dynamics are relative to. In chapter 2 the mathematics needed to describe the relative orientation between two coordinate reference frames was established. In this section, the different reference frames used to describe the satellites dynamics are presented.

### Earth Centered Inertial (ECI) frame

The Earth-centered inertial frame, ECI, denoted  $\mathcal{F}_i$ , is centered in the earth's center. The  $x_i$  axis points towards vernal equinox, the point where the ecliptic, or plane of the Earth's orbit about the Sun, crosses the Equator going from south to north. The  $z_i$  axis points through the geographic north pole and the  $y_i$  axis completes the right hand rule. As the name implies, this reference frame doesn't rotate, and is used as the inertial reference frame for the system. For inertial frames, the axes are fixed, and thus have no acceleration. Newtons laws can therefore be applied to this reference frame.

### Earth Centered, Earth Fixed (ECEF) frame

The Earth-centered, Earth-fixed frame, ECEF, denoted  $\mathcal{F}_e$  has it's origin in center of the earth. The axes are fixed with  $x_e$  pointing through  $0^\circ$  latitude  $0^\circ$  longitude,  $z_e$  towards the geographical north pole and  $y_e$  follows the right hand rule. The frame rotates relative to the ECI frame around the  $z_i$  axis with one revolution per day, giving a constant angular rate of  $\omega_e = 7.2921 \times 10^{-5}$  rad/s.

### Satellite orbit frame

The satellite orbit frame,  $\mathcal{F}_o$ , is centered in the mass center of the satellite. The  $x_o$  axis points in the satellites velocity direction, the  $z_o$  axis towards nadir, the direction towards Earth's center, while the  $y_o$  axis completes the right hand rule. The frame can be seen as the reference frame for the body frame, and the attitude of the spacecraft can be described how the body frame is oriented in the orbit frame.

### Satellite body frame

The satellite body frame,  $\mathcal{F}_b$  is fixed in the satellites center of mass. If the body frame axes coincide with the satellites principal axes, the inertia tensor products vanishes, and the inertia matrix becomes diagonal. This simplifies the dynamic equations and is therefore used. Since the spacecraft will have its longest side in the velocity direction, with the scientific payload in front, the  $x_b$  axis will point in this direction. The two other axes,  $y_b$  and  $z_b$ , will point through two of the long sides according to the right hand rule. Rotation about the axis  $x_b$ ,  $y_b$  and  $z_b$  is defined as roll, pitch and yaw, respectively.



## 3.2 Equations of Motion

In this section the equations of motion are presented. The spacecraft is modeled as a rigid body, and Euler's equation is applicable. In the case where satellites are using liquid thrusters, the fuel will lap, in addition to lose weight over time due to the use of the thrusters. In the extreme environment in space the spacecraft will experience a severe temperature change. This may cause thermal deformations on the spacecraft, and change it's dynamics. In addition, antennas and scientific instruments can oscillate, making the spacecraft not rigid. However, because the CubeSTAR satellite is small, with no liquids on-board and small flexible parts, the rigid body model will be a good approximation. This chapter is based on Hughes [18], Sidi [36], Wertz [42].

### 3.2.1 Angular momentum

Euler's moment equation can be formulated as [36]

$$\boldsymbol{\tau}_A = \dot{\mathbf{h}}_A^i = \dot{\mathbf{h}}_A^{ib} + \boldsymbol{\omega}_b^{ib} \times \mathbf{h}_A^i \quad (3.1)$$

This equation shows that the applied torque,  $\boldsymbol{\tau}_A$ , to a system will change the derivative of the angular momentum of the system.

The angular momentum is defined as

$$\mathbf{h}_A^{ib} = \mathbf{I}_b \boldsymbol{\omega}_b^{ib} \quad (3.2)$$

where the inertia matrix  $\mathbf{I}_b$  is expressed as

$$\mathbf{I}_b = \begin{bmatrix} I_{xx} & -I_{xy} & -I_{xz} \\ -I_{yx} & I_{yy} & -I_{yz} \\ -I_{zx} & -I_{zy} & I_{zz} \end{bmatrix} = \begin{bmatrix} \int_M (y^2 + z^2) dm & -\int_M xy dm & -\int_M xz dm \\ -\int_M yx dm & \int_M (x^2 + z^2) dm & -\int_M yz dm \\ -\int_M zx dm & -\int_M zy dm & \int_M (x^2 + y^2) dm \end{bmatrix} \quad (3.3)$$

Since  $\mathbf{I}_b$  is a real, symmetric matrix, it has real eigenvalues and orthogonal eigenvectors. This means that it's possible to place the  $\mathcal{F}_b$  frame in such a way that  $\mathbf{I}_b$  becomes a diagonal matrix. By assuming a uniform mass distribution and letting the principle axes coincide with the body reference system it can be shown that the inertia tensors can be written as

$$I_{xx} = \frac{m}{12}(b^2 + c^2) \quad (3.4a)$$

$$I_{yy} = \frac{m}{12}(a^2 + c^2) \quad (3.4b)$$

$$I_{zz} = \frac{m}{12}(a^2 + b^2) \quad (3.4c)$$

where  $m$  is the total mass of the satellite and  $a, b, c$  is the length of the  $x, y, z$  axes, respectively. It must be mentioned that the shape of the spacecraft in this case is a cuboid, a right rectangular prism.

From equation 3.4a-3.4c, it's easy to see that, when a uniform mass distribution is considered, the shape of the spacecraft has a huge impact on how the satellite will behave in space.

### 3.2.2 Dynamics

The dynamics of the satellite describes how the angular velocity evolves over time, and how external torques acts on the satellite. The Newton-Euler equation is only defined in the inertial frame, and can be expressed as [36]

$$\mathbf{I}_b \dot{\boldsymbol{\omega}}_b^{ib} + \boldsymbol{\omega}_b^{ib} \times \mathbf{I}_b \boldsymbol{\omega}_b^{ib} = \boldsymbol{\tau}_{coils} + \boldsymbol{\tau}_{gg} + \boldsymbol{\tau}_{dis} = \boldsymbol{\tau} \quad (3.5)$$

where  $\mathbf{I}_b$  is the inertia matrix,  $\boldsymbol{\tau}_{coils}$  is the torque created by the magnetic coils described in section 3.3,  $\boldsymbol{\tau}_{dis}$  are the disturbance torques described in section 3.4 along with the gravity gradient torque  $\boldsymbol{\tau}_{gg}$ . The cross product  $\boldsymbol{\omega}_b^{ib} \times \mathbf{I}_b \boldsymbol{\omega}_b^{ib}$  arises due to the fact that the dynamics are described in a rotating coordinate frame, namely the body frame, in the inertial frame.

By looking at the system without any external torques, the individual elements of the dynamics can be written as

$$\dot{\omega}_{b,x}^{ib} = \frac{I_y - I_z}{I_x} \omega_{b,y}^{ib} \omega_{b,z}^{ib} = k_x \omega_{b,y}^{ib} \omega_{b,z}^{ib} \quad (3.6a)$$

$$\dot{\omega}_{b,y}^{ib} = \frac{I_z - I_x}{I_y} \omega_{b,x}^{ib} \omega_{b,z}^{ib} = k_y \omega_{b,x}^{ib} \omega_{b,z}^{ib} \quad (3.6b)$$

$$\dot{\omega}_{b,z}^{ib} = \frac{I_x - I_y}{I_z} \omega_{b,x}^{ib} \omega_{b,y}^{ib} = k_z \omega_{b,x}^{ib} \omega_{b,y}^{ib} \quad (3.6c)$$

By using the equations in 3.6a-3.6c, these homogeneous equations can be used to analyze spin stability. In general, a rigid body is angular motion stable if the body spins about it's minimum or maximum moment of inertia.

### 3.2.3 Kinematics

The kinematics can be used to describe the orientation of the spacecraft in the orbit as a result of the spacecrafts angular velocity described by the dynamics. The kinematic differential equation using the Euler parameters can be expressed as [36]

$$\dot{\mathbf{q}} = \frac{1}{2} \mathbf{W}(\boldsymbol{\omega}_b^{ob}) \cdot \mathbf{q} \quad (3.7)$$

where  $\mathbf{W}(\boldsymbol{\omega})$  is the  $4 \times 4$  skew symmetric matrix of the angular velocity, and can be written as

$$\mathbf{W}(\boldsymbol{\omega}_b^{ob}) = \begin{bmatrix} 0 & \omega_3 & -\omega_2 & \omega_1 \\ -\omega_3 & 0 & \omega_1 & \omega_2 \\ \omega_2 & -\omega_1 & 0 & \omega_3 \\ -\omega_1 & -\omega_2 & -\omega_3 & 0 \end{bmatrix} \quad (3.8)$$

Here,  $\boldsymbol{\omega}_b^{ob}$  is the angular velocity of the spacecraft seen from the orbit represented in the satellite body. From equation 3.5 the angular velocity of the spacecraft seen from the inertial frame,  $\boldsymbol{\omega}_b^{ib}$ , was solved. It's therefore necessary to rotate the angular velocity into the correct frame. The transformation can be expressed as

$$\boldsymbol{\omega}_b^{ib} = \boldsymbol{\omega}_b^{ob} + \boldsymbol{\omega}_b^{io} \quad (3.9)$$

By knowing the orbit angular velocity,  $\omega_0$ , and having defined the different coordinate frames,  $\boldsymbol{\omega}_b^{ob}$  can be written as

$$\boldsymbol{\omega}_b^{ob} = \boldsymbol{\omega}_b^{ib} - \boldsymbol{\omega}_b^{io} = \boldsymbol{\omega}_b^{ib} - \omega_o \mathbf{j}_0 \quad (3.10)$$

where  $\mathbf{j}_0$  is the column in the rotation matrix from the inertial frame to the orbit frame describing the rotation of the angular velocity of the orbit in the inertial frame.

### 3.3 Magnetic torquers

To understand how the interaction between a spacecraft and earth's magnetic field, it's necessary to examine how magnetic fields can cause torques to act on a spacecraft. The CubeSTAR satellite will use three magnetic coils. These coils will create a magnetic dipole reacting with the earth's magnetic field. Electromagnetic coils creates a magnetic dipole when electrical current flows through the windings. This current is proportional to the ampere-turns and the area enclosed by the coil, yielding

$$m(t) = ni(t)A \quad (3.11)$$

where  $m$  is the produced magnetic moment,  $n$  is the number of turns,  $i$  is the electrical current and  $A$  is the face area of the coil.

The magnetic moment vector created by the coils follows the laws of magnetism, and will therefore act perpendicular on the earth's magnetic field vector in the body frame. This can be described by a cross product, and written as

$$\boldsymbol{\tau}_{coils} = \mathbf{m}_{coils} \times \mathbf{b}_b \quad (3.12)$$

where  $\mathbf{b}_b$  is the geomagnetic field in the body frame.

By using the skew-symmetric matrix we can represent the magnetic torque as

$$\boldsymbol{\tau}_{coils} = \mathbf{S}(\mathbf{m}_{coils})\mathbf{b}_b = \begin{bmatrix} b_z m_y - b_y m_z \\ b_x m_z - b_z m_x \\ b_y m_x - b_x m_y \end{bmatrix} \quad (3.13)$$

The magnetic coils acts, as already mentioned, perpendicular on the geomagnetic field. This means that if a coils is parallel to the geomagnetic field vector, no torque will be created. It's therefore possible to use a mapping of the magnetic torque to create a control torque that only includes the perpendicular parts of the magnetic moment. By separating the parallel and perpendicular magnetic moments, it's possible to write

$$\boldsymbol{\tau} = (\mathbf{m}_{\parallel} + \mathbf{m}_{\perp}) \times \mathbf{b} = \mathbf{m}_{\perp} \times \mathbf{b} \quad (3.14)$$

Then, by including an extra cross product of the geomagnetic field and the norm of the field, a mapping of the magnetic moment insures that the control torque only acts on the geomagnetic field perpendicular to the magnetorquers.

$$\boldsymbol{\tau}_{coils} = \frac{\mathbf{m}_{coils} \times \mathbf{b}_b}{|\mathbf{b}_b|} \times \mathbf{b}_b \quad (3.15)$$

## 3.4 Environmental Models

### 3.4.1 Earth's Geomagnetic Field

The earth is surrounded by a magnetic field, also called the geomagnetic field. This field can approximately be modeled as a magnetic dipole, with the magnetic south pole near the geographical north pole, approximately  $11.5^\circ$  south of the pole, and the magnetic north pole near the geographic south pole. The magnetic field is very important for life on earth, as this field protects us from solar winds amongst other things. The geomagnetic field is higher close to the ground, and decrease with the altitude. In addition, at higher altitudes the solar magnetic field cause perturbations, making the geomagnetic complicated to model. The earth's magnetic field is constantly changing, and the magnetic poles moves over time.

The International Geomagnetic Reference Field (IGRF) is a standard mathematical description of the Earth's magnetic field. The model describes both the magnetic field and the secular variations in the field. IGRF is updated every fifth year. and the validity of current model is year 2010 to 2015.

The current version, IGRF-11, is a 13th order model, with a precision of one tenth of a nT(nano Tesla). IGRF-11 uses Gauss coefficients which define a spherical harmonic expansion of the geomagnetic potential. This can be expressed as [42]

$$V(r, \theta, \phi, t) = a \cdot \sum_{n=1}^k \left(\frac{a}{r}\right)^{n+1} \sum_{m=0}^n (g_n^m \cos(m\phi) + h_n^m \sin(m\phi) P_n^m(\theta)) \quad (3.16)$$

where  $r$  is the geocentric distance from earth,  $\theta$  is the co-elevation, that is latitude  $-90^\circ$  and  $\phi$  is the longitude.  $a$  is the equatorial radius of the earth,  $g_n^m$  and  $h_n^m$  is the Gaussian coefficients.  $P_n^m(\theta)$  are the Schmidt semi-normalized associated Legendre functions of degrees  $n$  and order  $m$ .

Figure 3.1-3.3 shows the magnetic field in the orbit frame at 300, 500 and 800 km altitude. The orbit is a circular orbit with an inclination of  $90^\circ$ . A modified version of the IGRF-11 mex file from the open-source Mirone project at Luis [25] was used to calculate the geomagnetic field for the considered orbits.

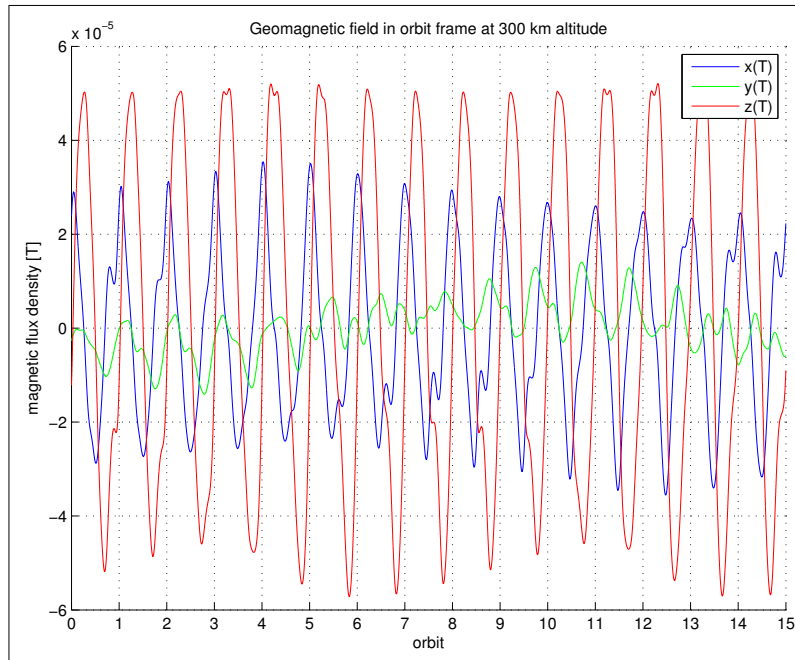


**Figure 3.1:** The geomagnetic field seen from the orbit frame at 300 km altitude. The circular orbit has an inclination of  $90^\circ$

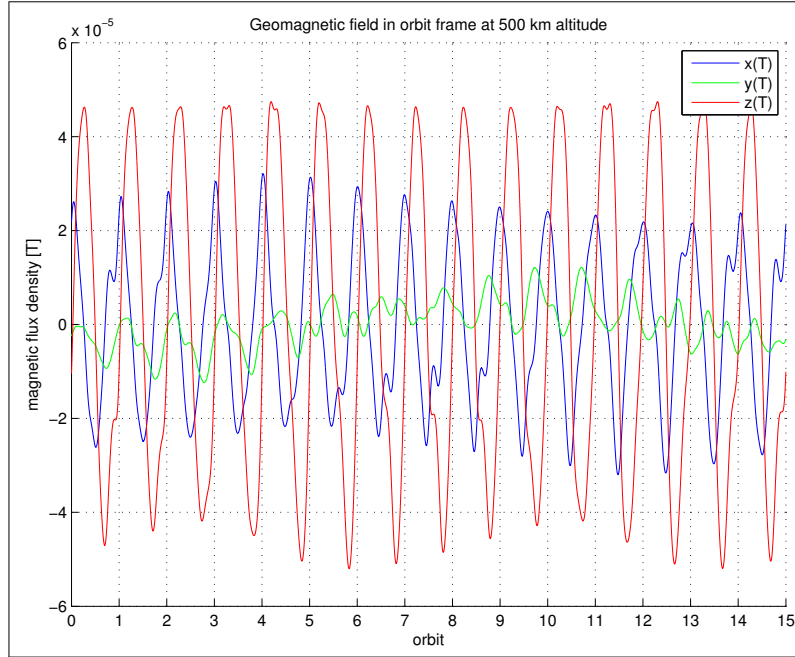


**Figure 3.2:** The geomagnetic field seen from the orbit frame at 500 km altitude. The circular orbit has an inclination of  $90^\circ$

### Dipole model

The IGRF model requires a lot of computation. Another way of estimating Earth's magnetic field is to use a dipole model. This model is easy to calculate, and many controllers are designed with the dipole model because this tends to create some robustness towards measurement errors on the magnetic field.

The dipole approximation model of the geomagnetic field, with no Earth rotation and no orbit precession, can be written as [32]

$$\tilde{\mathbf{b}}_0(t) = \begin{bmatrix} b_1(t) \\ b_2(t) \\ b_3(t) \end{bmatrix} = \frac{\mu_f}{a^3} \begin{bmatrix} \cos(\omega_0 t) \sin(i_m) \\ -\cos(i_m) \\ 2 \sin(\omega_0 t) \sin(i_m) \end{bmatrix} \quad (3.17)$$

where  $i_m$  is the orbit's inclination with respect to the geomagnetic equator and this is currently about 11.5 degrees south of the geographic north pole.  $\mu_f = 7.9 \cdot 10^{15} \text{Wbm}$  is the dipole strength,  $\omega_0$  is the orbit angular velocity, and  $a$  is the semi-major axis, equal the radius of a circular orbit.

In figure 3.4, the geomagnetic field is shown in the orbit frame with a circular orbit at 500 km altitude and an inclination of  $90^\circ$ . As can be seen from the figure, the dipole

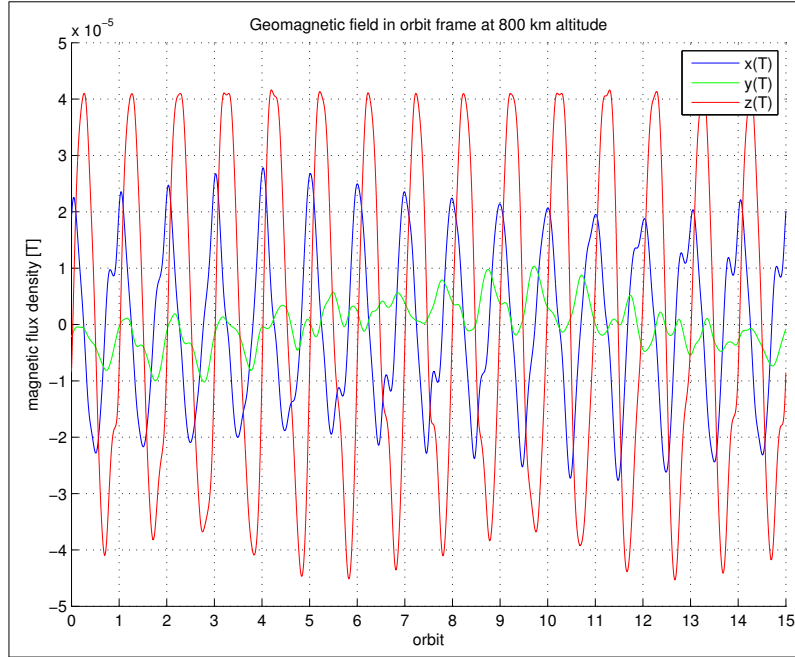


**Figure 3.3:** The geomagnetic field seen from the orbit frame at 800 km altitude. The circular orbit has an inclination of  $90^\circ$

model gives good results compared to the 13th order IGRF-11 model.

### 3.4.2 Gravity Gradient torque

Gravity gradient is a property of every asymmetric object in the presence of a gravity field. The axis of least inertia tends to align the field direction, while the largest inertia axis aligns normal to the gravity field. If the gravitational field is uniform over a body, then the center of mass is the center of gravity, and the gravitational torque about the mass center will then be zero. In space, however, the gravitational field is not uniform, and the gravity gradient can be expressed as

$$\boldsymbol{\tau}_{gg} = \frac{3\mu}{r_o^3} \mathbf{u}_e \times \mathbf{I} \mathbf{u}_e \quad (3.18)$$

where  $\mu = 3.986 \cdot 10^{14} m^3/s^2$  is the earth's gravitational coefficient,  $r_o$  is the distance from the earth's center,  $\mathbf{I}$  is the inertia matrix and  $\mathbf{u}_e$  is the unit vector towards nadir.

By inserting equation 3.18 in the body frame, this yields:

$$\boldsymbol{\tau}_{gg} = \frac{3\mu}{r_o^3} \mathbf{c}_3 \times \mathbf{I} \mathbf{c}_3 = 3\omega_o^2 \mathbf{c}_3 \times \mathbf{I} \mathbf{c}_3 \quad (3.19)$$

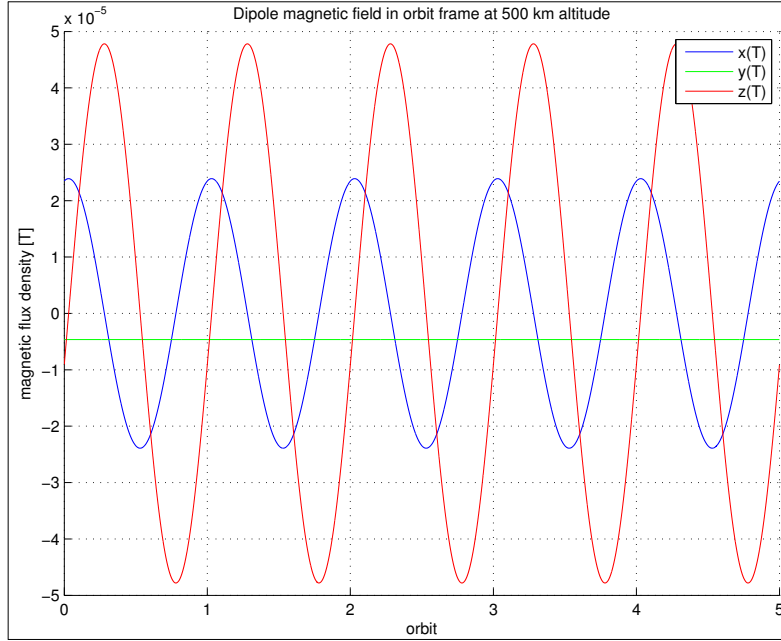


**Figure 3.4:** The geomagnetic field seen from the orbit frame at 500 km altitude using the dipole approximation. The circular orbit has an inclination of  $90^\circ$

where  $c_3$  is the third column of the rotation matrix from the body frame to the orbit frame, and is the nadir pointing unit vector of the orbit frame.

Over time, every asymmetric object will, theoretically, align the gravity field. However, other disturbances will deviate the satellite from this orientation, unless the spacecraft is gravity gradient stable. This can be achieved in the design of the spacecraft, or by using a gravity gradient boom. From [36], two sub-regions of gravity gradient stability are defined by

$$I_y > I_x > I_z \quad I_y < I_x + I_z \quad (3.20)$$

or

$$I_x > I_x > I_y \quad I_x < I_y + I_z \quad (3.21)$$

When designing satellites, it's therefore important to design a spacecraft that is in one of these two sub-regions.

### 3.4.3 Aerodynamic Torque

Spacecrafts in low earth orbits will not travel through near empty space, but will be surrounded by the earth's atmosphere. The atmosphere consists of particles, and when the spacecraft collides with these particles, this causes a force on the satellite.



The aerodynamic force acting on the spacecraft can be written as (Wertz and Larson [43])

$$\mathbf{F}_{aero} = \frac{1}{2} \rho C_d A v^2 \mathbf{u}_{aero} \quad (3.22)$$

where  $\rho$  is the atmospheric density,  $C_d$  is the aerodynamic drag coefficient (usually between 2.0 and 2.5),  $v$  is the spacecraft orbit velocity and  $\mathbf{u}_{aero}$  is the vector describing the direction of the force on the satellite. Finally,  $A$  is the cross-sectional area facing the satellite's orbit velocity, and it's this area that collides with the atmospheric particles. The cross-sectional area is assumed constant in equation 3.22, but will in reality vary in some degree depending on how the satellite is oriented in the orbit. The lowest area will occur in this case, when the satellite is in equilibrium, that is the body frame coincides with the orbit frame.

The air density, is higher close to ground and will gradually weaken as the hight increases. In orbits with altitude lower then approximately 400km, the aerodynamic drag is the dominant disturbance (Wertz [42]). In table 3.1, the air density for the specific altitudes for this work are shown[43]. From this it can be seen that maximum air density at an altitude of 300 km is around ten thousand times larger than the minimum air density at an altitude of 800 km, and hence the orbit altitude plays a major part in the aerodynamic disturbance acting on the spacecraft.

**Table 3.1:** Air density in the atmosphere for specific altitudes.

Altitude [km]	Atmospheric Density $\rho$ [kg/m <sup>3</sup> ]		
	Minimum	Mean	Maximum
300	$8.19 \times 10^{-12}$	$1.95 \times 10^{-11}$	$3.96 \times 10^{-11}$
500	$8.98 \times 10^{-14}$	$4.89 \times 10^{-13}$	$1.80 \times 10^{-12}$
800	$2.96 \times 10^{-15}$	$9.63 \times 10^{-15}$	$4.39 \times 10^{-14}$

The aerodynamic force will act in the negative satellite orbit velocity direction, and by using the defined orbit frame,  $\mathbf{u}_{aero}$  can be expressed in the orbit frame as

$$\mathbf{u}_{aero}^o = \begin{bmatrix} -1 \\ 0 \\ 0 \end{bmatrix} \quad (3.23)$$

Because the aerodynamic force acting on the spacecraft is working in the negative orbit velocity direction, it's lowering the orbit velocity and hence the altitude. This is however not treated in this work where a constant circular orbit is considered. However, this torque is also acting on the center of pressure, and if the Center of Mass (CoM) is not in the Geometric Center (GC), this creates a torque on the satellite. This torque is given as

the cross product of the displacement vector between the CoM and the GC,  $\mathbf{r}_{CoM-GC}$ , and the aerodynamic force vector,  $\mathbf{F}_{aero}$ , hence (Hughes [18])

$$\boldsymbol{\tau}_{aero} = \mathbf{r}_{CoM-GC} \times \mathbf{F}_{aero} \quad (3.24)$$

The displacement vector,  $\mathbf{r}_{CoM-GC}$ , is an important factor to these kinds of torques, and it's important that this vector is made as small as possible in the design. In fact, if this vector is not present there will be theoretically no disturbing torque of this kind, although this is very unlikely. The standard requirement for CubeSats is that the center of mass must be within 2cm of the geometric center [40].

### 3.4.4 Solar Radiation Torque

The sun radiates electromagnetic waves in a large spectrum, from x-rays to radio waves. These waves, together with the solar winds, causes physical pressure on the spacecraft's body when in direct view of the sun. In eclipse, however, these pressures are not present. The Earth is also radiating, mainly reflecting the waves from the sun, but also emitting radiation produced by the earth. This radiation will act on the spacecraft at any time in orbit, and is higher closer to the earth. The radiation from the earth is typical one third of the solar radiation (Hughes [18]), and will therefore not be further investigated. For precise calculations on radiation acting on the spacecraft, radiation from earth should be taken into account. The solar winds consists mainly of ionized nuclei and electrons. However, these winds are 100-1000 times smaller than the momentum flux of the solar radiation, and can therefor be neglected compared to the solar radiation. All other types of radiation, such as galactic rays, will also be neglected.

The momentum flux of solar radiation varies according to time of year(distance to sun) and other factors, such as solar activity level. The mean momentum flux,  $P_{rad}$ , of the solar radiation is given as [36]

$$P_{rad} = \frac{F_e}{c} = 4.5 \times 10^{-6} \text{kgm}^{-1}\text{sec}^{-2} \quad (3.25)$$

where  $c$  is the speed of light and  $F_e$  is the mean integrated energy flux at earth's position. The solar radiation pressure,  $\mathbf{F}_{rad}$  is given as [36]

$$\mathbf{F}_{rad} = P_{rad} A C_P \mathbf{u}_{rad} \quad (3.26)$$

where  $A$  is the cross-sectional area of the satellite facing the sun,  $\mathbf{u}_{rad}$  is the vector describing the direction of the force on the spacecraft and  $C_P$  is the spacecraft surface absorption characteristic.  $C_P$  lies between 1 and 2, where  $C_P = 1$  is a perfectly absorbing material and  $C_P = 2$  is a material reflecting all light. In equation 3.26 it's assumed that the surface absorption characteristic is equal for the total area surface. This is seldom the case, but due to the small characteristic changes, the small size of CubeSats

and the uncertainty of the value, a constant surface absorption characteristic is assumed in this work. The cross-sectional area is also assumed constant as done in section 3.4.3.

When the solar waves hits the spacecraft, this creates a force pushing the spacecraft in the same direction. If the CoM lies in the GC, the force created is evenly distributed and the spacecraft is only pushed in the sunlight direction without creating torque on the spacecraft itself. For a satellite orbiting the Earth, this means that the sun pushes the satellite towards earth most of the time, and thus lowering the altitude and changing the orbit. This effect is not taken into account in this work where a constant circular orbit is considered. If, however, the CoM is not in the GC, the solar radiation will also create a torque on the spacecraft. This torque will be created on the axes perpendicular to the solar waves, that is the cross-product of the displacement vector between the CoM and the GC,  $\mathbf{r}_{CoM-GC}$ , and the solar radiation force vector  $\mathbf{F}_{rad}$ . The solar pressure torque acting on the body can therefore be written, similar to equation 3.24, as [18]

$$\boldsymbol{\tau}_{rad} = \mathbf{r}_{CoM-GC} \times \mathbf{F}_{rad} \quad (3.27)$$

### 3.4.5 Residual Dipole Torques

Although the satellite is controlled by magnetic coils, this is not the only magnetic field produced by the spacecraft. Electric components also create magnetic fields, in addition to ferromagnetic materials. These fields can be considered as disturbances as they are not wanted, and have an effect on the satellite's attitude. It's therefore necessary to avoid these disturbances as much as possible by designing the satellite with this in mind. This includes designing and using electrical components and materials that creates as small as possible magnetic moments. However, these dipole moments are usually time-invariant, and can theoretically be removed by measuring and estimating the residual dipoles, and using these values as biases in the magnetic coil control.

The residual dipole torque is expressed essentially the same as for the magnetorquers, and is written as

$$\boldsymbol{\tau}_{res} = \mathbf{m}_{res} \times \mathbf{b}_t \quad (3.28)$$

For more details on determining dipole moments, see Lee et al. [21].

## 3.5 Linearized model

In the previous sections the satellite model was derived, and these equations are nonlinear by nature. In order in order to apply linear system theory and control law synthesis procedures, the dynamics of the spacecraft must be linearized. A linear time variant system can be expressed as [9]

$$\dot{\mathbf{x}}(t) = \mathbf{F}(t)\mathbf{x}(t) + \mathbf{G}(t)\mathbf{u}(t) \quad (3.29)$$

where  $\mathbf{x}(t)$  is the total state vector,  $\mathbf{F}(t)$  is the plant system matrix,  $\mathbf{u}$  is the control input and  $\mathbf{G}$  is the input matrix.

As mentioned before, it's desirable to stabilize the satellite in such a way that the multi-Needle Langmuir Probe system is pointing in the velocity direction, the  $x$ -axis. This will be the same as a nadir, vector describing the direction of the center of the earth, pointing satellite.

To be able to linearize the nonlinear system a equilibrium must be chosen. The natural choice would be to let the angular velocity with respect to the reference be zero, and that the attitude is such that the body coordinate system coincides with the reference. This gives the equilibrium

$$\boldsymbol{\omega}_{b,ref}^{ib} = \begin{bmatrix} 0 \\ -\omega_0 \\ 0 \end{bmatrix}, \quad \mathbf{q}_{ref} = \begin{bmatrix} 0 \\ 0 \\ 0 \\ 1 \end{bmatrix} \quad (3.30)$$

By using the Taylor expansion, the linearization can be done by adding a perturbation to the system plant with respect on the states around the equilibrium.

The Euler parameters can then be expressed as

$$\delta \mathbf{q} = \begin{bmatrix} \delta \mathbf{q}_1 \\ \delta \mathbf{q}_2 \\ \delta \mathbf{q}_3 \\ \delta \mathbf{q}_4 \end{bmatrix} \approx \begin{bmatrix} \delta \boldsymbol{\epsilon} \\ 1 \end{bmatrix} \quad (3.31)$$

and the body angular velocities as

$$\delta \boldsymbol{\omega}_b^{ib} = \begin{bmatrix} \delta \omega_{b,x}^{ib} \\ \delta \omega_{b,y}^{ib} - \omega_0 \\ \delta \omega_{b,z}^{ib} \end{bmatrix} \quad (3.32)$$

From equation 3.7 the kinetic differential equation was found to be

$$\dot{\mathbf{q}} = \frac{1}{2} \mathbf{W}(\boldsymbol{\omega}_b^{ob}) \cdot \mathbf{q} \quad (3.33)$$

Because  $\eta$ , the fourth Euler parameter is defined by the other three parameters,  $\eta = \sqrt{1 - q_1^2 - q_2^2 - q_3^2}$ , this value can be omitted in the linearization.

By selecting the linearized state vector as

$$\begin{bmatrix} \delta\boldsymbol{\omega} \\ \delta\boldsymbol{\epsilon} \end{bmatrix} = \begin{bmatrix} \delta\omega_x \\ \delta\omega_y \\ \delta\omega_z \\ \delta q_1 \\ \delta q_2 \\ \delta q_3 \end{bmatrix} \quad (3.34)$$

where  $\boldsymbol{\omega} = \boldsymbol{\omega}_b^{ib}$  for simplicity, the linearization of the kinetic differential equation can be expressed as

$$\delta\dot{\boldsymbol{\epsilon}} = \begin{bmatrix} \frac{1}{2} & 0 & 0 & 0 & 0 & \frac{1}{2}\omega_0 \\ 0 & \frac{1}{2} & 0 & 0 & 0 & 0 \\ 0 & 0 & \frac{1}{2} & -\frac{1}{2}\omega_0 & 0 & 0 \end{bmatrix} \begin{bmatrix} \delta\omega_x \\ \delta\omega_y \\ \delta\omega_z \\ \delta q_1 \\ \delta q_2 \\ \delta q_3 \end{bmatrix} \quad (3.35)$$

The homogeneous dynamic differential equation from equation 3.5 is

$$\mathbf{I}^b \dot{\boldsymbol{\omega}}_b^{ib} + \boldsymbol{\omega}_b^{ib} \times \mathbf{I} \boldsymbol{\omega}_b^{ib} = 0 \quad (3.36)$$

The cross-product can be written as

$$\begin{aligned} -\mathbf{I}^{-1}(\boldsymbol{\omega}_b^{ib} \times \mathbf{I} \boldsymbol{\omega}_b^{ib}) &= -\mathbf{I}^{-1} \mathbf{S}(\boldsymbol{\omega}_b^{ib}) \mathbf{I} \boldsymbol{\omega}_b^{ib} \\ &= \begin{bmatrix} \frac{(I_y - I_z)}{I_x} \omega_{b,y}^{ib} \omega_{b,z}^{ib} \\ \frac{(I_z - I_x)}{I_y} \omega_{b,x}^{ib} \omega_{b,z}^{ib} \\ \frac{(I_x - I_y)}{I_z} \omega_{b,x}^{ib} \omega_{b,y}^{ib} \end{bmatrix} = \begin{bmatrix} \sigma_x \omega_{b,y}^{ib} \omega_{b,z}^{ib} \\ \sigma_y \omega_{b,x}^{ib} \omega_{b,z}^{ib} \\ \sigma_z \omega_{b,x}^{ib} \omega_{b,y}^{ib} \end{bmatrix} \end{aligned} \quad (3.37)$$

where

$$\sigma_x = \frac{I_y - I_z}{I_x}, \quad \sigma_y = \frac{I_z - I_x}{I_y}, \quad \sigma_z = \frac{I_x - I_y}{I_z} \quad (3.38)$$

Because of the perturbations,  $\delta\omega_i \delta\omega_j \approx 0$ , and the cross product is approximately

$$-\mathbf{I}^{-1}(\boldsymbol{\omega}_b^{ib} \times \mathbf{I} \boldsymbol{\omega}_b^{ib}) \approx \begin{bmatrix} \sigma_x (\omega_o + \delta\omega_{b,y}^{ob}) \delta\omega_{b,z}^{ob} \\ \sigma_y \delta\omega_{b,x}^{ob} \delta\omega_{b,z}^{ob} \\ \sigma_z (\omega_o + \delta\omega_{b,y}^{ob}) \delta\omega_{b,x}^{ob} \end{bmatrix} \approx \begin{bmatrix} \sigma_x \omega_o \delta\omega_{b,z}^{ob} \\ 0 \\ \sigma_z \omega_o \delta\omega_{b,x}^{ob} \end{bmatrix} \quad (3.39)$$

Disturbance torques are not linearized because of their complexity, except from the gravity gradient.

The gravity gradient from equation 3.19 was found to be

$$\boldsymbol{\tau}_{gg} = 3\omega_o^2 \mathbf{c}_3 \times \mathbf{I} \mathbf{c}_3 \quad (3.40)$$

where  $\mathbf{c}_3$  can be expressed as

$$\mathbf{c}_3 = \begin{bmatrix} 2(q_1q_3 - q_2q_4) \\ 2(q_2q_3 + q_1q_4) \\ -q_1^2 - q_2^2 + q_3^2 + q_4^2 \end{bmatrix} \quad (3.41)$$

Because  $\delta q_i \cdot \delta q_j \approx 0$  for  $i, j = 1, 2, 3$  and  $\delta q_i^2 \approx 0$  for  $i = 1, 2, 3$ , the linearized gravity gradient becomes

$$\mathbf{I}^{-1}\boldsymbol{\tau}_{gg} = 6\omega_0^2 \begin{bmatrix} -\sigma_x \delta q_1 \\ \sigma_y \delta q_2 \\ 0 \end{bmatrix} \quad (3.42)$$

The linearized dynamics, including gravity gradient, can then be written as

$$\delta \dot{\boldsymbol{\omega}} = \begin{bmatrix} 0 & 0 & -k_x \omega_0 & -6k_x \omega_0^2 & 0 & 0 \\ 0 & 0 & 0 & 0 & 6k_y \omega_0^2 & 0 \\ -k_z \omega_0 & 0 & 0 & 0 & 0 & 0 \end{bmatrix} \begin{bmatrix} \delta \omega_x \\ \delta \omega_y \\ \delta \omega_z \\ \delta q_1 \\ \delta q_2 \\ \delta q_3 \end{bmatrix} + \mathbf{I}^{-1}\boldsymbol{\tau}_{coils} \quad (3.43)$$

The magnetic moment is already linear, and was found to be from equation 3.15

$$\boldsymbol{\tau}_{coils} = \frac{\mathbf{m}_{coils} \times \mathbf{b}_b}{|\mathbf{b}_b|} \times \mathbf{b}_b \quad (3.44)$$

By using the skew-symmetric form, this can be written as

$$\boldsymbol{\tau}_{coils} = \frac{1}{|\mathbf{b}_b|} \mathbf{S}(\mathbf{b}_b)^T \mathbf{S}(\mathbf{b}_b)^T \mathbf{m}_{coils} \quad (3.45)$$

### 3.5.1 Linearized equations of motion

The total linearized system plant can be expressed as

$$\begin{bmatrix} \delta \dot{\boldsymbol{\omega}} \\ \delta \dot{\boldsymbol{\epsilon}} \end{bmatrix} = \mathbf{F} \begin{bmatrix} \delta \boldsymbol{\omega} \\ \delta \boldsymbol{\epsilon} \end{bmatrix} + \mathbf{G}(t) \mathbf{m}_{coils} + \begin{bmatrix} \mathbf{I}^{-1} \\ \mathbf{0} \end{bmatrix} \boldsymbol{\tau}_{dist} \quad (3.46)$$

where

$$\mathbf{F} = \begin{bmatrix} 0 & 0 & -k_x \omega_0 & -6k_x \omega_0^2 & 0 & 0 \\ 0 & 0 & 0 & 0 & 6k_y \omega_0^2 & 0 \\ -k_z \omega_0 & 0 & 0 & 0 & 0 & 0 \\ \frac{1}{2} & 0 & 0 & 0 & 0 & \frac{1}{2} \omega_0 \\ 0 & \frac{1}{2} & 0 & 0 & 0 & 0 \\ 0 & 0 & \frac{1}{2} & -\frac{1}{2} \omega_0 & 0 & 0 \end{bmatrix} \quad (3.47)$$

and

$$\mathbf{G}(t) = \begin{bmatrix} \mathbf{I}^{-1} \\ |\mathbf{b}_b| \end{bmatrix} \begin{bmatrix} -b_y^2(t) - b_z^2(t) & b_x(t)b_y(t) & b_x(t)b_z(t) \\ b_x(t)b_y(t) & -b_x^2(t) - b_z^2(t) & b_y(t)b_z(t) \\ b_x(t)b_z(t) & b_y(t)b_z(t) & -b_x^2(t) - b_y^2(t) \end{bmatrix} \begin{bmatrix} 0 & 0 & 0 \\ 0 & 0 & 0 \\ 0 & 0 & 0 \end{bmatrix} \quad (3.48)$$

### 3.6 Controllability

Investigating controllability on non-linear systems may not be trivial due to its complexity. Therefore, the linearized system model will be investigated. A linear system is said to be controllable if there exists a control,  $\mathbf{u}$ , which can get an arbitrary state  $\mathbf{x}(t_0)$  to an arbitrary state  $\mathbf{x}(t_1)$  for  $t_1 > t_0$ . The controllability condition states that the state and input matrix,  $\mathbf{A}$ ,  $\mathbf{B}$ , satisfy that [13]

$$\Theta = [\mathbf{B} | \mathbf{A}\mathbf{B} | \dots | \mathbf{A}^{n-1}\mathbf{B}] \quad (3.49)$$

has rank  $n$ .

From the system 3.46,  $\eta$  is equal zero, and hence the system is uncontrollable. In fact, this is the only uncontrollable state. In addition, the controllability matrix is nearly singular, and this reflects that there is always one axis not controllable. In order for the system to be stabilizable, this uncontrollable state needs to be stable.

### 3.7 Stabilizability

In order for an uncontrollable linear system to be stabilizable, all eigenvalues corresponding to the uncontrollable modes must be stable. This can be done by using the Kalman canonical decomposition. The original uncontrollable linear system with  $\text{rank}(\Theta) = n_1 < n$ , where  $\Theta$  is given in 3.49, is decomposed into controllable and uncontrollable subspaces. From Chen [9] it's shown that it's possible to form a  $n \times n$  matrix  $\mathbf{P}^{-1}$  with the  $n_1$  first columns are linearly independent columns of  $\Theta$ . The transformation  $\mathbf{x} = \mathbf{P}^{-1}\bar{\mathbf{x}}$  can then be transformed into

$$\begin{bmatrix} \dot{\bar{\mathbf{x}}}_{uc} \\ \dot{\bar{\mathbf{x}}}_c \end{bmatrix} = \begin{bmatrix} \bar{\mathbf{A}}_{uc} & \mathbf{0} \\ \bar{\mathbf{A}}_{12} & \bar{\mathbf{A}}_c \end{bmatrix} \begin{bmatrix} \bar{\mathbf{x}}_{uc} \\ \bar{\mathbf{x}}_c \end{bmatrix} + \begin{bmatrix} \mathbf{0} \\ \bar{\mathbf{B}}_c \end{bmatrix} \mathbf{u} \quad (3.50)$$

$$\mathbf{y} = [\bar{\mathbf{C}}_{uc} \quad \bar{\mathbf{C}}_c] \begin{bmatrix} \bar{\mathbf{x}}_{uc} \\ \bar{\mathbf{x}}_c \end{bmatrix} + \mathbf{D}\mathbf{u} \quad (3.51)$$

where the controllable block  $\bar{\mathbf{A}}_c$  is a  $n_1 \times n_1$  matrix and the uncontrollable block  $\bar{\mathbf{A}}_{uc}$  is a  $(n - n_1) \times (n - n_1)$  matrix.

By including  $\eta$  in the linear system, the canonical system can be found. The averaged geomagnetic field is used to create a time invariant linear system in order of simplicity. The eigenvalues of the uncontrollable block is found to be stable, and hence the system is stabilizable.

## 3.8 Summary

In this chapter the reference frames for the considered satellite was defined. Later, the non-linear equations of motion for the satellite was derived along with the respective environmental models. In order to use linear control theory, the linearized equations of motion was derived and analyzed in terms of stability and stabilizability. It was found that the linear model was not controllable, but stabilizable.

The disturbance torques can seem to be relatively high when looked at individually. When worst case disturbances are used, it's unlikely that all the disturbances will act in the same direction on the spacecraft. Instead, torque cancellation may occur, resulting in lower realistic total disturbance torques.

The spacecraft must be orbiting the Earth in an altitude between 300 and 800 km because of the scientific instrument. The solar disturbance torque is relatively constant over this interval. However, there is a very huge difference in the aerodynamic drag disturbance. At higher altitudes, the air density is lower, and less aerodynamic force. Even though the geomagnetic field is also lower at higher altitudes, this can be compensated by using larger magnetic coils. In order to keep the disturbances as low as possible, a higher orbit altitude may be of interest.



## Chapter 4

---

# Magnetorquer Design

---

In the previous chapter, the spacecraft dynamics were presented along with the dynamic properties of the magnetic coils. In this chapter, the magnetic coil design will be investigated. In order to manufacture magnetic coils for the satellite, it's necessary to check if the preliminary design specifications are suitable or if changes must be made. This chapter only investigated the basic properties, and doesn't cover the entire magnetorquer design. In this thesis, the interesting part is to examine if the given dimensions and power restrictions can give a possible producible magnetic moment big enough to control the spacecraft. Problems such as physical layout, production, driver circuit, current sensor, self inductance, eddy currents, hysteresis and other disturbances in addition to validation is not treated in this work.

### 4.1 Design specification

At the time being, the satellite will have, because of the spacecraft dimensions, two different types of coils. Two coils will have the dimension of  $190 \times 75\text{mm}$ , and will hereby be called the long side coils. The coil on the short side of the satellite will be  $75 \times 75\text{mm}$ , and named the short side coil. The coils are positioned in the satellite so that all three coils are orthogonal to each other. Because of the restricted space available inside the satellite, the maximum coil cross-sectional area is set to  $2 \times 5\text{mm} = 10\text{mm}^2$ . Work on the power supply indicates that it's possible to use a maximum coil voltage of 3 volts, and each coil is restricted to around 100mA. In table 4.1 the constraints for the magnetorquer design are listed.

### 4.2 Magnetic coil design

The electromagnetic coils can be made with or without a metal core. With a metal core, a greater magnetic field can be produced by the same coil compared to an air core coil. However, metal cores are heavy and use more space. Therefore, air core magnetorquers will be used in this thesis.

**Table 4.1:** Magnetorquer design constraints

Parameter	Symbol	Value	Unit
Maximum width	$b_{\max}$	75	mm
Maximum height short side	$h_{s,\max}$	75	mm
Maximum height long side	$h_{l,\max}$	190	mm
Maximum face area short side	$a_{s,\max}$	5625	mm <sup>2</sup>
Maximum face area long side	$a_{l,\max}$	14250	mm <sup>2</sup>
Maximum coil cross-sectional width	$b_{c,\max}$	5	mm
Maximum coil cross-sectional height	$h_{c,\max}$	2	mm
Maximum coil cross-sectional area	$a_{c,\max}$	10	mm <sup>2</sup>
Mean width ( $b_{\max} - h_{c,\max}$ )	$b_{\text{mean}}$	73	mm
Mean height short side ( $h_{s,\max} - h_{c,\max}$ )	$h_{s,\text{mean}}$	73	mm
Mean height long side ( $h_{l,\max} - h_{c,\max}$ )	$h_{l,\text{mean}}$	188	mm
Mean face area short side	$a_{s,\text{mean}}$	5329	mm <sup>2</sup>
Mean face area long side	$a_{l,\text{mean}}$	13724	mm <sup>2</sup>
Mean circumference shortside ( $2(b_{\text{mean}} + h_{s,\text{mean}})$ )	$l_{cs,\text{mean}}$	292	mm
Mean circumference longside ( $2(b_{\text{mean}} + h_{l,\text{mean}})$ )	$l_{cl,\text{mean}}$	522	mm
Voltage at full load	$U_C$	3.0	V
Maximum allowed current	$I_{\max}$	100	mA
Maximum power at full load	$P_{\max}$	300	mW
Minimum temperature	$T_{\min}$	-60	°C
Nominal temperature	$T_{\text{norm}}$	25	°C
Maximum temperature	$T_{\max}$	100	°C

The magnetic moment for a coil is given by

$$m(t) = n_{coil} i_{coil}(t) A_{coil} \quad (4.1)$$

where  $m$  is the magnetic moment,  $n$  is the number of turns,  $i$  is the electrical current and  $A$  is the face area of the coil. From simulations and previous work such as Graversen et al. [15] and Giebelmann [14] the desired magnetic moment is set to  $100\text{mAm}^2$ , and is a fairly large number for a small satellite such as CubeSTAR. This value is only used as a maximum reference value, and much lower magnetic moments can control the spacecraft, and exceed the disturbances.

From equation 4.1, since the coil face area is fixed, the magnetic moment is increased by either increasing the amount of turns or by increasing the electrical current. This will, however, increase the weight and power usage, respectively. The number of turns of a coil must therefore be chosen in such a way that the weight of the coils are reasonable and the power restrictions are not violated. In addition, larger number of windings can lead to a larger possibility of coil failure, i.e. short circuiting.

At this point, there exists no weight restrictions on the magnetorquers. However, satellites, especially Cubesats, have a strict weight limitation, and CubeSTAR can weight maximum 2 kg. By setting an upper boundary of 5% of the total weight, that is 100 grams for all three coils, this value can be used for comparison with the final design result. Note that these limits only include the wiring, and not other electrical components and/or circuits necessary to implement the magnetorquers.

In order to design the magnetic coils, several properties must be investigated. The following material is adopted from Serway and Jewett [35].

The maximum current in a coil will be at the minimum temperature due to the fact that the resistance is temperature dependent. The coil resistance can be written as

$$R = \frac{nl\sigma(T)}{a_w} \quad (4.2)$$

where  $n$  is the number of turns,  $l$  is the circumference and  $a_w$  is the wire cross sectional area. The wire material resistivity,  $\sigma(T)$ , of a conductor varies, over a limited temperature range, approximately linearly with the temperature and can be found by knowing the resistivity at a specific temperature,  $\sigma_0$ , and the temperature coefficient of resistivity,  $\alpha$ , yielding

$$\sigma = \sigma_0[1 + \alpha(T - T_0)] \quad (4.3)$$

Although aluminium has better properties for use in magnetic coils[15], very thin aluminium wire is not commercial available. Therefore, copper may be the best choice

of material. In table 4.3 the copper properties from [35] are listed.

The mass of a coil is given by

$$M_c = nla_w\rho \quad (4.4)$$

where  $m_c$  is the mass [kg],  $n$  is the number of turns,  $l$  is the length [m],  $a_w$  the the cross sectional area and  $\rho$  is the material density.

The power can be expressed as

$$P = UI = I^2R \quad (4.5)$$

In equation 4.2, the ohmic resistance increases with decreasing lead cross-section. Therefore there exists a minimum wire cross sectional area, and the chosen wire diameter must not exceed this value. For more on design development and production of electromagnetic coils, see Aydinlioglu [2].

**Table 4.2:** Copper properties

Parameter	Symbol	Value	Unit
Density	$\rho$	$8.92 \cdot 10^3$	kg/m <sup>3</sup>
Resisivity @ 20°C	$\sigma_0$	$1.7 \cdot 10^{-8}$	$\Omega\text{m}$
Temperature coefficient of resistivity	$\alpha$	$3.9 \cdot 10^{-3}$	1/°C

### 4.3 Design results

In table 4.3 and table 4.4, the results of the short side and long side coils design are shown, respectively. As can be seen from the tables, the coils give necessary magnetic moments as well as meeting the design criteria. The two different types of coils where designed in a way that they essentially weights the same, and thus resulting in different produceable magnetic moments. The coils could have been designed with the magnetic moment in mind, as this would lead to different weights.

### 4.4 Summary

In this chapter the magnetic coil design was investigated. It was found that with the design restrictions at the time being, it's possible to produce magnetic air coils able to create large enough magnetic moments to control the satellite. Although aluminium is a better choice of material, there is not commercial available very thin aluminium wires. An important property of the coils is the rise time constant, the time before the magnetic

**Table 4.3:** Magnetorquer design results for the short side coil

Parameter	Symbol	Value	Unit
Number of turns	$N_s$	258	
Mass	$M_s$	11.9	kg
Wire diameter	$d_w$	0.15	mm
Wire cross sectional area	$a_w$	0.01767	mm <sup>2</sup>
Coil cross sectional area	$a_{s,c}$	4.56	mm <sup>2</sup>
Maximum Current at $T_{\min}$	$I_{s,-60}$	60	mA
Maximum Current at $T_{\text{nom}}$	$I_{s,25}$	40.6	mA
Maximum Current at $T_{\max}$	$I_{s,100}$	31.5	mA
Maximum Power at $T_{\min}$	$P_{s,-60}$	180	mW
Maximum Power at $T_{\text{nom}}$	$P_{s,25}$	121.8	mW
Maximum Power at $T_{\max}$	$P_{s,100}$	95.5	mW
Coil Resistance at $T_{\min}$	$R_{s,-60}$	50	$\Omega$
Coil Resistance at $T_{\text{nom}}$	$R_{s,25}$	73.89	$\Omega$
Coil Resistance at $T_{\max}$	$R_{s,100}$	95.09	$\Omega$
Produceable magnetic moment at $T_{\min}$	$m_{s,-60}$	82.5	mAm <sup>2</sup>
Produceable magnetic moment at $T_{\text{nom}}$	$m_{s,25}$	55.8	mAm <sup>2</sup>
Produceable magnetic moment at $T_{\max}$	$m_{s,100}$	43.3	mAm <sup>2</sup>

**Table 4.4:** Magnetorquer design results for the long sides

Parameter	Symbol	Value	Unit
Number of turns	$N_l$	144	
Mass	$M_l$	11.8	kg
Wire diameter	$d_w$	0.15	mm
Wire cross sectional area	$a_w$	0.01767	mm <sup>2</sup>
Coil cross sectional area	$a_{l,c}$	2.55	mm <sup>2</sup>
Maximum Current at $T_{\min}$	$I_{l,-60}$	60	mA
Maximum Current at $T_{\text{nom}}$	$I_{l,25}$	40.7	mA
Maximum Current at $T_{\max}$	$I_{l,100}$	31.6	mA
Maximum Power at $T_{\min}$	$P_{l,-60}$	180	mW
Maximum Power at $T_{\text{nom}}$	$P_{l,25}$	122.1	mW
Maximum Power at $T_{\max}$	$P_{l,100}$	94.8	mW
Coil Resistance at $T_{\min}$	$R_{l,-60}$	50	$\Omega$
Coil Resistance at $T_{\text{nom}}$	$R_{l,25}$	73.73	$\Omega$
Coil Resistance at $T_{\max}$	$R_{l,100}$	94.88	$\Omega$
Produceable magnetic moment at $T_{\min}$	$m_{l,-60}$	118.6	mAm <sup>2</sup>
Produceable magnetic moment at $T_{\text{nom}}$	$m_{l,25}$	80.4	mAm <sup>2</sup>
Produceable magnetic moment at $T_{\max}$	$m_{l,100}$	62.4	mAm <sup>2</sup>

field occurs after the electrical current has been turned on, and the time it takes before the magnetic field is removed after the current has been shut off. Without going into details, the work of Busterud [8], Graversen et al. [15] indicates a rise time constant of about  $100\mu s$ . This is very small, and should not cause trouble in the magnetic coil control.

## Chapter 5

---

# Attitude Control

---

In the previous chapters, the spacecraft's dynamics has been presented, analyzed and discussed. The CubeSTAR scientific instrument needs to point in the orbit velocity direction in order to use the measurements. An pointing accuracy of around 10 degrees can be seen as necessary to fulfill this.

Based on the previous work that has been reviewed, three different control laws has been investigated. The first is the B-dot control law for detumbling the satellite. The last two controllers can be used for stabilization of the spacecraft. Based on the simulation results and implementation issues, one of these control laws will be implemented on a FPGA.

Because this thesis only focus on the attitude control, no attitude determination is applied. This means that the full-state feedback is the output of the non-linear system models. Because the accuracy of the determination is unknown, the "real" states are used, and there is no uncertainties in the state measurements. This is however not realistic, and the attitude controllers must be tested with the attitude determination system when this is available.

## 5.1 Detumbling

When the satellite has relatively high angular velocity, it's said to be tumbling. This happens usually right after the release from the launch pod. The uncontrolled satellite can also over time start to tumble due to disturbances. These disturbances can increase the rotational kinetic energy in the spacecraft if they act on the spacecraft in a non-periodic way. In addition, deployment of mechanical parts, such as antennas, can cause tumbling.

When the satellite is tumbling, it's desirable to bring the angular velocities down before starting to stabilize the spacecraft. There are many reasons for this. Firstly, the stabilization controllers may not be stable with high angular velocities. Attitude determination sensor may get problems regarding measurements, and it's therefore not

possible to estimate the attitude of the orientation. In addition, when using a gravity gradient boom, high angular velocity can stress the boom under deployment and cause damage.

In this thesis, the B-dot algorithm will be used as a detumbling controller. The B-dot controller was first introduced in Stickler and Alfriend [38]. Later, Wisniewski [47] derived a modified version of this controller with use of the Lyapunov direct method. The controller only uses measurements from a 3-axis magnetometer, and no information about the spacecraft attitude or orbital position is required. The controller can therefore be employed at any point of time.

The original B-Dot control law is given as [38]

$$\mathbf{m} = -K\dot{\mathbf{b}}_b \quad (5.1)$$

where  $\mathbf{m}$  is the magnetic output moment,  $K$  is a positive constant gain, and  $\dot{\mathbf{b}}_b$  is the derivative of the measured magnetic field in the body frame. The controller acts like a compass needle following the geomagnetic field. The smallest theoretical angular velocity achieved by the B-dot controller is therefore the change of the geomagnetic field in the orbit. It must be noted that the sampling rate of the magnetometer is of great importance. Faster sampling rates will improve the performance of the detumbler as the magnetic field is continuously changing in the orbit, in addition to the spin of the spacecraft.

The kinetic energy can be expressed as [47]

$$E_k = \frac{1}{2} \boldsymbol{\omega}_b^{ibT} \mathbf{I}_b \boldsymbol{\omega}_b^{ib} \quad (5.2)$$

By using the assumption that the change of the magnetic field vector is being the result of the rotation of the spacecraft only, the derivative of the magnetic field can be expressed as

$$\dot{\mathbf{b}}_b \approx \mathbf{b}_b \times \boldsymbol{\omega}_b^{ib} \quad (5.3)$$

From this, it can be shown that the control law in equation 5.1 will reduce the angular velocity of the satellite. The gain in equation 5.1 determines how fast the angular velocity of the spacecraft will be decreased. Higher gain gives faster dissipation of kinetic energy, but at the cost of higher power consumption and possibly instability.

## 5.2 Magnetic Stabilization

When the satellite is not tumbling, it's desired that the scientific instrument points in the orbit velocity direction. It's therefore necessary to use a control law that stabilize the



spacecraft with as high accuracy as possible. When magnetic coils is used as actuators, normal attitude control laws cannot be used as the magnetic coils can only produce a torque in the plane perpendicular to the magnetic field.

Based on a study of the literature on ADCS using magnetic coils, an adaptive PD-like control law and the LQR optimal control problem has been decided to be further investigated for magnetic stabilization of the CubeSTAR satellite. The LQR control problem is investigated as a constant gain controller, and a periodic gain controller.

### 5.2.1 Proportional-Derivative Control

PD is a very common control law. Although they are essentially the same, there exist a various number of different PD-controllers. A simple PD-control can be written on the form when using attitude and angular velocity error feedback as

$$\boldsymbol{\tau} = - \begin{bmatrix} \mathbf{K}_d & \mathbf{K}_d \end{bmatrix} \begin{bmatrix} \boldsymbol{\omega}_e \\ \mathbf{q}_e \end{bmatrix} \quad (5.4)$$

where  $\boldsymbol{\omega}_e = \boldsymbol{\omega}_{ref} - \boldsymbol{\omega}_b^{ob}$  and  $\mathbf{q}_e$  is the attitude error quaternion vector.  $\mathbf{K}_d$  and  $\mathbf{K}_d$  are gain matrices. These gains does not need to be matrices, as they can also be treated as scalars or vectors. For the system 5.4, where  $\boldsymbol{\omega}_e = [\omega_{e,1} \ \omega_{e,2} \ \omega_{e,3}]^T$  and  $\mathbf{q}_e = [q_{e,1} \ q_{e,2} \ q_{e,3}]^T$ , the gains can be written as

$$\mathbf{K}_p = \begin{bmatrix} k_{p11} & k_{p12} & k_{p13} \\ k_{p21} & k_{p22} & k_{p23} \\ k_{p31} & k_{p32} & k_{p33} \end{bmatrix}, \quad \mathbf{K}_d = \begin{bmatrix} k_{d11} & k_{d12} & k_{d13} \\ k_{d21} & k_{d22} & k_{d23} \\ k_{d31} & k_{d32} & k_{d33} \end{bmatrix} \quad (5.5)$$

However, standard PD-control on small satellites using only magnetorquers does not necessarily give good results [27].

In this thesis, the work of Lovera and Astolfi [22] has been decided to be further investigated. This work does not rely on the frequently adopted assumption of periodicity of the geomagnetic field. Instead it uses a adoption mechanism of the measured geomagnetic field.

From chapter 3 the deterministic dynamics of the spacecraft was found to be

$$\mathbf{I}\dot{\boldsymbol{\omega}}_b^{ib} + \mathbf{S}(\boldsymbol{\omega}_b^{ib})\mathbf{I}\boldsymbol{\omega}_b^{ib} = \boldsymbol{\tau}_{coils} \quad (5.6)$$

By writing the system as

$$\mathbf{I}\dot{\boldsymbol{\omega}}_b^{ob} = \mathbf{S}(\boldsymbol{\omega}_b^{ib})\mathbf{I}\boldsymbol{\omega}_b^{ob} + \boldsymbol{\Gamma}(t)\mathbf{u} \quad (5.7)$$

where

$$\boldsymbol{\Gamma}(t) = \mathbf{S}^T(\tilde{\mathbf{b}}(t))\mathbf{S}(\tilde{\mathbf{b}}(t)) \geq 0 \quad (5.8)$$

and

$$\tilde{\mathbf{b}}(t) = \frac{\mathbf{b}(t)}{\|\mathbf{b}(t)\|} \quad (5.9)$$

it's possible to prove that the control input

$$\mathbf{u} = \begin{cases} -\epsilon k_v \boldsymbol{\omega}_r & t \leq \bar{t} \\ -\hat{\Gamma}_{av}^{-1}(\epsilon^2 k_p \mathbf{q}_r + \epsilon k_v \boldsymbol{\omega}_r) & t > \bar{t} \end{cases} \quad (5.10)$$

can stabilize the system. The control law cannot use  $\Gamma(t)$  before the requirement in equation 5.8 is fulfilled at time  $\bar{t}$ . Before time  $\bar{t}$ , the controller acts as a detumbler.

The differential equation

$$\dot{\hat{\Gamma}}_{av} = \frac{1}{t}(\Gamma - \hat{\Gamma}_{av}), \quad t > 0 \quad (5.11)$$

with initial condition

$$\hat{\Gamma}_{av}(0) = \Gamma(0) \quad (5.12)$$

can be seen as a adoption mechanism on the geomagnetic field.

## 5.2.2 Linear-Quadratic Regulator

In this section, the LQR optimal control problem is investigated. From the work of Gießelmann [14], Psiaki [32], Scholz [34], Wisniewski [45] amongst others, the LQR problem is well documented for use on spacecrafts with the use of magnetorquers. The problem is based on Pontryagin's optimal theory, and can be stated as finding the control input that minimizes a given criteria. For further reading, the reader should refer to Anderson [1].

The LQR utilizes the state feedback in order to find the optimal control. In general, in order to take system model uncertainties into account, and/or if the full state feedback is not available, the states must be estimated. This can be done with for example Kalman filtering, see [13], and the Linear Quadratic Gaussian control problem can be used to find the optimal control.

The infinite-horizon optimal control is found by minimizing a quadratic cost criteria given by

$$J = \frac{1}{2} \int_0^{\infty} [\mathbf{x}^T(t) \mathbf{Q}(t) \mathbf{x}(t) + \mathbf{u}^T(t) \mathbf{R}(t) \mathbf{u}(t)] dt \quad (5.13)$$

where

$$\left. \begin{aligned} \mathbf{u}^T(t) \cdot \mathbf{R} \cdot \mathbf{u}(t) &> 0 \\ \mathbf{x}^T(t) \cdot \mathbf{Q} \cdot \mathbf{x}(t) &\geq 0 \end{aligned} \right\} \text{for } \mathbf{u}(t), \mathbf{x}(t) \neq 0 \quad (5.14)$$

In equation 5.14,  $\mathbf{Q}$  and  $\mathbf{R}$  must be semi-positive definite and positive definite, respectively. This ensures that all energy added to the system has a cost, and no energy is given for free.

The LQR problem can, however, only be used on linear systems. As previously mentioned in chapter 3, the continuous-time linear deterministic system can be described by the state space model

$$\dot{\mathbf{x}}(t) = \mathbf{F}(t)\mathbf{x}(t) + \mathbf{G}(t)\mathbf{u}(t) \quad (5.15)$$

$$\mathbf{y}(t) = \mathbf{C}\mathbf{x}(t) \quad (5.16)$$

The linearized system model found in chapter 3 must therefore be used. This model does not behave the same as the non-linear system, but can be used in small deviations around the equilibrium.

The solution to the optimal control, where  $J$  is minimized, can be written as

$$\mathbf{u}(t) = -\mathbf{K}\mathbf{x}(t) \quad (5.17)$$

where the gain  $\mathbf{K}$  is the solution to the optimal control problem, and is obtained as

$$\mathbf{K} = \mathbf{R}^{-1}\mathbf{B}^T\mathbf{P} \quad (5.18)$$

In order to solve equation 5.18, the Riccati equation must be solved. The Riccati differential equation can be used to solve minimalization problems when dealing with quadratic cost functions. The Riccati equation is given as [1]

$$\dot{\mathbf{P}}(t) = -\mathbf{P}(t)\mathbf{A}(t) - \mathbf{A}^T(t)\mathbf{P}(t) - \mathbf{Q} + \mathbf{P}(t)\mathbf{G}(t)\mathbf{R}^{-1}(t)\mathbf{G}^T(t)\mathbf{P}(t) \quad (5.19)$$

If the system is controllable or stabilizable,  $\mathbf{P}(t)$  converges to a stationary solution, yielding

$$\mathbf{0} = \mathbf{F}^T\mathbf{P} + \mathbf{P}\mathbf{F} - \mathbf{P}\mathbf{G}\mathbf{R}^{-1}\mathbf{G}^T\mathbf{P} + \mathbf{Q} \quad (5.20)$$

This equation is called the algebraic Riccati equation (ARE), and can be used because the linear model was found stabilizable in chapter 3, and thus simplifies the calculation of the optimal gain.

The closed-loop system can be written as

$$\dot{\mathbf{x}}(t) = (\mathbf{A} - \mathbf{B}\mathbf{K})\mathbf{x}(t) = \mathbf{A}_c\mathbf{x}(t) \quad (5.21)$$

If the system is observable or detectable, as in this case, the optimal state feedback is asymptotically stable, or equally,  $\mathbf{A}_c$  is Hurwitz, if every eigenvalue of  $\mathbf{A}_c$  has strictly negative real part[1].

### Periodic LQR control

A periodic is a system that repeat itself after a period of time, hence the name. Because the geomagnetic field can be modeled as a near periodic field, periodic system theory can be applied. Based on this, it's possible to create a periodic gain LQR control law. The following is based on Wisniewski [47]

Consider the following linear system

$$\dot{\mathbf{x}}(t) = \mathbf{A}(t)\mathbf{x}(t) + \mathbf{B}(t)\mathbf{u}(t) \quad (5.22a)$$

$$\mathbf{y}(t) = \mathbf{C}(t)\mathbf{x}(t) \quad (5.22b)$$

where the state and input vector is given as  $\mathbf{x}(t) \in \mathbb{R}^n$  and  $\mathbf{u}(t) \in \mathbb{R}^m$ , respectively. The matrices  $\mathbf{A}(t)$  and  $\mathbf{B}(t)$  are periodic matrices of period  $T$ , and the system is periodic system where

$$\mathbf{A}(t + T) = \mathbf{A}(t), \quad \mathbf{B}(t + T) = \mathbf{B}(t) \quad (5.23)$$

It's then possible to calculate the LQR gain matrix for each time step over one orbit, and use this value in a look-up table. The gain is precalculated off-line, and the optimal control can be used for each time step over the orbit. The geomagnetic field is, however, not periodic over each orbit because the Earth is rotating. The solution will only be an approximation, and the performance may vary. However, the orbit will, after several laps, end up in the same position as previous. The geomagnetic field can therefore be averaged over this number of orbits for each time step. This will create an average periodic geomagnetic field vector that can be used for calculating the periodic LQR gain matrix.

The average geomagnetic field can be calculated as

$$\hat{\mathbf{G}} = \frac{1}{T} \int_0^T \mathbf{G}(t)dt \quad (5.24)$$

The periodic LQR gain matrix can then be calculated as above over one orbit, achieving the gain matrix

$$\mathbf{K}(t) = \mathbf{K}(t + T) \quad (5.25)$$

### Floquet Theory

When dealing with periodic linear system, Floquet theory can be used for stability analysis. Because the stability of periodic systems are considered over time, the transition matrix, see [13], can be calculated over one period. When the transition matrix is calculated over one period, it's called the monodromy matrix. The eigenvalues of the monodromy matrix can then be found, and the placement of the eigenvalues can determine if the system is stable. The material in this section is based on Wisniewski [47].

Consider the zero input system

$$\dot{\mathbf{x}}(t) = \mathbf{A}_c(t)\mathbf{x}(t) \quad (5.26)$$

where  $\mathbf{A}_c(t)$  can be the closed-loop system matrix from equation 5.21. The transition matrix,  $\Phi(t, t_0)$ , of the system 5.26 can be expressed as

$$\Phi(t + T, t_0) = \Phi(t, t_0)\mathbf{C} \quad (5.27)$$

where  $t_0$  is the initial time,  $T$  is the period and  $\mathbf{C}$  is a constant matrix. By writing

$$\dot{\Phi} = \mathbf{A}_c(t)\Phi \quad (5.28)$$

it's possible to show that

$$\dot{\Phi}(t + T, t_0) = \mathbf{A}_c(t + T)\Phi(t + T, t_0) \quad (5.29)$$

There exist a constant matrix  $\mathbf{R}$  such that  $\mathbf{C} = e^{\mathbf{R}T}$  and together with the initial condition

$$\Phi(t_0, t_0) = \mathbf{I} \quad (5.30)$$

it follows that

$$\Phi(t_0 + T, t_0) = e^{\mathbf{R}T} \quad (5.31)$$

$\Phi(t_0 + T, t_0)$  is called the monodromy matrix at  $t_0$ , and the eigenvalues of the monodromy matrix are independent of  $t_0$ . The system is asymptotically stable, if and only if the eigenvalues of the  $\mathbf{R}$  matrix have negative real parts.

Another way of determine if the system is stable or not is to solve the monodromy matrix differential equation

$$\dot{\Phi}(t + T, t_0) = \mathbf{A}_c(t)\Phi(t + T, t_0) \quad (5.32)$$

If the eigenvalues of the monodromy matrix after one period, called the characteristic multipliers of  $\mathbf{A}_c(t)$ , belongs on the open unit disc, the system is stable.

### Constant gain LQR control

Instead of using the periodic assumption, a constant gain LQR matrix can be found. The control matrix  $\mathbf{G}(t)$ , was found to be time variant, and included the geomagnetic field in the body frame. In order to find a constant gain LQR control law, the average of this field must be found. This can be done by solving

$$\hat{\mathbf{G}} = \frac{1}{T} \int_0^T \mathbf{G}(t) dt \quad (5.33)$$

over several orbits.

This averaged geomagnetic field vector can be used to calculate a constant gain matrix,  $\mathbf{K}$ , and tested for stability with Floquet analysis. The advantage of using this method over the periodic assumption is that less memory is required, and is more simpler to implement.

### Choosing Q and R

In order to get a stable LQR control law, the weighting matrices must be correct chosen. More weighting on the states will give a faster response, but will increase the power consumption. If the control output is weighted more, the power consumption will be lower, but with a slower state response. To little weighting can lead to a non-stabilizing system, while to much weighting can lead to a unstable system. There exist no exact way to select the weighting matrices, but there are several “rules of thumb” that can give good results. These weighting matrices can indeed be time variant in the case of the periodic LQR problem, but using time invariant weighting matrices usually give good results. In addition, the weighting usually doesn’t need to be changed over time, as the importance hierarchy of the states and control input doesn’t change over time. It’s important to notice that when dealing with time variant and time invariant systems, a stable time variant LQR controller doesn’t necessary needs to be stable on the time invariant system, and vice versa.

If the designer has sufficient knowledge of the system, the maximum value of the individual states and control inputs can be used to find the weighting matrices as

$$\mathbf{R}(i, i) = \frac{1}{u_{i,max}^2} \quad \mathbf{Q}(i, i) = \frac{1}{x_{i,max}^2} \quad (5.34)$$

However, this is usually not the case, and other methods of selecting the weighting matrices must be used.

One usual way is to hold the control weighting matrix,  $\mathbf{R}$ , constant and equal the identity matrix.

$$\mathbf{R} = \mathbf{I}_{3 \times 3} \quad (5.35)$$

The state weighting matrix,  $\mathbf{Q}$  is then selected in a way that gives the best results. Choosing  $\mathbf{Q}$  can be done in several ways. One common way is to let the matrix be diagonal.

$$\mathbf{Q} = \text{diag}([k_{v1} \ k_{v2} \ k_{v3} \ k_{p1} \ k_{p2} \ k_{p3}]) \quad (5.36)$$

In [15], another way of selecting  $\mathbf{Q}$  was found to give good results.

$$\mathbf{Q} = \begin{bmatrix} qk_1\mathbf{I} & \mathbf{0} \\ \mathbf{0} & qk_2\mathbf{I} \end{bmatrix}^T \begin{bmatrix} 0.5\mathbf{I} & 0.5\mathbf{I} \\ 0.5\mathbf{I} & 0.5\mathbf{I} \end{bmatrix} \begin{bmatrix} qk_1\mathbf{I} & \mathbf{0} \\ \mathbf{0} & qk_2\mathbf{I} \end{bmatrix} \quad (5.37)$$

where  $\mathbf{I}$  is the  $3 \times 3$  identity matrix, and  $q$ ,  $k_1$  and  $k_2$  are scaling factors.

The chosen weighting matrices must be checked for stability. This can be done by using Floquet theory described in section 5.2.2. A less rigorous method is to test the calculated controller in terms of simulation.

## 5.3 Summary

In this chapter, the B-Dot control law used for detumbling was presented. Right after separation of the launch pod, relatively high angular velocities may occur. This controller is able reduce the satellites angular velocity by only using magnetometer measurements.

For magnetic stabilization, an adaptive PD-like controller where presented. This controller is quite complex, but does not rely on the frequently adopted assumption of a periodic geomagnetic field. The LQR control problem where investigated, along with both a periodic and constant gain solution. The stability of the LQR controller can be tested with Floquet theory, and some material on choosing the weights in the optimization criteria where discussed.





## Chapter 6

# Simulations

As previous mentioned, there exists very little data about the CubeSTAR satellite at this moment. In order to simulate and test the examined controllers, several parameters must be chosen. These parameters are best guesses and values suggested by references such as Wertz and Larson [43].

In this chapter, the controllers found in chapter 5 are tested with simulations. The controllers to be tested are the detumbling controller B-dot, the adaptive PD-regulator and LQR controllers. The disturbances in chapter 3 are added for a more realistic simulation. Because no attitude determination system is present, the full-state feedback will be the “real” states from the non-linear system models, and hence no noise. In table 6.1 the simulation parameters are shown.

**Table 6.1:** Simulation Model Parameters

Parameter	Symbol	Value	Unit
Total mass	$m_s$	2.0	kg
Inertia Matrix	$[I]$	$\begin{bmatrix} 0 & 0 & 0 \\ 0 & 0 & 0 \\ 0 & 0 & 0 \end{bmatrix}$	kg · m <sup>2</sup>
Displacement vector of CoM to GC	$\mathbf{r}_{\text{CoM-GC}}$	$\begin{bmatrix} 0 & 0 & 0 \end{bmatrix}^T$	m
Coefficient of drag	$C_D$	2.0	–
Coefficient of solar preassure	$C_P$	1.6	–
Area of drag	$A_D$	0.03	m <sup>2</sup>
Area of solar preassure	$A_P$	0.03	m <sup>2</sup>

The displacement vector  $\mathbf{r}_{\text{CoM-GC}}$ , is selected rather low. When simulated with higher values, the satellite became uncontrollable because the solar radiation torque and the aerodynamic torque became larger. This shows the importance of that the displacement vector must be made as low as possible in the design process. The residual dipole disturbance is ignored due to the fact it was not possible to find an estimate of the value. In addition, it could be possible to remove this disturbance by using this constant

disturbance as a bias in the magnetic coil control.

In the simulations, the axes of importance are the  $y$  and  $z$  axes. This is because the m-NLP system is mounted on the  $x$  axis. Stabilization about this axis is not necessarily needed, because the scientific instrument only will spin about its own axis. However, the  $x$ -axis is coupled with the other axes, and, because of the spin stability, will have an effect on the  $y$  and  $z$  axes as well.

A lot of the work in this thesis was done regarding the tuning of the different controllers. Although all the controllers did stabilize in the deterministic case, this was not the case when the disturbances was added. The tuning of the controllers did give usable results for the adaptive PD-control and the constant gain LQR controller, but it was not possible to stabilize the spacecraft with the periodic controller in the presence of disturbances.

The magnetic coils are modeled as linear actuators, with saturation on the maximum values found in chapter 4. As can be seen from the simulations, the maximum magnetic moment for each coil is large enough.

The satellite is simulated in a circular orbit with an inclination of  $90^\circ$  at 500 km altitude. This value was chosen because it lies in the middle of the CubeSTARs desired altitudes, 300 to 800 km. However, from chapter 3 it was found that the aerodynamic disturbance is the only disturbance that changes with the altitude. This can indicate that in order to reduce the disturbances, higher altitudes are of interest.

The Matlab and simulink source code can be found in appendix B and C.

## 6.1 The Uncontrolled Satellite

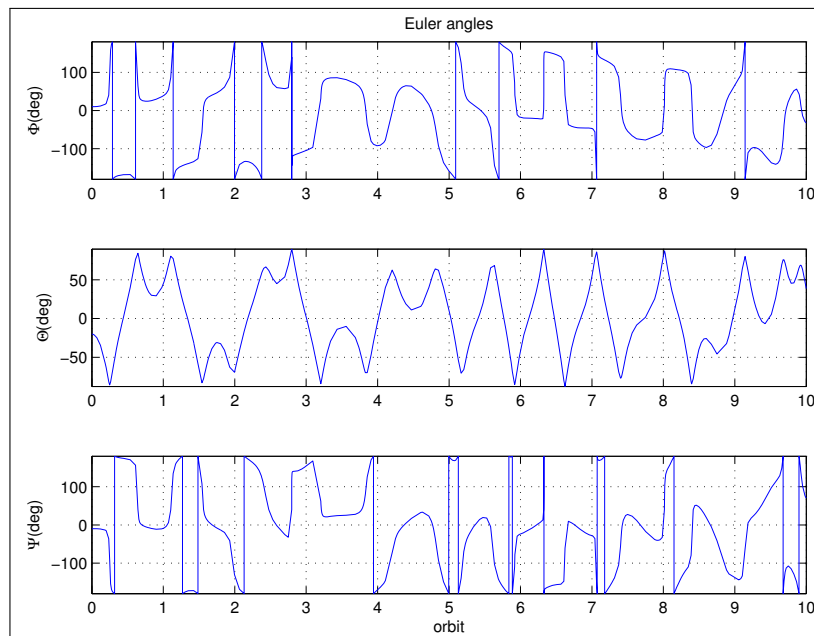
Before simulating the controllers found in the previous chapter, it's interesting to see how the uncontrolled spacecraft behaves. The non-linear system is added disturbances, and the noise will be the same as used for the controllers later in this chapter in order to see how much influence the disturbances has on the attitude of the satellite. From figures 6.1-6.4 it can be seen that, with the initial values shown in table 6.2, the satellite quickly moves away from the initial attitude. and starts to tumble. The maximum disturbance torques are identified as (Nm)

$$\tau_{dist,max} = \begin{bmatrix} 4.78 \cdot 10^{-10} \\ -8.99 \cdot 10^{-10} \\ 1.38 \cdot 10^{-9} \end{bmatrix} \quad (6.1)$$

This is rather small values. If the satellite was designed in another way, the system would be spin stable and gravity gradient stable, larger disturbance torques could possibly be added to the system without losing stability.

**Table 6.2:** Initial conditions for the uncontrolled satellite simulation

Initial Angles	$[\Phi_0 \ \Theta_0 \ \Psi_0]^T$	$[10 \ -20 \ -10]^T$
Initial body angular velocity (rad/s)	$\omega_{b,0}^{ob}$	$[0 \ 0 \ 0]^T$

**Figure 6.1:** Euler angles from the uncontrolled satellite

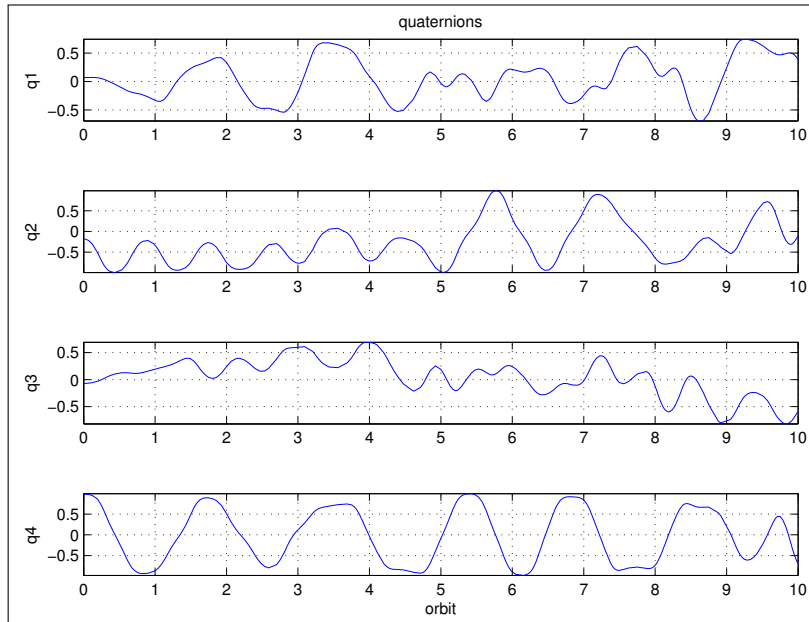


Figure 6.2: Quaternions from the uncontrolled satellite

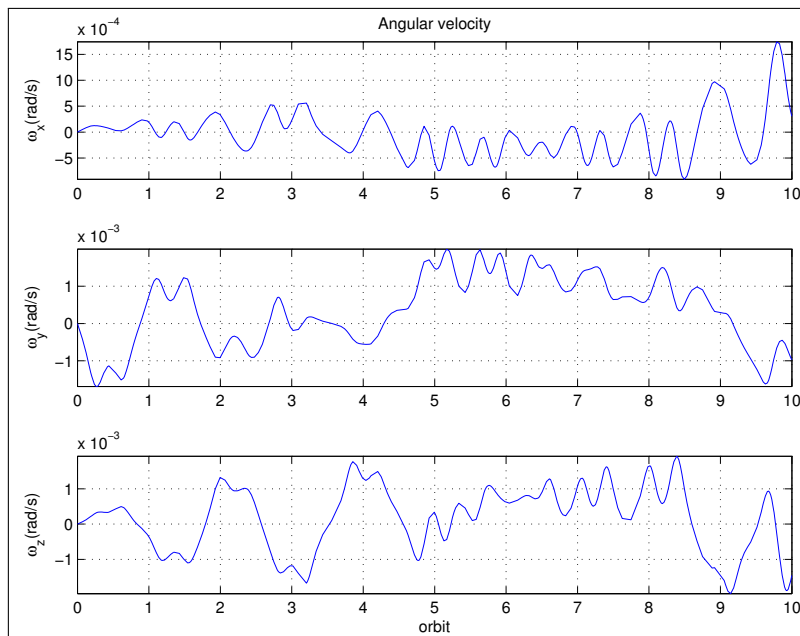
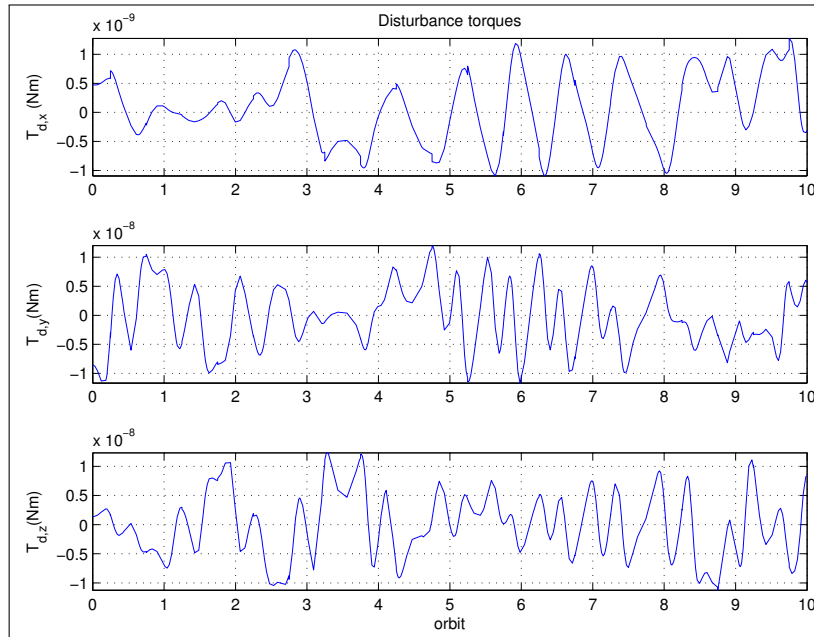


Figure 6.3: Angular velocity from the uncontrolled satellite



**Figure 6.4:** Disturbance torques acting on the uncontrolled satellite

## 6.2 Detumbling simulation

As mentioned in chapter 5.1, the initial angular body rates can become large, especially right after the separation of the P-POD. For simulation purposes, the initial conditions was chosen as specified in table 6.3.

**Table 6.3:** Initial conditions and gain value for the B-dot detumbling simulation

Initial Angles	$[\Phi_0 \ \Theta_0 \ \Psi_0]^T$	$[10 \ -20 \ -10]^T$
Initial body angular velocity (rad/s)	$\omega_{b,0}^{ob}$	$[0 \ 0.1 \ 0]^T$
Detumbling gain	$K$	10000

The performance of the simple controller from equation 5.1 can be seen in figures 6.5-6.9. The B-dot controller is able to reduce the initial body rates to around 0.002rad/s within 3 orbits. Because the controller only uses the magnetic field measurements, the lowest theoretical angular body rate would be the rate of change of the earth's magnetic field in the orbit frame.

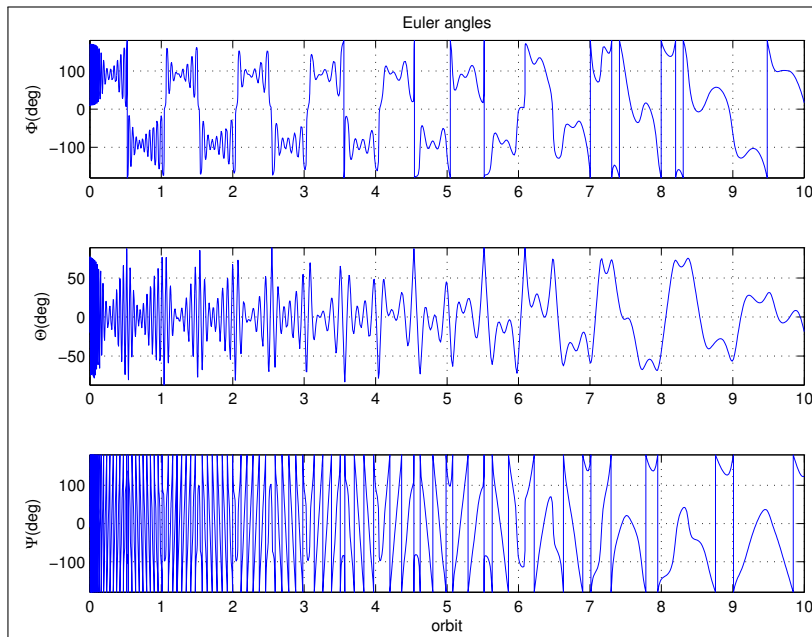


**Figure 6.5:** Euler angles from the B-dot control simulation

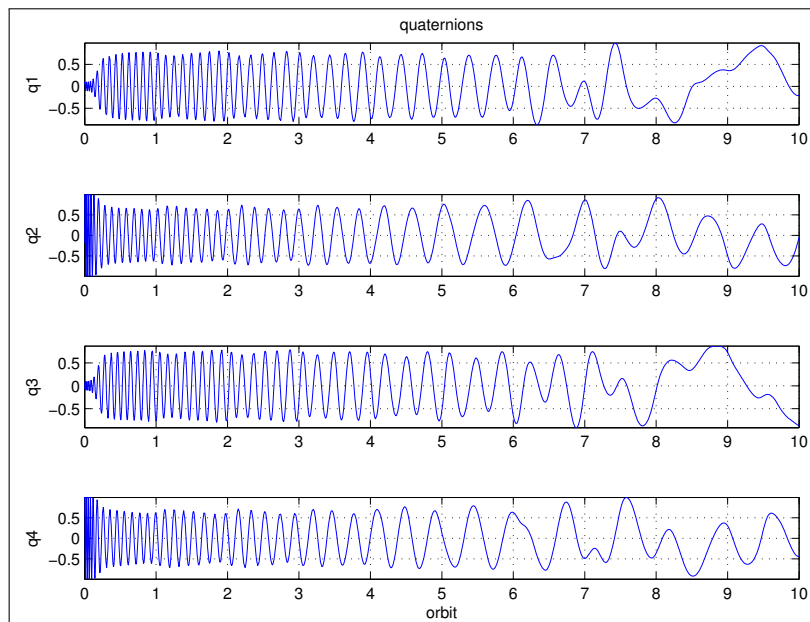


**Figure 6.6:** Quaternions from the B-dot control simulation

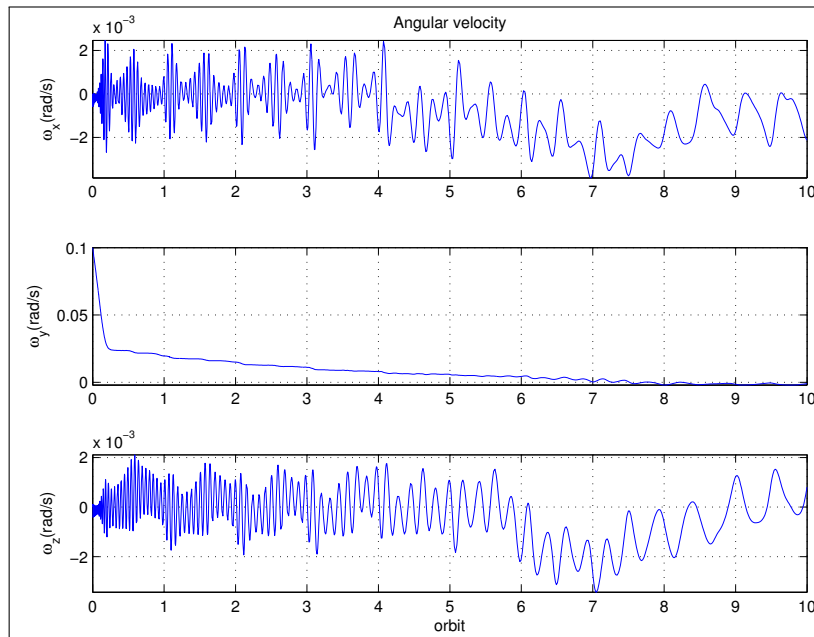


Figure 6.7: Angular velocity from the B-dot control simulation

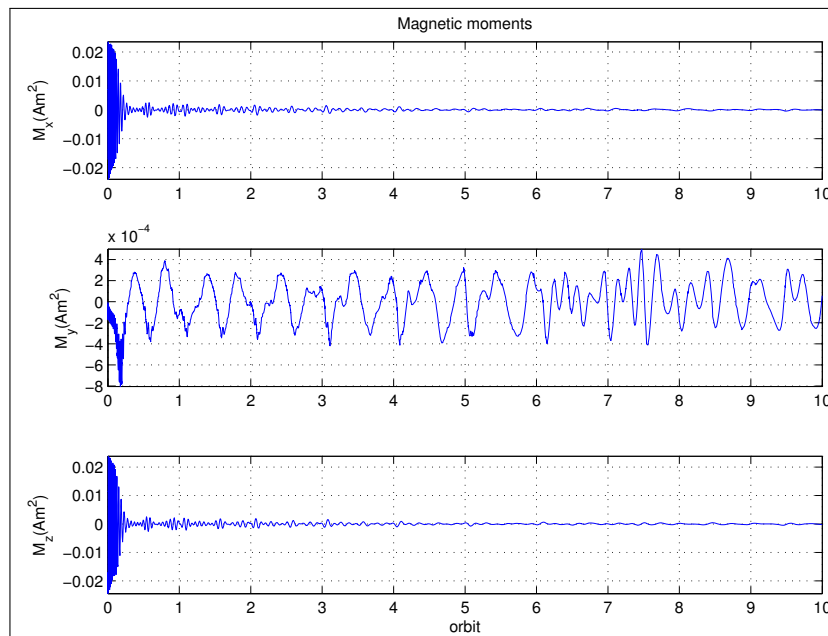
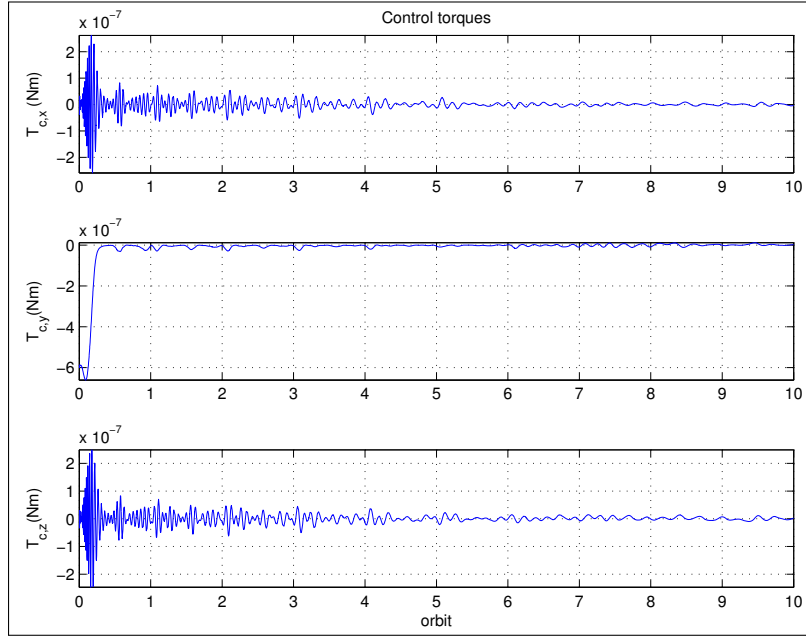


Figure 6.8: Magnetic moments from the B-dot control simulation



**Figure 6.9:** Magnetic torques from the B-dot control simulation

### 6.3 PD-Control simulation

For simulation of the adaptive PD-like control law, the same disturbances as used in the uncontrolled satellite simulation are used. In table 6.4 the initial conditions and gain values are shown.

**Table 6.4:** Initial conditions and gain value for the adaptive PD-control simulation

Initial Angles	$[\Phi_0 \ \Theta_0 \ \Psi_0]^T$	$[10 \ -20 \ -10]^T$
Initial body angular velocity (rad/s)	$\omega_{b,0}^{ob}$	$[0 \ 0 \ 0]^T$
Weighting factor	$\epsilon$	0.001
Quaternion weighting vector	$k_p$	$[0.2 \ 0.4 \ 0.2]^T$
Body angular velocity weighting vector	$k_v$	$[0.01 \ 0.2 \ 0.1]^T$

The gains was found with trial and error, and the performance of the controller can be seen in figures 6.10-6.15. As can be seen from the figures, the maximum pointing accuracy is identified as approximately

$$\begin{aligned}
 \Phi &= +8^\circ \quad \text{and} \quad -45^\circ \\
 \Theta &= \pm 4^\circ \\
 \Psi &= \pm 15^\circ
 \end{aligned} \tag{6.2}$$



Although the  $z$ -axis has a somewhat large maximum value, the angle is usually within  $10^\circ$ . The  $x$ -axis has very large values, but has no effect on the accuracy of the m-NLP instrument, as already mentioned. It can therefore be concluded that the adaptive PD-like controller is able to stabilize the spacecraft with disturbances added to the system. The larger error at the end of the simulation is due to the fact that the geomagnetic field is constantly changing. By ignoring the oscillations, the satellite is stabilized in about one orbit.

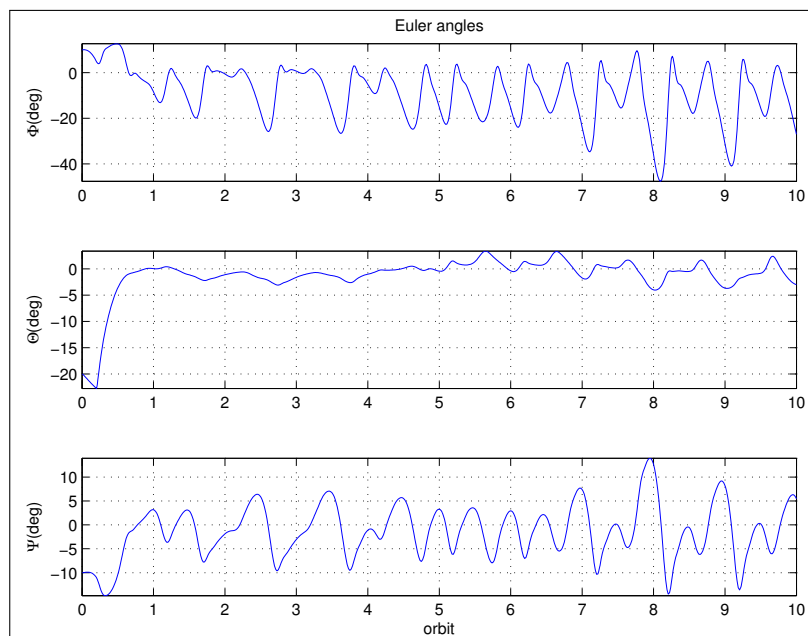


**Figure 6.10:** Euler angles from the PD control simulation

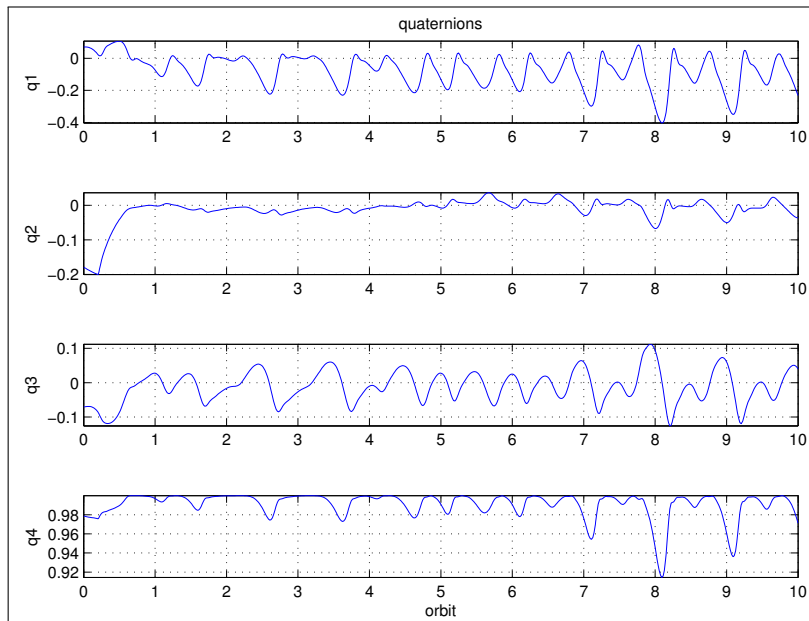


**Figure 6.11:** Quaternions from the PD control simulation

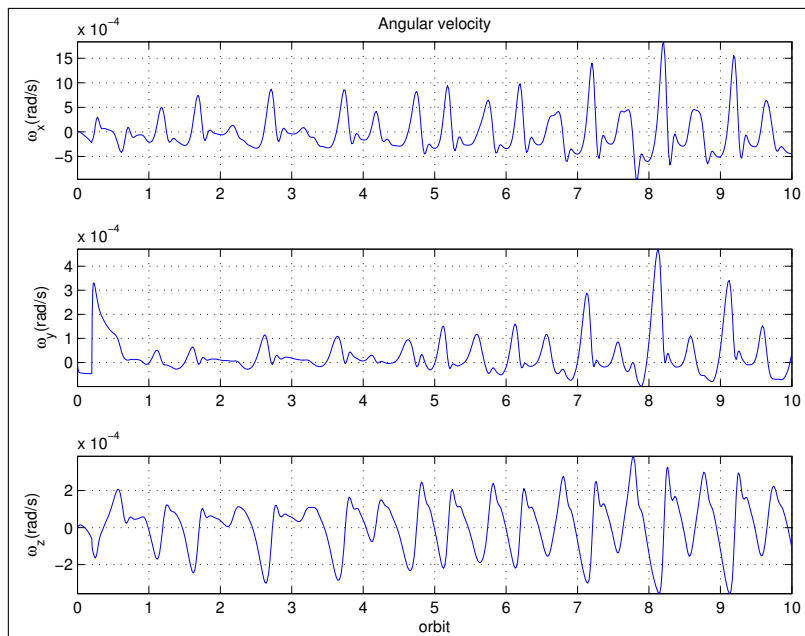


**Figure 6.12:** Angular velocity from the PD control simulation

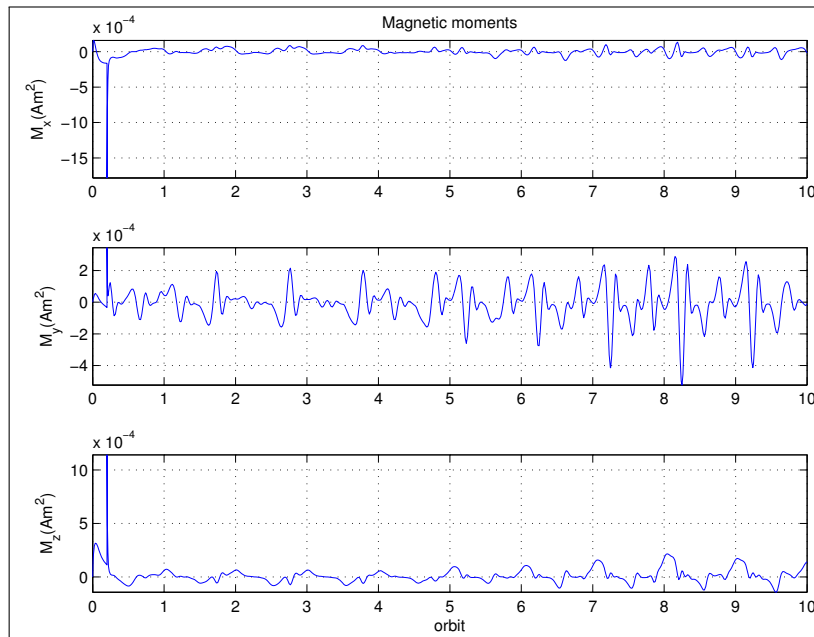


**Figure 6.13:** Magnetic moments from the PD control simulation

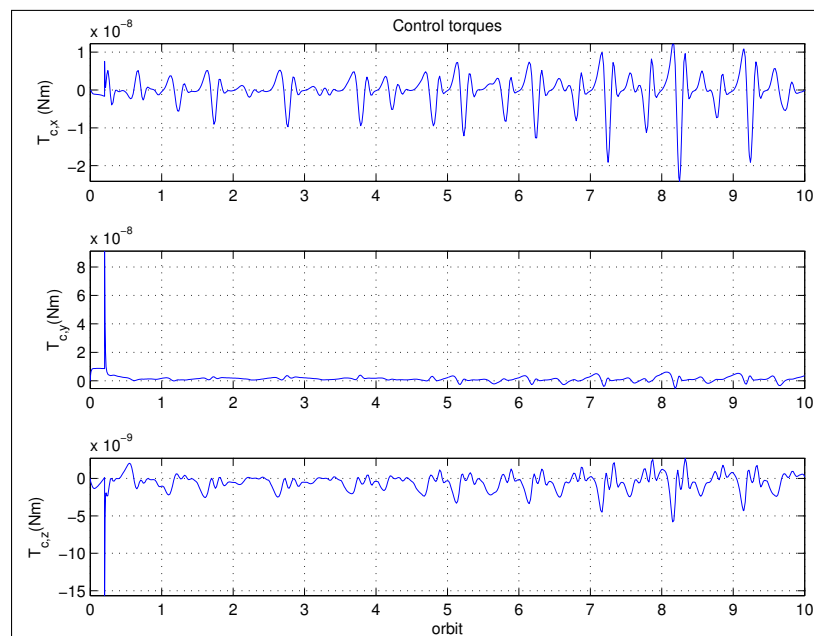


**Figure 6.14:** Magnetic torques from the PD control simulation

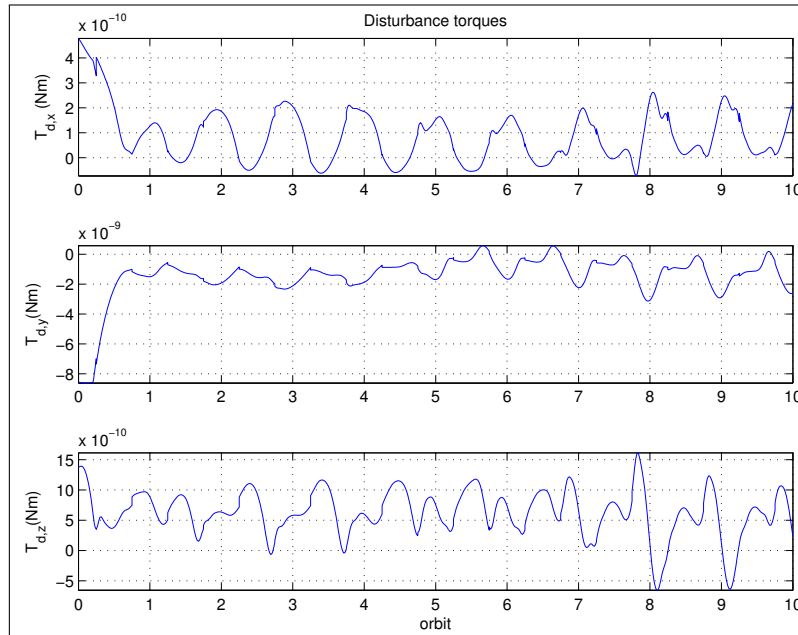


**Figure 6.15:** Disturbance torques from the PD control simulation

## 6.4 LQR Control

In this section, the LQR control laws are simulated. First, the periodic controller was tested. Although stabilization was achieved without disturbances, it was not possible to stabilize the spacecraft when disturbances were added. The periodic LQR control law simulation results are therefore not shown. Many different tunings were tried, and it seems like the gap between an unstabilizable controller and an unstable controller was very small, making it very hard to find a stable periodic control law. However, when the inertia matrix was changed, a stable controller was found. This shows the importance that the satellite must be designed with stability in mind, and an uniform mass distribution is not of interest.

### 6.4.1 Constant Gain

For the simulation of the constant gain LQR control, the initial condition and gain values shown in figure 6.5 were used.

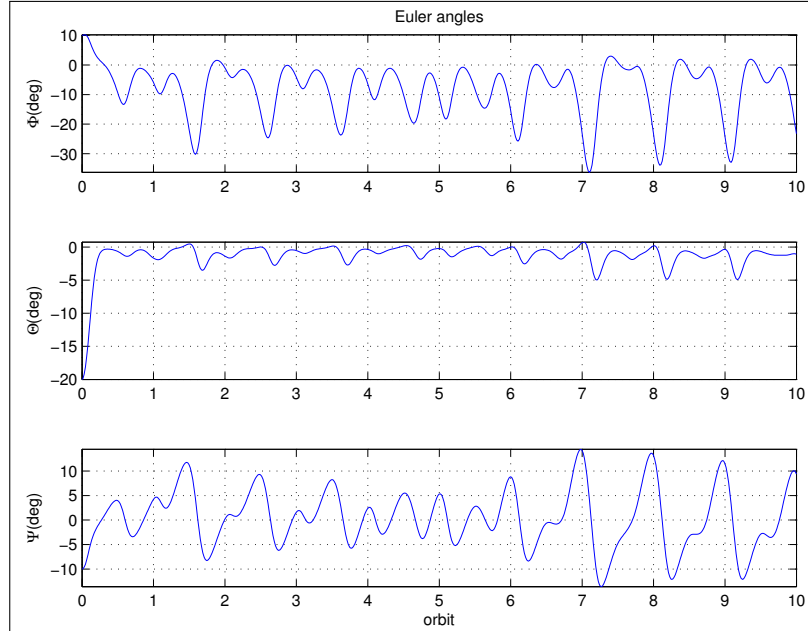
The disturbance torques are the same as in previous simulations. The performance of the constant gain controller is shown in figures 6.16-6.21. The maximum pointing accuracy is identified as approximately

**Table 6.5:** Initial conditions and gain value for the constant gain LQR control simulation

Initial Angles	$\begin{bmatrix} \Phi_0 \\ \Theta_0 \\ \Psi_0 \end{bmatrix}$	$[10 \quad -20 \quad -10]^T$
Initial body angular rate	$\omega_{b,0}^{ob}$	$[0 \quad 0 \quad 0]^T$
State weighting matrix	$Q$	$10^3 \cdot \text{diag}([5000, 5000, 5000, 8.5, 200, 8.5])$
Control weighting matrix	$R$	$\text{diag}([1 \quad 1 \quad 1])$

$$\begin{aligned}
 \Phi &= +3^\circ \quad \text{and} \quad -35^\circ \\
 \Theta &= +1^\circ \quad \text{and} \quad -5^\circ \\
 \Psi &= \pm 15^\circ
 \end{aligned}
 \tag{6.3}$$

These results are similar to the PD-control simulation, but better pointing accuracy is achieved. By ignoring the oscillations, the satellite is stabilized in about one orbit.

**Figure 6.16:** Euler angles from the constant gain LQR control simulation

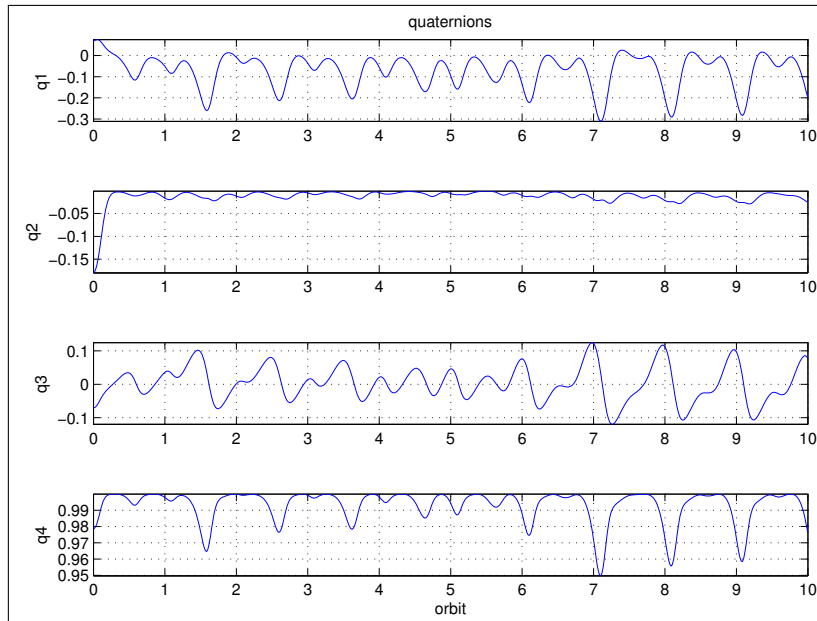


**Figure 6.17:** Quaternions from the constant gain LQR control simulation

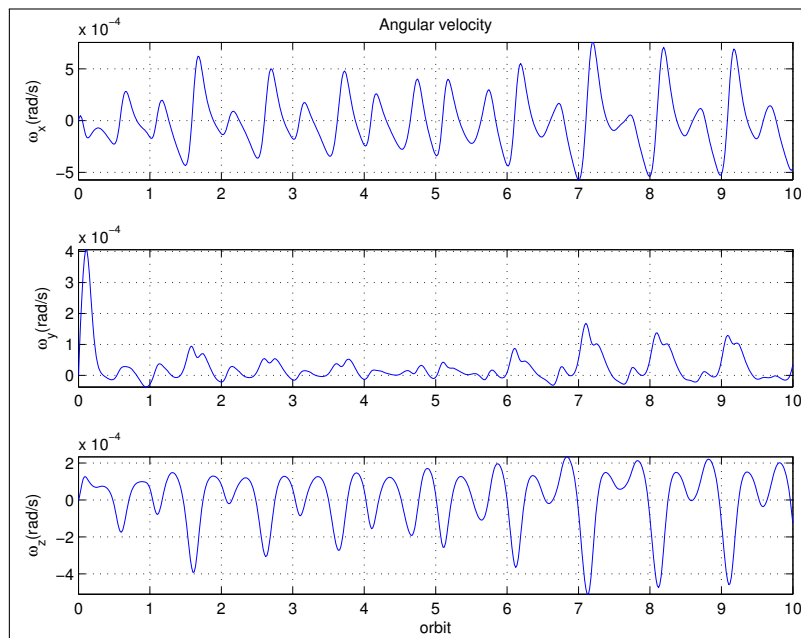


**Figure 6.18:** Angular velocity from the constant gain LQR control simulation

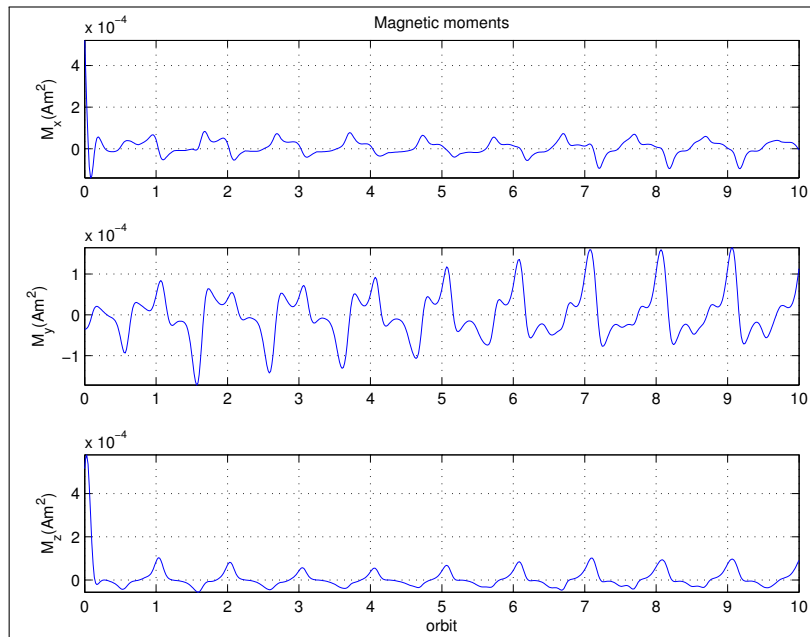


**Figure 6.19:** Magnetic moments from the constant gain LQR control simulation

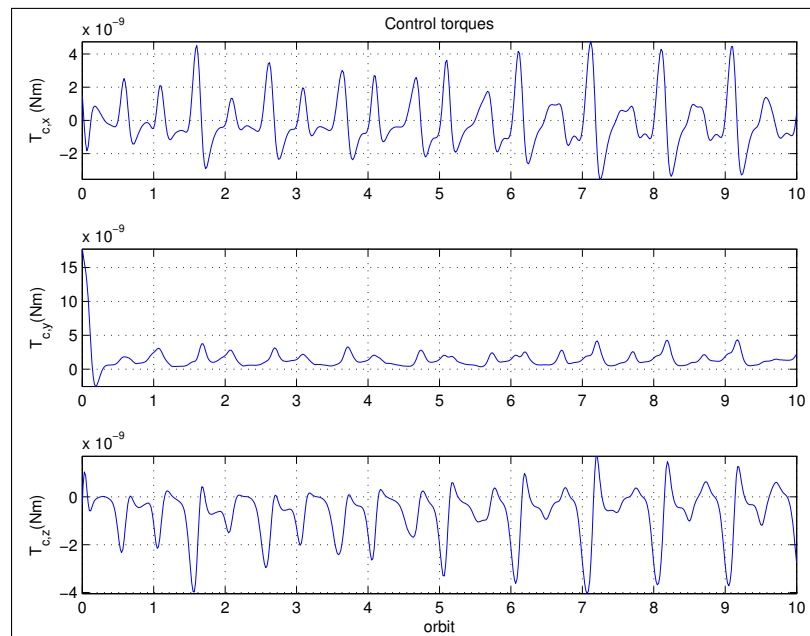


**Figure 6.20:** Magnetic torques from the constant gain LQR control simulation

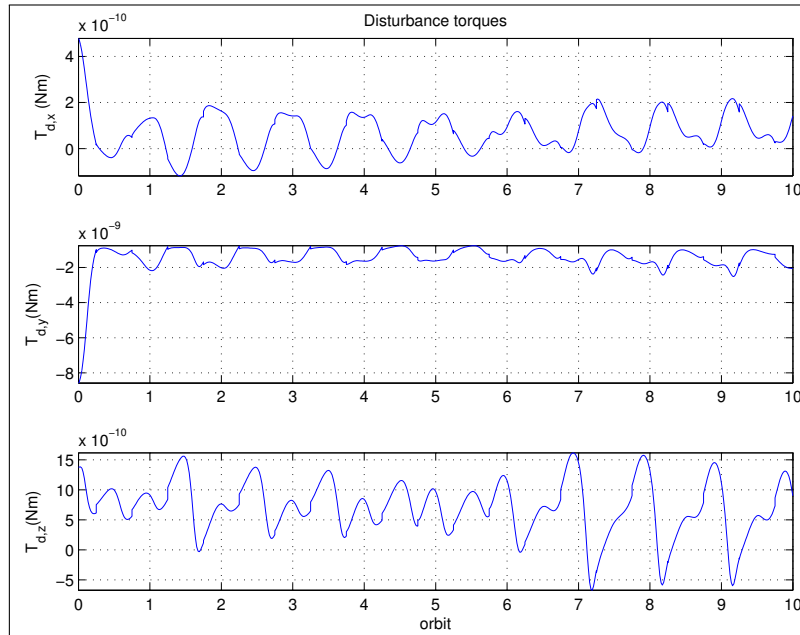


**Figure 6.21:** Disturbance torques from the constant gain LQR control simulation

## 6.5 Discussion

In this chapter, the performance of the different control laws was shown by simulations. The B-dot detumbler control law works well for detumbling the satellite in the presence of disturbances, and is able to reduce relatively high initial angular rates in a relatively short time. The B-dot control law is very simple, and hence easy to implement.

Based on the results, the constant gain LQR control law is a suitable choice for the magnetic stabilization of the CubeSTAR satellite as this controller gives the best results of the magnetic stabilization controllers. The controller is able to stabilize the satellite in the presence of disturbances, and an accuracy within the specification has been achieved. In addition, this controller is also the least complex. After calculating the gain matrix off-line, the attitude control system only needs to store the gain matrix, and calculate the optimal control by multiplying the gain with the state vector estimated by the attitude determination system.

The adaptive PD-like controller nearly gave as good results the constant gain controller. However, this controller is much more complex, and is much harder to implement. The advantage of this controller, however, is that it doesn't use the assumption of a periodic magnetic field. This makes it robust to geomagnetic model errors.



The last controller investigated was the periodic LQR controller. In the presence of disturbances, it was not possible to stabilize the spacecraft.

As can be seen from the simulations, the magnetic coils give large enough magnetic moments in order to stabilize the spacecraft.



## Chapter 7

---

# Implementation

---

For the scientific mission on the CubeSTAR satellite it's intended to use a Field Programmable Gate Array (FPGA) to perform calculations necessary to obtain the necessary data. A FPGA is an integrated circuit that can be configured by the user. The FPGA can be programmed in general by using a hardware description language (HDL). Due to this, it would be interesting and practical to implement the ADCS on the same device. Implementing the ADCS on a FPGA is, as far as the author know, not previous done on a satellite. Because of this, it's therefore necessary to investigate to see if it's possible to implement the attitude controller on the FPGA using the "DSP builder" tool-box for Matlab/Simulink by Altera to compile HDL, how this is done, and how the FPGA performs as a attitude controller.

Altera has created DSP builder which is essentially a tool-box compatible with MATLAB/simulink. A lot of the work in this thesis went to finding out how the DSP builder works, and how the tool can be used to compile and implement software on a FPGA. The work was implemented and tested on a "BeMicro FPGA-based MCU Evaluation Board" with a Cyclone III FPGA and the more advanced "DSP Development Kit, Cyclone III Edition".

The main problem with using the DSP builder tool-box for this project is the fact that matrix/vector calculations are not supported. In order to use the DSP builder tool-box, the vector/matrix calculations must be created from scratch using the implemented scalar functions. This work is tedious, and will be very complex when dealing with for example multiplication and inverting of large matrices with bad numerical properties. One solution to this problem is to write the ADCS directly in HDL.

Because of the fact that vector/matrix calculations is not supported in DSP-builder, the constant gain LQR controller from chapter 5.2.2 was chosen. In addition to being the simplest controller for stabilizing the spacecraft, it also gave the best results from the simulations. For the FPGA simulink source code, see appendix D.

## 7.1 HIL Simulation

The controller was implemented on the FPGA, and the HIL tool from DSP builder was used in order to simulate and test the controller. HIL simulation is a simulation where hardware is used in the simulation loop. The DSP-builder includes a HIL-simulation tool that can be used for simulating together with FPGAs. The FPGA kits were connected to a computer and the non-linear models including the environmental models were simulated on the computer. Meanwhile, the angular velocity and quaternions were sent to the FPGA, and the FPGA performed the attitude control calculations. The controller inputs were sent back to the computer, and used in the non-linear system model.

Because this simulation only will show the feasibility of the FPGA, no disturbances were added in the simulation.

The initial Euler angles were selected as

$$\begin{bmatrix} \Phi_0 \\ \Theta_0 \\ \Psi_0 \end{bmatrix} = \begin{bmatrix} -160^\circ \\ -80^\circ \\ 20^\circ \end{bmatrix} \quad (7.1)$$

and the initial body angular rate as

$$\omega_{b,0}^{ob} = \begin{bmatrix} 0 \\ 0 \\ 0 \end{bmatrix} \quad (7.2)$$

The constant gain was calculated as

$$\mathbf{K} = \begin{bmatrix} 9500 & -0.123 & -3404.7 & 36.1 & -3.6e-4 & 5.75 \\ -0.04 & 19726 & 0.079 & -1.53e-5 & 66.7 & -2.6e-4 \\ -359.4 & 0.0067 & 13977.8 & -21.96 & 1.53e-5 & 7.63 \end{bmatrix} \quad (7.3)$$

As can be seen from figures 7.1 -7.5, the spacecraft stabilizes in about one orbit, aligning the equilibrium perfectly. From this, it's possible to conclude that the attitude control can be implemented on a FPGA using the DSP-builder software.

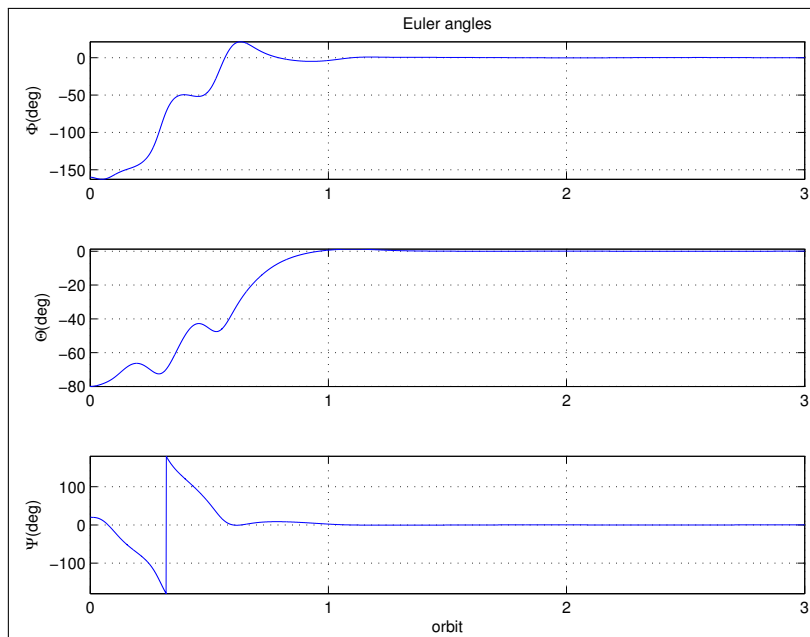


**Figure 7.1:** Euler angles from the FPGA HIL simulation

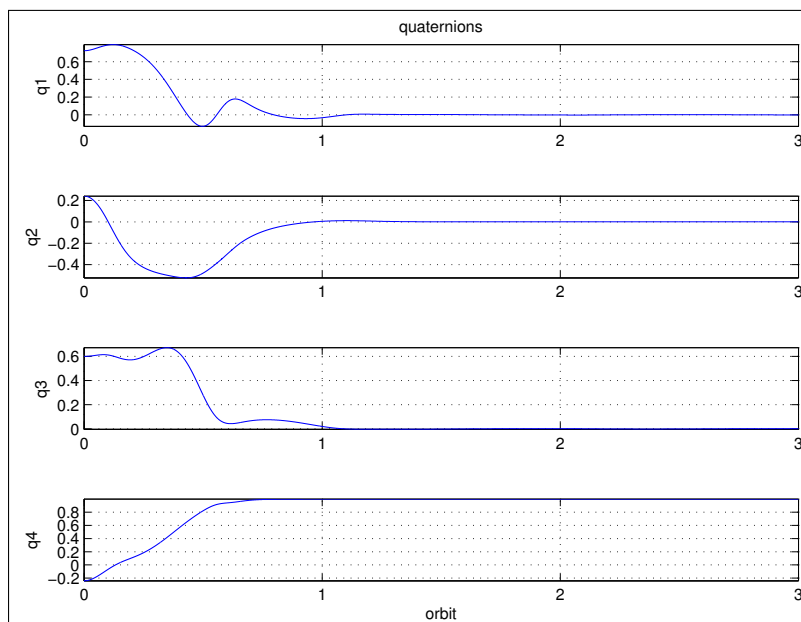


**Figure 7.2:** Quaternions from the FPGA HIL simulation

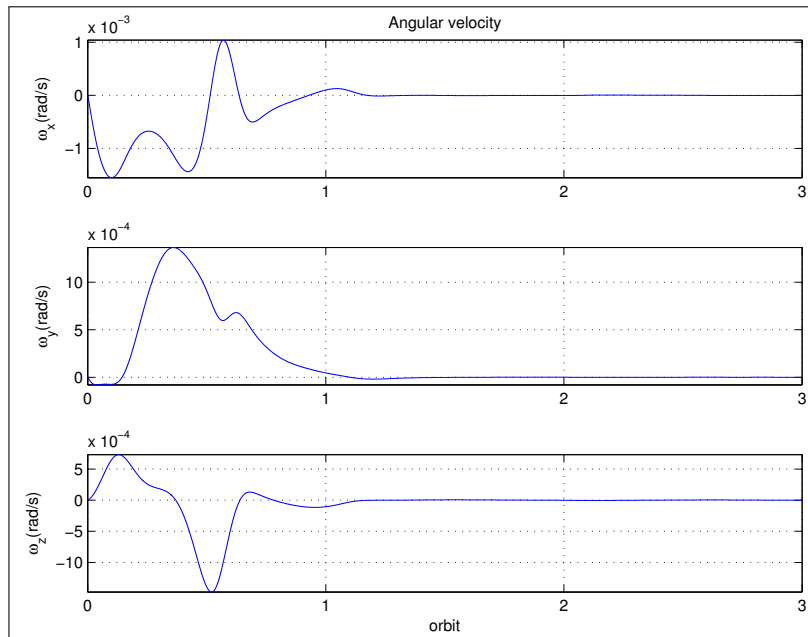


**Figure 7.3:** Angular velocity from the FPGA HIL simulation

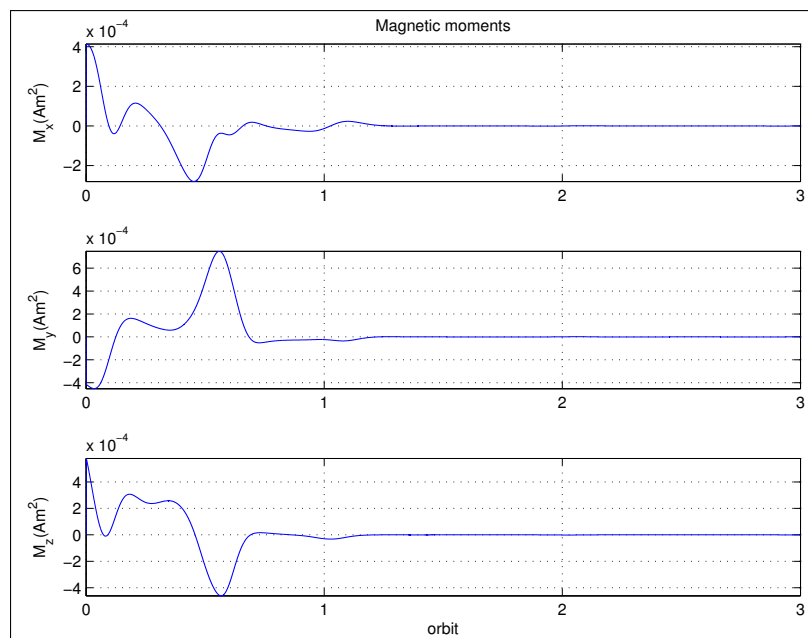


**Figure 7.4:** Magnetic moments from the FPGA HIL simulation

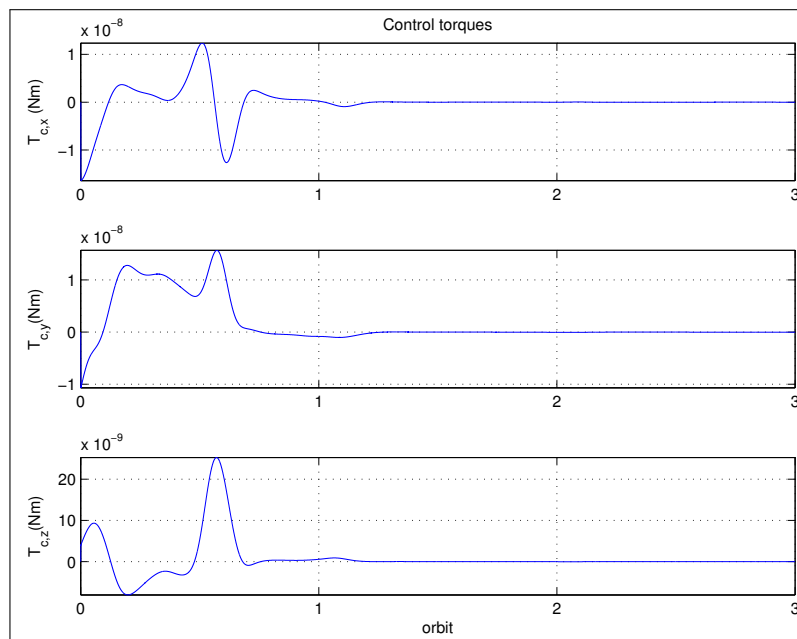


**Figure 7.5:** Magnetic torques from the FPGA HIL simulation





## Chapter 8

---

# Conclusions

---

### 8.1 Discussion of Results

In this thesis, the attitude control problem for the CubeSTAR satellite has been presented. The magnetic coils design was developed, and two different types of attitude controllers were investigated in addition to a detumbler control law.

The design of the magnetic coils showed that it's possible to manufacture magnetic coils that is able to control the spacecraft and meeting the design specifications. The coils are very light, but is able to create a relatively large magnetic moment.

From the simulations, it was found that the B-dot detumbling control law performed good, and reduced the satellites angular velocity from a relatively high initial value in the presence of disturbances. The control law is very simple to implement, and is suitable as a detumbler controller for the CubeSTAR satellite.

Regarding the magnetic stabilization, it was found that the constant gain LQR control law gave the best results. This controller is simple to implement, and requires very little memory. The controller gave a tolerated accuracy, but may be improved by more tuning of the regulator parameters, changing the spacecraft properties and reduce the disturbances. The satellite became stable after about one orbit.

The adaptive PD-like control law also gave usable results, but was not chosen because of its complexity and a somewhat lesser pointing accuracy. The periodic LQR control law failed to stabilize the system when realistic disturbances was added.

The constant gain control law was implemented on a FPGA, and tested using HIL simulations. It was found that it is possible to implement the ADCS on a FPGA using DSP builder, but because of the lack of matrix support in the DSP-builder software, the ADCS should be written in HDL.

Better pointing accuracy could also have been achieved by changing the inertia matrix of

the satellite. This could have been done by not using a uniform mass distribution, and thus creating a spin stable and gravity gradient stable satellite. In addition, by moving the m-NLP system and antennas to the longest sides of the satellite, the equilibrium would change, resulting in that the longest side of the satellite would point towards nadir. This layout would be much easier to make gravity gradient stable, and hence better results.

In addition, the pointing accuracy will also be improved by reducing the disturbances. The residual dipole disturbance could be reduced by avoiding ferromagnetic materials and canceling current loops. It was found that the displacement vector of the geographic center to center of mass has a huge impact on the solar pressure and aerodynamic disturbances. The solar pressure disturbance does not change with respect to the altitude. This is not the case for the aerodynamic drag disturbance, where this becomes very low at high altitudes. It's therefore desirable to use an orbit with as high altitude as possible to reduce disturbances, and hence increasing the stabilization. In deed, the geomagnetic field also weakens at higher altitudes, but this can be compensated by more windings in the coils.

## 8.2 Recommendation for Future Work

As this thesis is the first work to examine the attitude control problem for the CubeSTAR project, there still exists a large amount of work to be done on the ADCS before the satellite is ready to launch. Some of the future work to be done on the attitude control system should consist of;

- It should be investigated if it's possible to tune the constant gain LQR matrix to improve the performance of the magnetic stabilization. An integral state can also be added to the state vector, and thus improving the stabilization by removing bias disturbances.
- The attitude determination system must be developed and incorporated with the attitude control system. In this way, a more realistic model of the satellite is achieved by using estimated system quaternion attitudes and angular velocities. The uncertainties in the sensors are then included, and more realistic simulations can be performed.
- Together with the attitude determination system, a complete HDL source code must be written for the implementation on the FPGA. This code can then be used on the FPGA, and verified in more realistic hardware in-the-loop simulations, including a physical model of the satellite with the magnetic coils and sensors.
- The magnetic coils must be further investigated, and physical models of the coils must be manufactured, tested and verified.

- The simulation parameters was selected by best-guesses and recommendations in the literature. These values must be determined by real hardware testing in order to get a more realistic performance result of the controllers. This includes orbit parameters, disturbance torques parameters and other properties of the satellite.
- Disturbance torques acting on the satellite must be minimized in order to improve the magnetic stabilization. This includes the displacement vector of the geographic center and the center of mass of the satellite, and residual magnetic dipole moments.
- If the pointing accuracy must be better, it's necessary to investigate if a gravity gradient boom or momentum wheels can be used. Another way to get better accuracy can be to redesign the satellite and move scientific instrument with respect to gravity gradient stability.



---

# Bibliography

---

- [1] Brian Anderson. *Optimal Control: Linear Quadratic Methods*. Prentice Hall Information and System Sciences Series. Prentice Hall, 1990.
- [2] Ali Aydinlioglu. Design development and production of electromagnetic coils for attitude control of a pico satellite. Master's thesis, University of Applied Sciences Aachen, 2006.
- [3] Thomas Bak, Mogens Blanke, and Rahpael Wisniewski. Flight results and lessons learned from the ørsted attitude control system. *Spacecraft Guidance, Navigation and Control Systems*, 2000.
- [4] Tore André Bekkeng. Prototype development of a multi-needle langmuir probe system. Master's thesis, University of Oslo, May 2009.
- [5] Søren Abildsten Bøgh and Mogens Blanke. Fault-tolerant control - a case study of the ørsted satellite. *Proceedings, IEEE Colloquium on Fault Diagnosis in Process Systems*, 1997.
- [6] Søren Abildsten Bøgh, Rafal Wisniewski, and Thomas Bak. Autonomous attitude control system for the ørsted satellite. .
- [7] H. Bolandi and B. G. Vaghei. Stable supervisory-adaptive controller for spinning satellite using only magnetorquers. *IEEE Transactions on Aerospace and Electronic Systems*, 45(1):192–207, January 2009.
- [8] B. E. Busterud. Orienteringsregulering av mikrosatellitter. Master's thesis, NTNU, 2003.
- [9] Chi-Tsong Chen. *Linear System Theory and Design*. Oxford University Press, third edition, 1999.
- [10] ECSS. ECSS-E-ST-10-04C. Space Engineering, Space Environment. ESA-ESTEC, November 2008.
- [11] O. Egeland and J.T. Gravdahl. *Modeling and simulation for automatic control*. Marine Cybernetics, 2002.

- 
- [12] Ola-Erik Fjellstad and Thor I. Fossen. Comments on "the attitude control problem". *IEEE Transaction on Automatic Control*, 39(3):699–700, March 1994.
- [13] A. Gelb. *Applied Optimal Estimation*. MIT Press, Cambridge, MA, 1974.
- [14] Jens Gießelmann. Development of an active magnetic attitude determination and control system for picosatellites on highly inclined circular low earth orbits. Master's thesis, RMIT University, 2006.
- [15] Torben Graversen, Michael Kvist Frederiksen, and Søren Vejlggaard Vedstesen. Attitude control system fro aau cubesat. Master's thesis, Aalborg University, 2002.
- [16] Øyvind Hegrenæs. Attitude control by means of explicit model predictive control, via multi-parametric quadratic programming. Master's thesis, NTNU, 2004.
- [17] Øyvind Hegrenæs, Jan Tommy Gravdahl, and Petter Tøndel. Spacecraft attitude control using explicit model predictive control.
- [18] P.C. Hughes. *Spacecraft attitude dynamics*. Dover Publications, 2004.
- [19] Kristian Krogh and Elmo Schreder. Attitude determination for aau cubesat. Master's thesis, AALBORG UNIVERSITY, 2002.
- [20] Thomas R. Krogstad, Jan Tommy Gravdahl, and Petter Tøndel. Explicit model predictive control of a satellite with magnetic torquers.
- [21] J. Lee, A. Ng, and R. Jobanputra. On determining dipole moments of a magnetic torquer rod - experiments and discussions. *Canadian Aeronautics and Space Journal*, 48(1), 2002.
- [22] M. Lovera and A. Astolfi. Global magnetic attitude control of spacecraft in the presence of gravity gradient. *Aerospace and Electronic Systems, IEEE Transactions on*, 42(3):796–805, july 2006. ISSN 0018-9251. doi: 10.1109/TAES.2006.248214.
- [23] Marco Lovera and Alessandro Astolfi. Global magnetic attitude control of spacecraft. In *43rd IEEE Conference on Decision and Control*, 2004.
- [24] Marco Lovera, Eliana De Marchi, and Sergio Bittanti. Periodic attitude control techniques for small satellites with magnetic actuators. *IEE Transactions on Control Systems Technology*, 10(1), January 2002.
- [25] Joaquim Luis. Mirone. <http://w3.ualg.pt/~jluis/mirone/>, 2010. [Online; last accessed 29-September-2010].
- [26] Kristin Makovec, Andrew Turner, and Christopher Hall. Design and implementation of a nanosatellite attitude determination and control system.

- [27] Kristin L. Makovec. A nonlinear magnetic controller for three-axis stability of nanosatellites. Master's thesis, Virginia Polytechnic Institute and State University, 2001.
- [28] F. Martel, P. Pal, and M. Psiaki. Active magnetic control system for gravity gradient stabilized spacecraft. *Proceedings of the 2nd Annual AIAA/USU Conf. on Small Satellites*, 1988.
- [29] K. L. Musser and L. E. Ward. Autonomous spacecraft attitude control using magnetic torquing only. In *Flight Mechanics Estimation Theory Symposium*. NASA, 1989.
- [30] Stian Søndersrød Ose. Attitude determination for the norwegian student satellite ncube. Master's thesis, NTNU, 2004.
- [31] Eli Jerpeseth Øverby. Attitude control for the norwegian student satellite ncube. Master's thesis, NTNU, 2004.
- [32] Mark L. Psiaki. Magnetic torquer attitude control via asymptotic periodic linear quadratic regulation.
- [33] Tiziano Pulecchi, Marco Lovera, and Andras Varga. Optimal discrete-time design of magnetic attitude control laws.
- [34] Arthur Scholz. Implementaion of advanced attitude determination and control techniques into a nanosatellite. Master's thesis, National Cheng Kung University, 2008.
- [35] Raymond A. Serway and John W. Jewett. *Physics for Scientists and Engineers*. Cengage Learning, 6th edition, 2004.
- [36] M.J. Sidi. *Spacecraft dynamics and control: a practical engineering approach*. Cambridge Univ Pr, 1997. ISBN 9780521787802.
- [37] Enrico Silani and Marco Lovera. Magnetic spacecraft attitude control a survey and some new results. *Control Engineering Practice*, 13:357–371, 2005.
- [38] A. C. Stickler and K. T. Alfriend. An elementary magnetic attitude control system. *Journal of Spacecraft and Rockets*, 13(5), 1976.
- [39] Kristian Svartveit. Attitude determination of the ncube satellite. Master's thesis, NTNU, 2003.
- [40] California Polytechnic State University. CubeSat Design Specification. Revision 12, August 09.

- 
- [41] John Ting-Yung Wen and Kenneth Kreutz-Delgado. The attitude control problem. *IEEE Transaction on Automatic Control*, 36(10):1148–1162, October 1991.
- [42] James R. Wertz, editor. *Spacecraft attitude determination and control*. Kluwer, 1978.
- [43] James R. Wertz and Wiley J. Larson, editors. *Space Mission Analysis and Design*. Space Technology Library. Microcosm Press & Springer, 3rd edition, 1999. ISBN 9781881883104.
- [44] John S. White, Fred H. Shigemoto, and Kent Bourquin. Satellite attitude control utilizing the earth's magnetic field. Technical report, NATIONAL AERONAUTICS AND SPACE ADMINISTRATION TN-D1068, 1961.
- [45] Rafal Wisniewski. Linear time varying approach to satellite attitude control using only electromagnetic actuation, 2000.
- [46] Rafal Wisniewski and Mogens Blanke. Fully magnetic attitude control for spacecraft subject to gravity gradient. *Automatica*, 35, 1999.
- [47] Rahpael Wisniewski. *Satellite attitude control using only electromagnetic actuation*. PhD thesis, Aalborg University, 1996.
- [48] Mark Wood, Wen-Hua Chen, and Denis Fertin. Model predictive control of low earth orbiting spacecraft with magneto-torquers. In *IEEE International Conference on Control Applications*, 2006.



## Appendix A

---

# Abstract submitted to the 61st International Astronautical Congress (IAC)

---

During solar storms, turbulent electron clouds are formed in the ionosphere, causing distortion in satellite communication signals. The phenomenon of electron clouds is far from fully understood. Research in this area gives us the knowledge that we can later use to notify about space weather, and to improve equipment such as GPS receivers.

CubeSTAR will measure the structures in the electron clouds and improve the resolution 2000-fold, from today's seven kilometers down to the meter level. To ensure correct measurements, it is important that the multi-Needle Langmuir Probes are pointing in the satellite's velocity direction. In recent years a lot of work has been dedicated to attitude control of spacecrafts using solely magnetic actuators. In this paper, several of these controllers are investigated, including linear optimal control and adaptive control laws. The controllers are discussed from a practical point of view concerning future on-board implementation. The satellite's dynamics are presented with corresponding disturbance torques along with considerations concerning the magnetic coils. Simulation results are given, which illustrate the performance of the different controllers, and recommendation for future work on the attitude control system for the CubeSTAR project.



## Appendix B

---

# MATLAB source code

---

### InitSatelliteModel.m

```
%Find all open Simulink scopes and return
%their handles to an array called hScopeFig.
hScopeFig = findall(0,'Type','Figure','Tag','SIMULINK_SIMSCOPE_FIGURE');

%Set the renderer for all open scopes to painters.
set(hScopeFig,'Render','painters');

%Turn off the Scope/Zbuffer warnings.
warning('off','Simulink:SL_ScopeRendererNotZBuffer');
%*****
%*           Initialization           *
%*****
clear all;
close all;

%Declare global variables
global I A B K B_O_x B_O_y B_O_z;
global u_f r_o i_m w_o
%load data files
load igrf11-2010-500km
load gamma
load gammaNorm
load gammaNorm2
load BDipole_avg.mat
load KPeriodic
load KConstant
load Gamma0SIM
%Constants
G = 6.67428e-11; %gravity constant [m^3kg^-1s^-2]
m_e = 5.9742e24; %earth mass [kg]
g_0 = G*m_e; %earth gravitation coefficient [m^3s^-2]
re_e = 6378.1e3; %earth equatorial radius [m]
re_p = 6356.8e3; %earth polar radius [m]
re_m = 6371.2e3; % Earth's mean radius [m]
```

```

T_e = 86400; % earth period (1 day) [s]
w_e = 2*pi/T_e; %angular velocity [rad/s]
h_o = 500e3; %height above sea level [m]

%Satellite and orbit properties
dim=[0.200,0.10,0.10]; %length,width,height [m]
m_s=2.0;%mass[kg]
r_o = re_m + h_o; %orbit radius [m]
w_o = sqrt(g_0/(r_o^3)); %angular velocity [rad/s]
T_o = 2*pi/w_o; %Orbit period [s]
N = 2; %Number of orbits
T_t = T_o*N; %Total time [s]

%Inertia tensors
I_xx=m_s/12*(dim(2)^2+dim(3)^2);
I_yy=m_s/12*(dim(1)^2+dim(3)^2);
I_zz=m_s/12*(dim(1)^2+dim(2)^2);
%I_xx=0.007;
%I_yy=0.008;
%I_zz=0.003;
%I_xx = 60;
%I_yy = 70;
%I_zz = 5;
I=diag([I_xx,I_yy,I_zz]); %Matrix of inertia
k_x = (I_yy-I_zz)/I_xx;
k_y = (I_zz-I_xx)/I_yy;
k_z = (I_xx-I_yy)/I_zz;

%Magnetorquer properties
i_max = 0.06; %Maximum current [A]
N_x = 258; %Number of windings
N_y = 144; %Number of windings
N_z = 144; %Number of windings
A_x = 5329e-6; %mean Coil area [m^2]
A_y = 13724e-6; %mean Coil area [m^2]
A_z = 13724e-6; %mean Coil area [m^2]
mx_max = i_max*N_x*A_x; %Maximum
my_max = i_max*N_y*A_y; %Maximum
mz_max = i_max*N_z*A_z; %Maximum

%angular velocity inertial to orbit
w_o_io = [0,w_o,0]';
%initial angular velocity orbit to body
w_b_ob_0 = [0.0,0,0]';
%initial attitude orbit to body
euler_0 = pi/180*[10,-20,-10];
q_0 = euler2q(euler_0);

%initial rotation matrix, body to orbit
R_b_o = Rquat(q_0);
%initial rotation matrix, orbit to body

```

```

R_o_b = R_b_o';
%initial angular velocity, inertial to body
w_b_ib_0 = w_b_ob_0 + R_o_b*w_o_io;

m_dipoleDist = [0,0,0]';

%Sun preasure coefficients
Pp = 4.5*10^-6;
Ap = 0.1*0.2;
Cp = 1.6;

%Aerodynamic drag coefficients
r = [0.005,0.001,0.001]';
%rho = 42.418*10^-11;%300 km
rho = 6.697*10^-13;%500 mean km
%rho = 1.170*10^-14;%800 km
Cd = 2.0;
v0 = 2*pi*r_o/T_o;

%Linearized dynamics
A = [0, 0, -w_o*k_x, -6*w_o^2*k_x, 0, 0;
     0, 0, 0, 0, 6*w_o^2*k_y, 0;
     -w_o*k_z, 0, 0, 0, 0, 0;
     0.5, 0, 0, 0, 0, 0.5*w_o;
     0, 0.5, 0, 0, 0, 0;
     0, 0, 0.5, -0.5*w_o, 0, 0];

%dipole model parameters
T = round(T_o);
u_f=7.9*10^15;
i_m = (90-11)*pi/180;
i_0 = 11*pi/180;
t=1;

%LQRConstantGain
B = [I\BDipole_avg;zeros(3)];
R = eye(3)*10^1;
Q=diag([5000000,5000000,5000000,8500,200000,8500]);
K=-lqr(A,B,Q,R);

%Floquet with Rung-Kutta2
Phi = eye(6);
Ts = 100;
for k=1:Ts:T-1
    Bs = [B_O_x(k),B_O_y(k),B_O_z(k)];
    B = [I\skew3(Bs)*skew3(Bs);zeros(3)];
    Ak = A + B*K;
    k1 = Ak*Phi;
    k2 = Ak*(Phi+Ts*Ak*Phi);

```

```

    Phi = Phi + Ts*(k1+k2)/2;
end
maxE=max(abs(eig(Phi)))

%FPGA K
K_FPGA = [9500,-0.123,-3404.7,36.1,-3.6e-4,5.75;...
    -0.04,19726,0.079,-1.53e-5,66.7,-2.6e-4;...
    -359.4,0.0067,13977.8,-21.96,1.53e-5,7.63];

%PD
Bs = R_o_b*[B_O_x(1),B_O_y(1),B_O_z(1)]';
Gamma0 = skew3(Bs)'*skew3(Bs)/norm(Bs)^2;
eps = 0.001;
k_v1 = 0.01;
k_v2 = 0.2;
k_v3 = 0.1;
k_p1 = 0.2;
k_p2 = 0.4;
k_p3 = 0.2;

```

### KPeriodic.m

```

global T_o u_f r_o i_m i_0 I A
%Calculate the periodic LQR gain
T = round(T_o);
K1=zeros(3,6,T);
b_0=zeros(3,1);
for t = 0:T-1
    b_0 = u_f/r_o^3*[cos(w_o*(t-i_0/w_o))*sin(i_m),...
        -cos(i_m),2*sin(w_o*(t-i_0/w_o))*sin(i_m)]';
    as(1:3,t+1)= b_0;
    B = [I\skew3(b_0)*skew3(b_0)/norm(b_0);zeros(3,3)];
    p=1*10^-15;
    k_1=1;
    k_2=0.01;
    Q=p*diag([k_1,k_1,k_1,k_2,k_2,k_2]);
    R = eye(3);
    K1(:, :, t+1) = -lqr(A,B,Q,R);
end
KP=0;
KP(1:3,1:6,1:T)=K1;
for i = 1:14
    KP(1:3,1:6,end+1:end+T) = K1;
end
%}
save('K1.mat','K1')
save('KPeriodic.mat','KP')

```

**igrfFieldOrbit.m**

```

%calculate the magnetic field using the igrf11 model
clear all;
close all;
G = 6.67428e-11; %gravity constant [m^3kg^-1s^-2]
m_e = 5.9742e24; %earth mass [kg]
g_0 = G*m_e; %earth gravitation coefficient [m^3s^-2]
T_e = 86400; % earth period (1 day) [s]
w_e = 2*pi/T_e; %angular velocity [rad/s]
lon0 = w_e*180/pi;
%300km
alt300 = 6371.2e3 + 300e3;
w_s300 = sqrt(g_0/(alt300^3));
lat300_0 = w_s300*180/pi;
%500km
alt500 = 6371.2e3 + 500e3;
w_s500 = sqrt(g_0/(alt500^3));
lat500_0 = w_s500*180/pi;
%800km
alt800 = 6371.2e3 + 800e3;
w_s800 = sqrt(g_0/(alt800^3));
lat800_0 = w_s800*180/pi;
T_s = 2*pi/w_s500;
T_s300 = 2*pi/w_s300;
T_s500 = 2*pi/w_s500;
T_s800 = 2*pi/w_s800;
%w_s300*T_s300=-2pi
%2*pi/(w_e*T_s)=15.2450 orbits
%300km
for i = 1:T_s300*15
    lon = lon0*i;
    lat300 = lat300_0*i;
    B300 = igrf_m(lon,lat300,alt300*10^-3,2010,'-Fxyz')*10^-9;
    box300(i) = B300(1);
    boy300(i) = B300(2);
    boz300(i) = B300(3);
    time300(i) = i;
end
%500km
for i = 1:T_s500*15
    lon = lon0*i;
    lat500 = lat500_0*i;
    B500 = igrf_m(lon,lat500,alt500*10^-3,2010,'-Fxyz')*10^-9;
    box500(i) = B500(1);
    boy500(i) = B500(2);
    boz500(i) = B500(3);
    time500(i) = i;
end

```

```

%800km
for i = 1:T_s800*15
    lon = lon0*i;
    lat800 = lat800_0*i;
    B800 = igrf_m(lon,lat800,alt800*10^-3,2010,'-Fxyz')*10^-9;
    box800(i) = B800(1);
    boy800(i) = B800(2);
    boz800(i) = B800(3);
    time800(i) = i;
end

savefile = 'igrf11-300km.mat';
save(savefile, 'time300', 'box300', 'boy300', 'boz300');

savefile = 'igrf11-500km.mat';
save(savefile, 'time500', 'box500', 'boy500', 'boz500');

savefile = 'igrf11-800km.mat';
save(savefile, 'time800', 'box800', 'boy800', 'boz800');

figure(1)
hold on
grid
legend('x(T)', 'y(T)', 'z(T)')
plot(box300, 'b')
plot(boy300, 'g')
plot(boz300, 'r')

figure(2)
hold on
grid
legend('x(T)', 'y(T)', 'z(T)')
plot(box500, 'b')
plot(boy500, 'g')
plot(boz500, 'r')

figure(3)
hold on
grid
legend('x(T)', 'y(T)', 'z(T)')
plot(box800, 'b')
plot(boy800, 'g')
plot(boz800, 'r')

```

### BDipoleavg.m

```

%Bavg computes the average B matrix in the linearized satellite dynamics
%using the geomagnetic field model data over one orbit period.

```



```

%The average of the B matrix divided with the 2-norm of the magnetic
%field, and the average of the B matrix divided with the squared 2-norm
%of the magnetic field are also calculated.
%Fredrik Stray 2010

global T_o i_m r_o u_f w_o i_0

%Calculating over one period
for t = 0:T_o
    b = u_f/r_o^3*[cos(w_o*(t-i_0/w_o))*sin(i_m);...
    -cos(i_m);2*sin(w_o*(t-i_0/w_o))*sin(i_m)];
    S = skew3(b)'*skew3(b)';
    S11(t+1)=S(1,1);
    S12(t+1)=S(1,2);
    S13(t+1)=S(1,3);
    S21(t+1)=S(2,1);
    S22(t+1)=S(2,2);
    S23(t+1)=S(2,3);
    S31(t+1)=S(3,1);
    S32(t+1)=S(3,2);
    S33(t+1)=S(3,3);
end

%Calculating the averages and saving
BDipole_avg=[sum(S11),sum(S21),sum(S31);
    sum(S12),sum(S22),sum(S32);
    sum(S13),sum(S23),sum(S33)]/t;
save('BDipole_avg.mat','BDipole_avg')

```

## Bavg.m

```

%Bavg computes the average B matrix in the linearized satellite
%dynamics using the geomagnetic field model data over one orbit
%period. The average of the B matrix divided with the 2-norm of
%the magnetic field,
%and the average of the B matrix divided with the squared 2-norm of the
%magnetic field are also calculated.
%Fredrik Stray 2010

%The geomagnetic field model data is loaded.
load igrf11-2010-500km

%Calculating over one period
for i = 1:length(B_O_x)
    vec=[B_O_x(i),B_O_y(i),B_O_z(i)]';
    S = skew3(vec)*skew3(vec)';
    S11(i)=S(1,1);
    S12(i)=S(1,2);

```

```

S13(i)=S(1,3);
S21(i)=S(2,1);
S22(i)=S(2,2);
S23(i)=S(2,3);
S31(i)=S(3,1);
S32(i)=S(3,2);
S33(i)=S(3,3);

S = skew3(vec)*skew3(vec)'/norm(vec)^2;
Ss11(i)=S(1,1);
Ss12(i)=S(1,2);
Ss13(i)=S(1,3);
Ss21(i)=S(2,1);
Ss22(i)=S(2,2);
Ss23(i)=S(2,3);
Ss31(i)=S(3,1);
Ss32(i)=S(3,2);
Ss33(i)=S(3,3);

S = skew3(vec)*skew3(vec)'/norm(vec);
Sss11(i)=S(1,1);
Sss12(i)=S(1,2);
Sss13(i)=S(1,3);
Sss21(i)=S(2,1);
Sss22(i)=S(2,2);
Sss23(i)=S(2,3);
Sss31(i)=S(3,1);
Sss32(i)=S(3,2);
Sss33(i)=S(3,3);
end

%Calculating the averages and saving
gamma=[sum(S11),sum(S21),sum(S31);
        sum(S12),sum(S22),sum(S32);
        sum(S13),sum(S23),sum(S33)]/i;
save('gamma.mat','gamma')

gammaNorm2=[sum(Ss11),sum(Ss21),sum(Ss31);
            sum(Ss12),sum(Ss22),sum(Ss32);
            sum(Ss13),sum(Ss23),sum(Ss33)]/i;
save('gammaNorm2.mat','gammaNorm2')

gammaNorm=[sum(Sss11),sum(Sss21),sum(Sss31);
           sum(Sss12),sum(Sss22),sum(Sss32);
           sum(Sss13),sum(Sss23),sum(Sss33)]/i;
save('gammaNorm.mat','gammaNorm')

```

**skew3.m**

```
function S = skew3(vec)

S=[0 -vec(3) vec(2);
   vec(3) 0 -vec(1);
   -vec(2) vec(1) 0];
```

### Wq.m

```
function W = Wq(q)
W = 0.5*[q(4) -q(3) q(2);
         q(3) q(4) -q(1);
        -q(2) q(1) q(4);
        -q(1) -q(2) -q(3)];
```

### euler2q.m

```
function q = euler2q(in)
% q = EULER2Q(phi,theta,psi) computes the unit quaternions
% q = [eps1 eps2 eps3 eta]
% from Euler angles phi, theta and psi
%
% Author:   Thor I. Fossen
% Date:     8th June 2000
% Revisions: 6 October 2001, T I. Fossen - eta as first element in q
%           2010 Fredrik Stray
phi=in(1);
theta=in(2);
psi=in(3);
R = Rzyx(phi,theta,psi);
R(4,4) = trace(R);
[Rmax,i] = max( [R(1,1) R(2,2) R(3,3) R(4,4)] );
p_i= sqrt(1+2*R(i,i)-R(4,4));
if i==1,
    p1 = p_i;
    p2 = (R(2,1)+R(1,2))/p_i;
    p3 = (R(1,3)+R(3,1))/p_i;
    p4 = (R(3,2)-R(2,3))/p_i;
elseif i==2,
    p1 = (R(2,1)+R(1,2))/p_i;
    p2 = p_i;
    p3 = (R(3,2)+R(2,3))/p_i;
    p4 = (R(1,3)-R(3,1))/p_i;
elseif i==3,
    p1 = (R(1,3)+R(3,1))/p_i;
    p2 = (R(3,2)+R(2,3))/p_i;
```

```

    p3 = p_i;
    p4 = (R(2,1)-R(1,2))/p_i;
else
    p1 = (R(3,2)-R(2,3))/p_i;
    p2 = (R(1,3)-R(3,1))/p_i;
    p3 = (R(2,1)-R(1,2))/p_i;
    p4 = p_i;
end

q = 0.5*[p1 p2 p3 p4]';
q = q/(q'*q);

```

### Rzyx.m

```

function R = Rzyx(phi,theta,psi)
% R = Rzyx(phi,theta,psi) computes the Euler angle
% rotation matrix R in SO(3) using the zyx convention
%
% Author:    Thor I. Fossen
% Date:     14th June 2001
% Revisions:

cphi = cos(phi);
sphi = sin(phi);
cth = cos(theta);
sth = sin(theta);
cpsi = cos(psi);
spsi = sin(psi);

R = [...
    cpsi*cth    -spsi*cphi+cpsi*sth*sphi    spsi*sphi+cpsi*cphi*sth
    spsi*cth    cpsi*cphi+sphi*sth*spsi    -cpsi*sphi+sth*spsi*cphi
    -sth        cth*sphi                    cth*cphi ];

```

### Rquat.m

```

function R = Rquat(q)
% R = Rquat(q) computes the quaternion rotation matrix R in SO(3)
% for q = [eps1 eps2 eps3 eta]
% Fredrik Stray 2010
eps = q(1:3);
eta = q(4);

S = skew3(eps);
R = eye(3) + 2*eta*S + 2*S^2;

```

**q2euler.m**

```
function euler = q2euler(q)
% [phi,theta,psi] = Q2EULER(q) computes the Euler angles from the unit
% quaternions q = [eps1 eps2 eps3 eta]
%
% Author:   Thor I. Fossen
% Date:    14th June 2001
% Edited by Fredrik Stray 2010

R = Rquat(q);

phi   = atan2(R(3,2),R(3,3));
theta = -asin(R(3,1));
psi   = atan2(R(2,1),R(1,1));

euler=180/pi*[phi theta psi];
```



## Appendix C

# SIMULINK source code

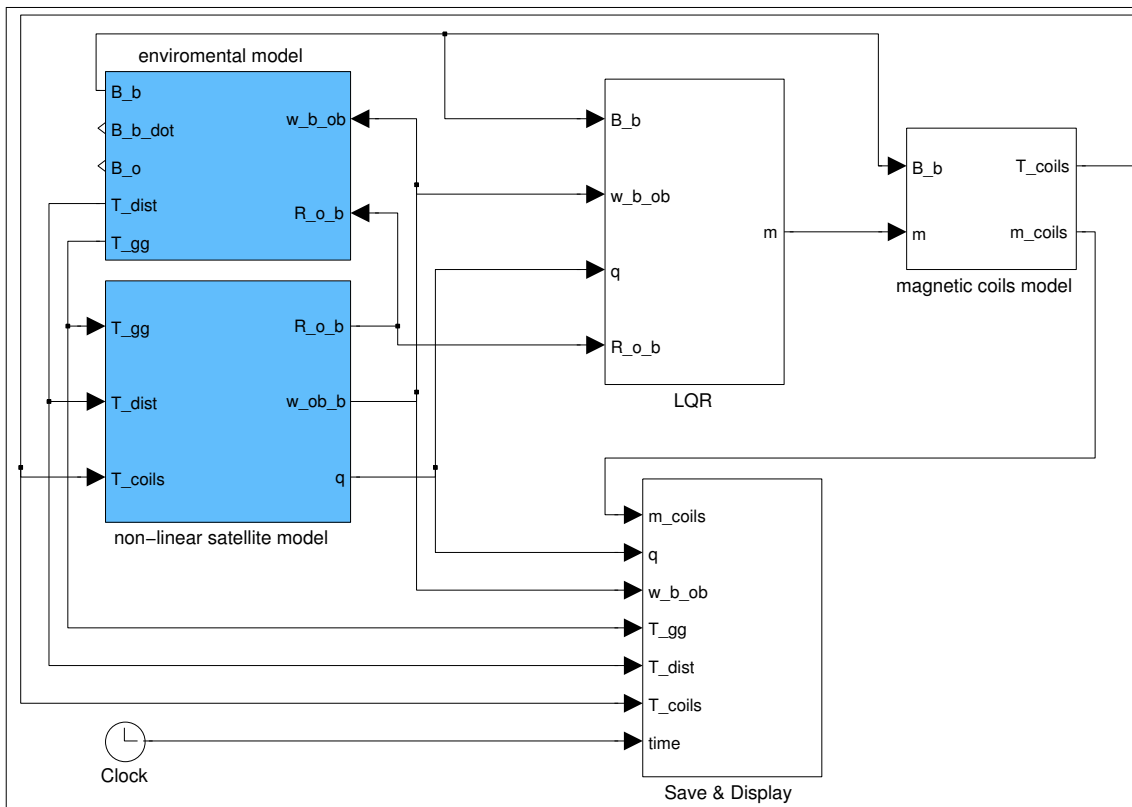


Figure C.1: Top-Level Block Diagram

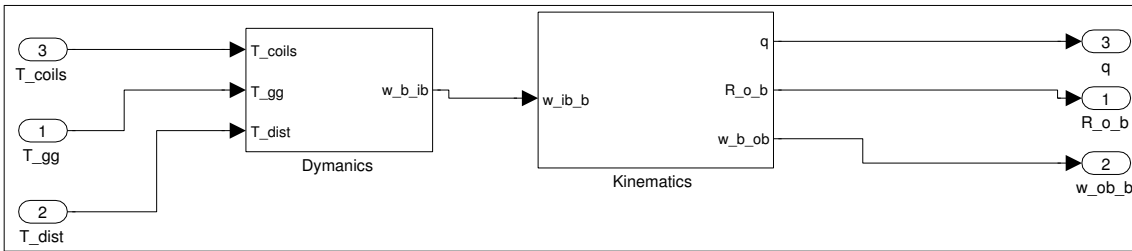


Figure C.2: Non-Linear System

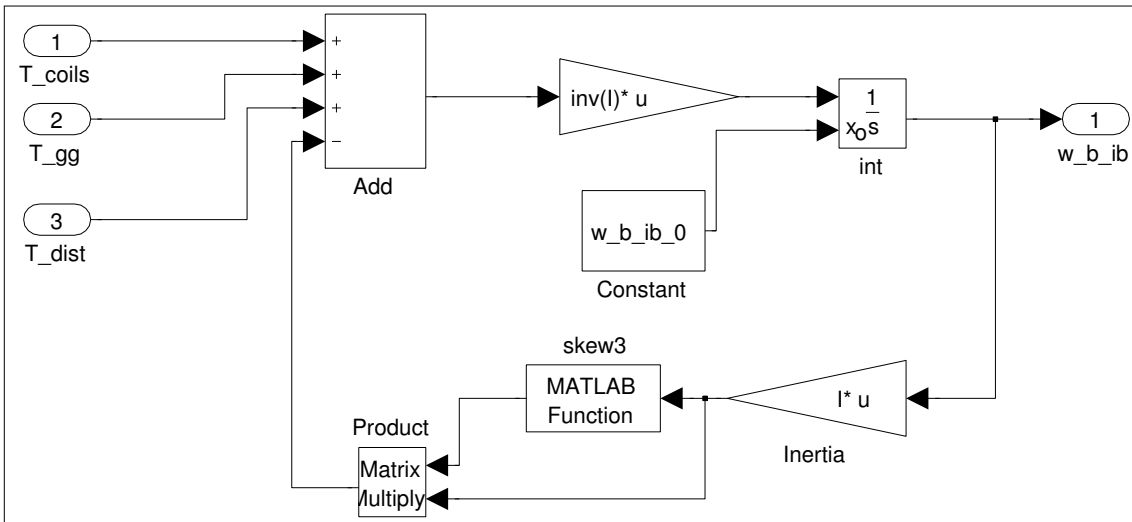


Figure C.3: Spacecraft Dynamics

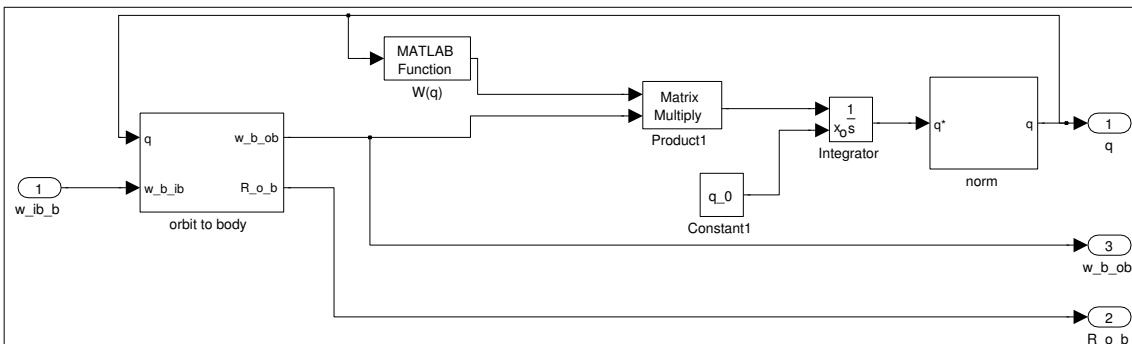


Figure C.4: Spacecraft Kinetics



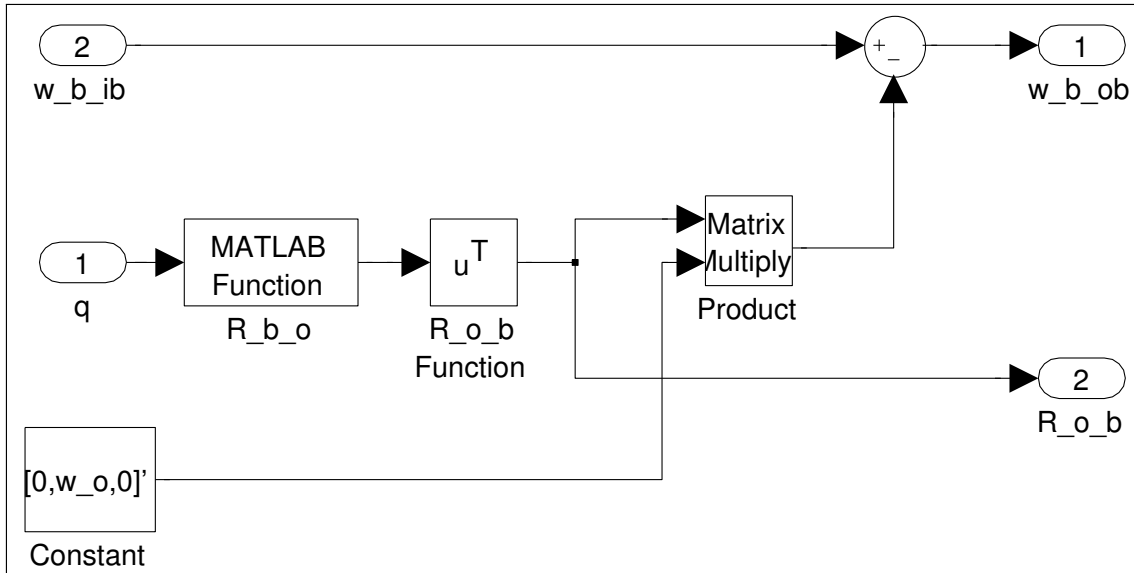


Figure C.5: orbit to body

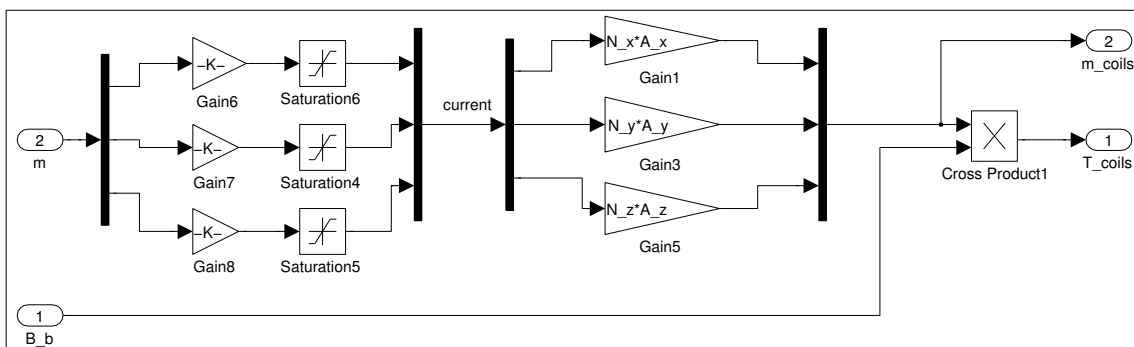


Figure C.6: Magnetic Coils model

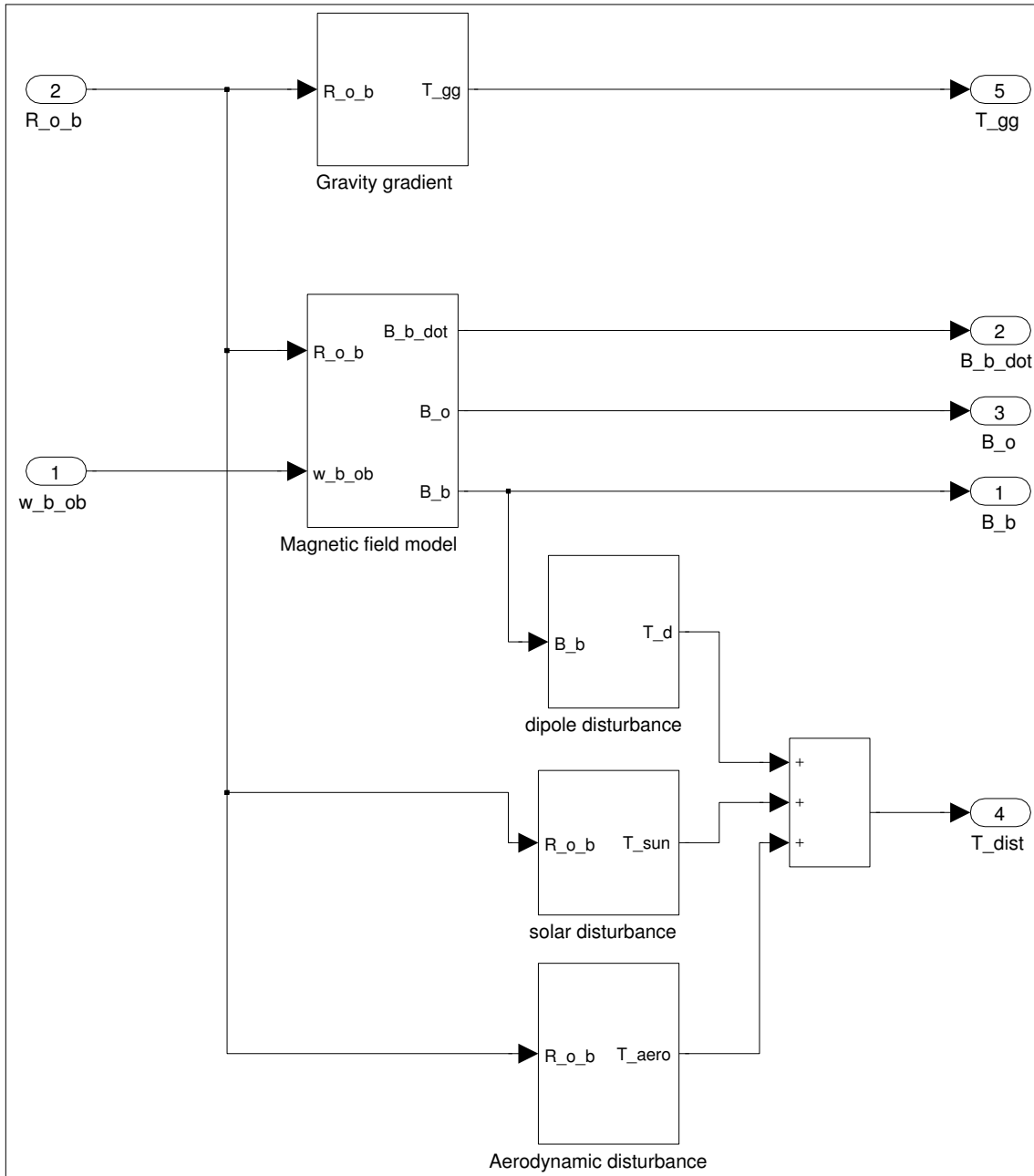


Figure C.7: Environmental Model

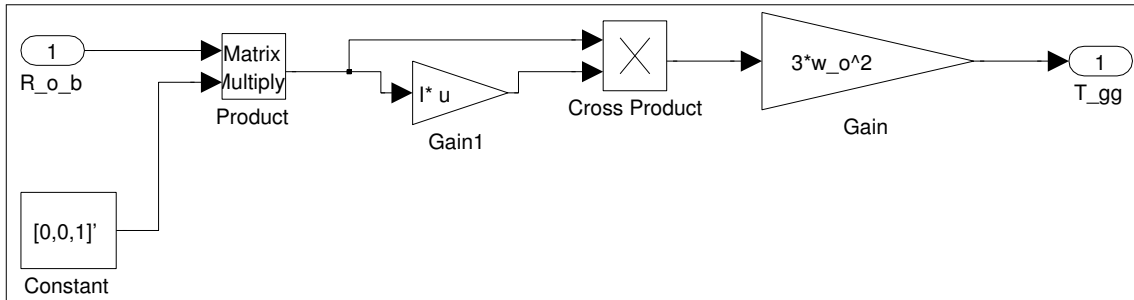


Figure C.8: Gravity Gradient Block

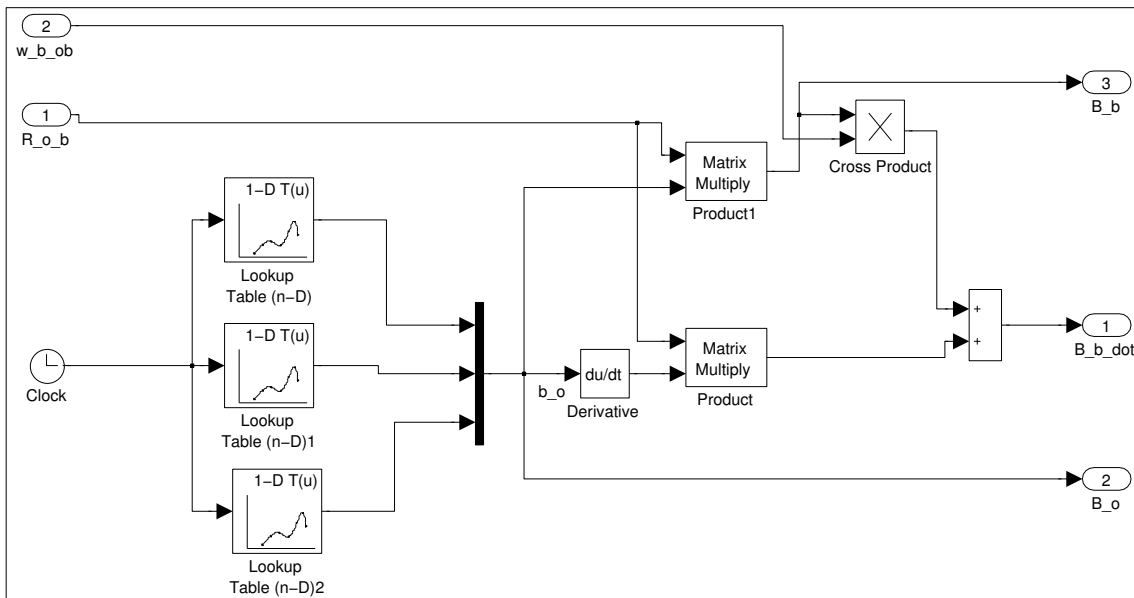


Figure C.9: Magnetic Field Block

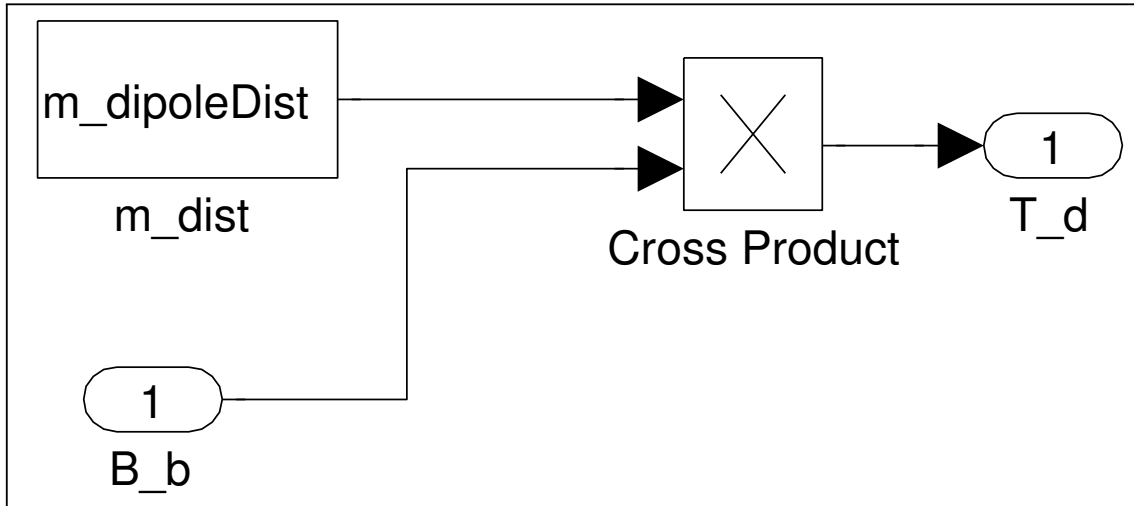


Figure C.10: Magnetic Dipole Disturbance Block

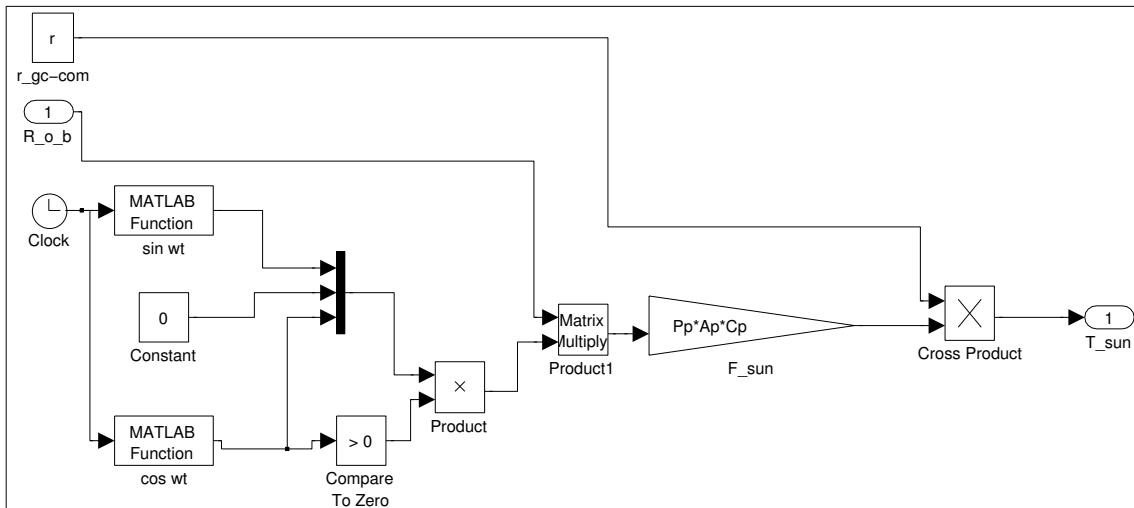


Figure C.11: Sun Pressure Block

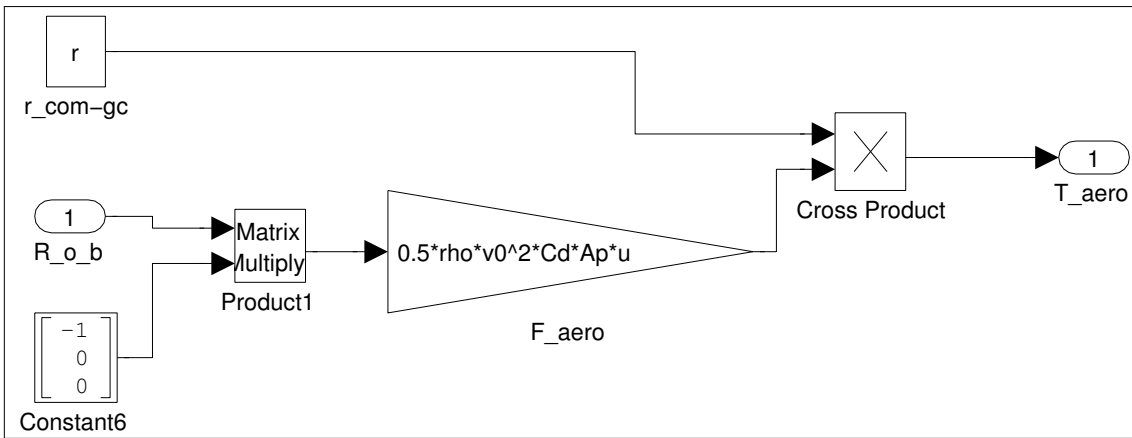


Figure C.12: Aerodynamic Pressure Block

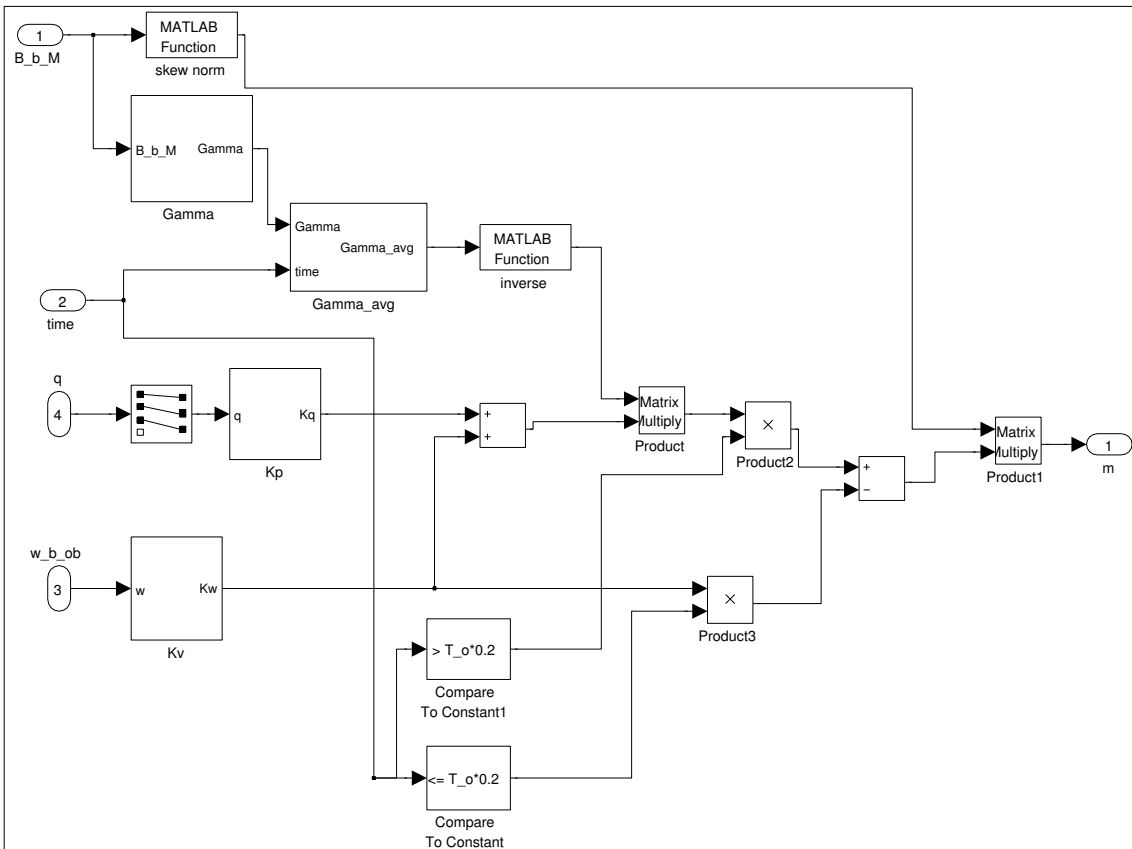


Figure C.13: Adaptive PD

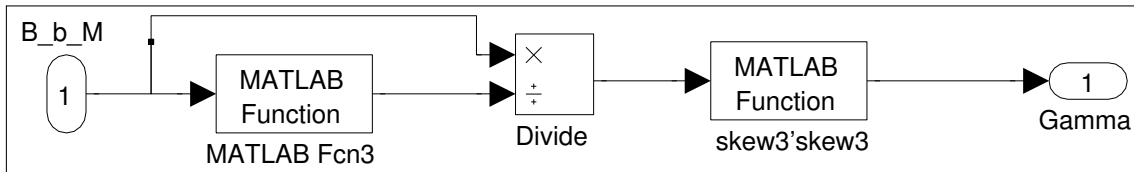


Figure C.14: Adaptive PD gamma

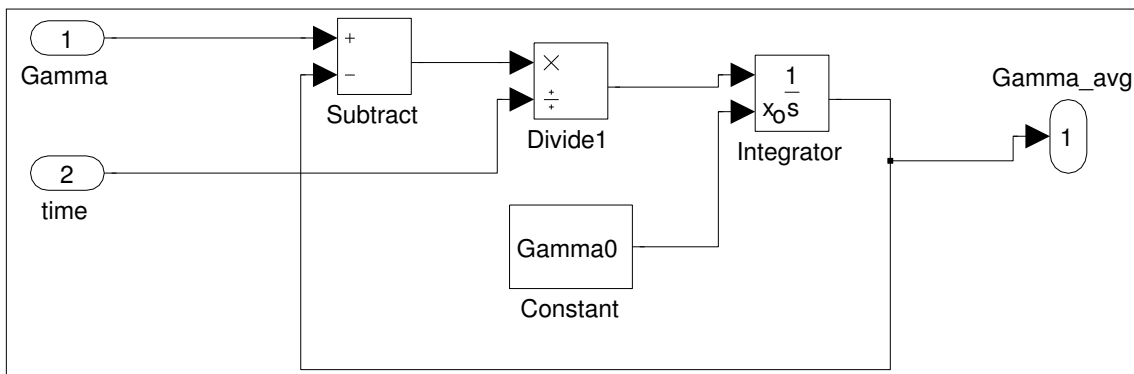
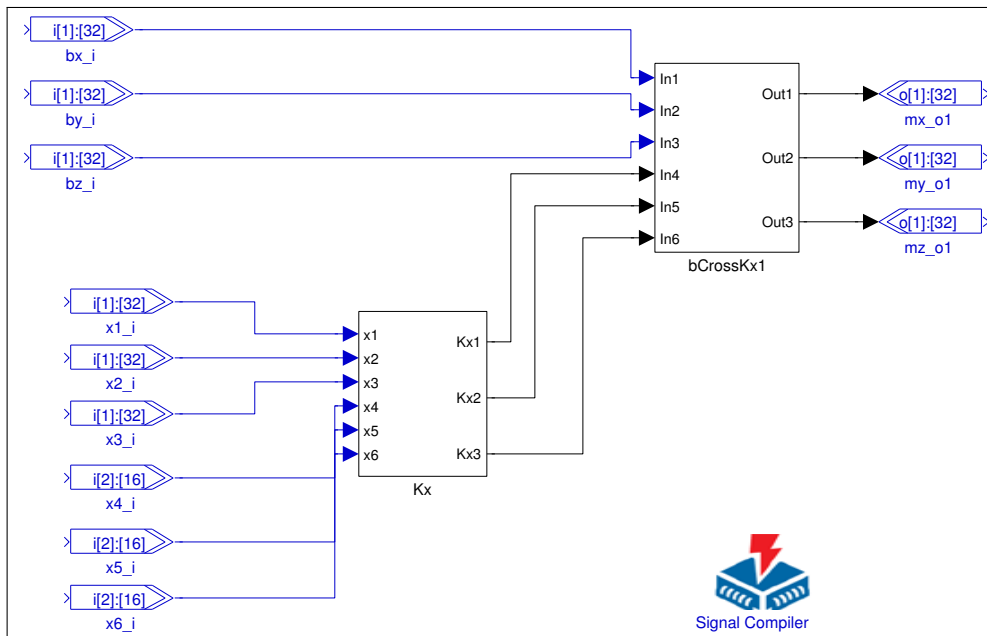


Figure C.15: Adaptive PD gamma average

## Appendix D

# DSP builder source code



**Figure D.1:** Top-Level Block Diagram of the FPGA attitude control.

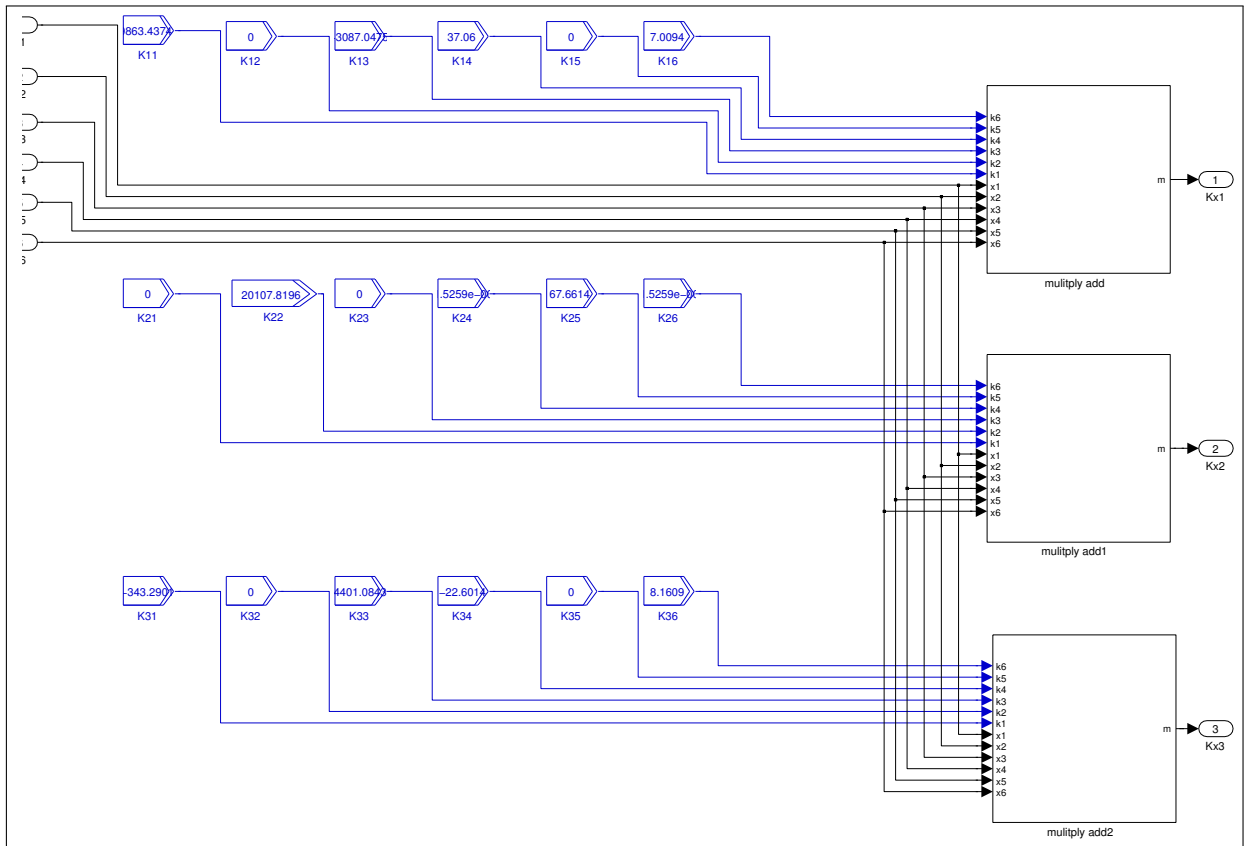


Figure D.2: Block Diagram of the FPGA gain



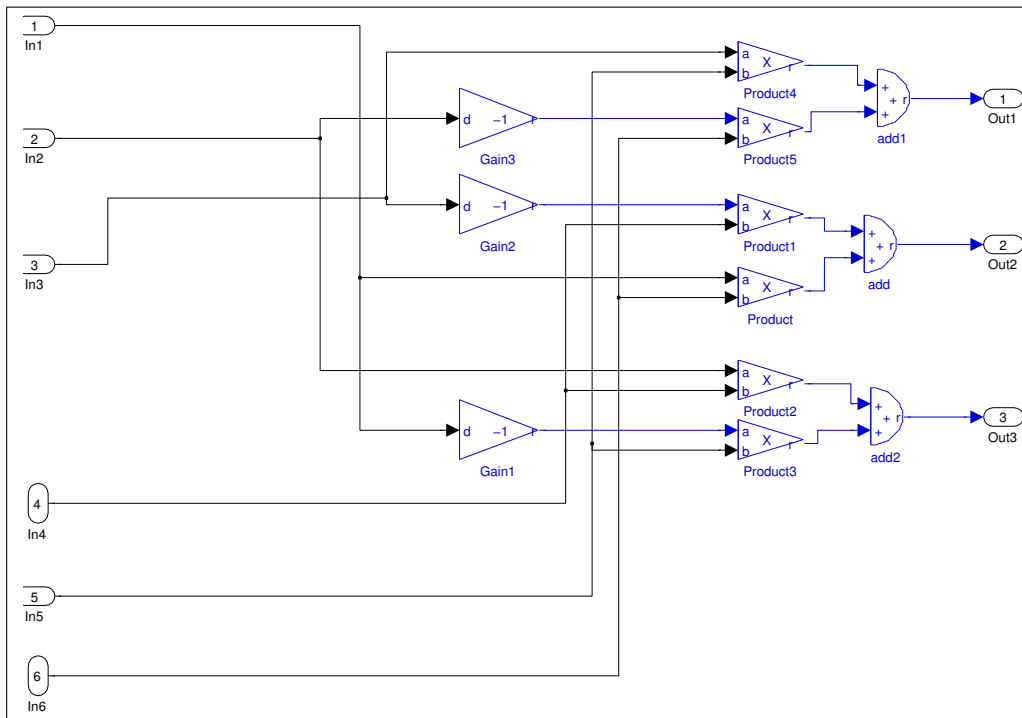


Figure D.3: Block Diagram of the FPGA matrix calculation

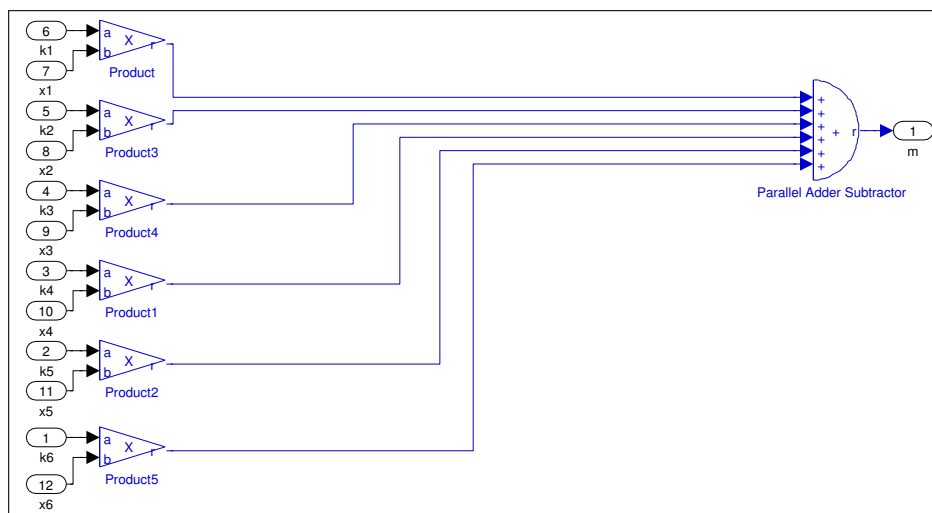


Figure D.4: Block Diagram of the FPGA matrix calculation